6-21-2022

Advanced Methods for Performance Enhancement in Modern Distribution Networks

Iresha Shamini Dharmasena Konara Mudiyanselage
Florida International University, ikona001@fiu.edu

FLORIDA INTERNATIONAL UNIVERSITY

Miami, Florida

ADVANCED METHODS FOR PERFORMANCE ENHANCEMENT IN MODERN DISTRIBUTION NETWORKS

A dissertation submitted in partial fulfillment of the

requirements for the degree of

DOCTOR OF PHILOSOPHY

in

ELECTRICAL AND COMPUTER ENGINEERING

by

Iresha Shamini Dharmasena, Konara Mudiyanselage

2022

To: Dean John Volakis
College of Engineering and Computing

This dissertation, written by Iresha Shamini Dharmasena, Konara Mudiyanselage, and entitled Advanced Methods for Performance Enhancement in Modern Distribution Networks, having been approved in respect to style and intellectual content, is referred to you for judgment.

We have read this dissertation and recommend that it be approved.

Jean H. Andrian

Sumit Paudyal

Berrin Tansel

Deepal Rodrigo

Arif Sarwat, Major Professor

Date of Defense: June 21, 2022

The dissertation of Iresha Shamini Dharmasena, Konara Mudiyanselage is approved.

Dean John Volakis
College of Engineering and Computing

Andrés G. Gil
Vice President for Research and Economic Development
and Dean of the University Graduate School

Florida International University, 2022

DEDICATION

To my dearest parents K.M Dharmasena and Sunethra Liyanage

ACKNOWLEDGMENTS

I would like to convey my sincere gratitude to my advisor Dr. Arif Sarwat for his continuous support and guidance throughout my doctoral studies. My gratitude extends to the dissertation committee, Dr. Jean H. Andrian, Dr. Sumit Paudyal, Dr. Deepal Rodrigo and Dr. Barrin Tansel for their constructive feedback and encouragement. With great pleasure I would like to also acknowledge all the faculty members at Florida International University, The University Akron, Ohio and University of Moratuwa, Sri Lanka and all the teachers I met in my life. Moreover, I would like to thank all past and present fellow researchers at the Energy, Power & Sustainability-Intelligence (EPS-i) laboratory for the collaboration rendered throughout, especially to my dear friend Temitayo Olowu. Furthurmore, my utmost heartfelt gratitude goes to my beloved parents for raising me up to the position today I am. I'm thankful to my husband and my baby boy for their unparalleled support and encouragement. The work in this dissertation is supported by the National Science Foundation (NSF) award number 1553494, Department of Energy under grant number DE-EE0009349, and the UGS Dissertation Year Fellowship.

ABSTRACT OF THE DISSERTATION

ADVANCED METHODS FOR PERFORMANCE ENHANCEMENT IN MODERN DISTRIBUTION NETWORKS

by

Iresha Shamini Dharmasena, Konara Mudiyanselage

Florida International University, 2022

Miami, Florida

Professor Arif Sarwat, Major Professor

Efforts towards decarbonized economy has added new pressures in the distribution network, especially with increased penetration of distributed generation, electrification of transportation, etc. It demands breakthrough technologies to be developed in different sectors such as in power systems, power electronics, communication, among others. The work of this dissertation investigates a twofold approach of distribution energy resources (DERs) implementation to address the challenges faced by modern power distribution network.

The first approach is to develop advance control techniques for smart inverters that interlinks DERs to the grid to facilitate grid support services. A complexity reduced finite control set model predictive direct power controller (FS-MPDPC) for active-reactive bidirectional power control of grid connected converter has been developed. This avoids the brute-force search inherent to FS-MPDC which cut down the computational complexity. Further, a fuzzy decision making (FDM) assisted MPDPC (fuzzy-MPDPC) is derived for a three-phase grid-connected converter that interlinks battery energy storage system (BESS) to the grid. The controller combines fuzzy logic and MPDPC theories to control bidirectional active, reactive power. Rather than using a layered control architecture for BESS scheduling and grid feed control, this work proposes an improved model predictive controller with fuzzy-

goal, fuzzy-constraint based objective function which dynamically adjusts according to external conditions.

The second approach is to develop resilience enhancement and quantification techniques for power distribution network. For that, an algorithm is formulated for optimal hosting and placement of DERs for network resiliency enhancement. This multi-objective nonlinear programming formulation incorporates a unique critical load (CL) ranking scheme to prioritize the CL nodes for the DER placement while achieving a maximum DER hosting capacity, improving resiliency and minimizing the system's active power loss while satisfying all network and power flow constraints. The developed algorithm is validated for different outage scenarios caused by a hurricane and the results verify the effectiveness. Secondly, a metric scheme has been developed to quantify the level of resilience of the network and to justify the resilience enhancements done on the system. The metrics are validated by showcasing the resilience enhancement before and after implementation of DERs through the metrics.

TABLE OF CONTENTS

LIST OF TABLES

LIST OF FIGURES

FIGURE PAGE

CHAPTER 1

INTRODUCTION

1.1 General Statement of Research Area

The modern day power distribution networks need to undergo massive transformations due to highly penetrated distributed generation (DG), mass electrification of everyday life including electrification of transportation, stringent technological requirements that are raised by the load-side, climate change and due to many other driving factors. The network improvements/changes needs much thought into the development of potential key enabler technologies in sectors such as power electronics, communication, sensing, measuring, monitoring technologies, control techniques [1]. The efforts of this research are aimed towards exploring new techniques for enhancing performance in the modern distribution network.

The escalating electricity demands over large geographical distances is a tremendous technical challenge in the modern distribution network for which DG is introduced as a solution. Most DGs are renewable energy resource based and the renewable energy generation is highly desired due to environmental concerns. However, the increased levels of penetration of renewable energy generation can weaken the rigidity and stability of the grid due to their intermittent nature. Some of the challenges that stem from increased penetration are power quality issues, low inertia, voltage and frequency fluctuations, among others [2]. Energy storage systems are introduced to the energy mix mainly to alleviate these stability issues by operating as a spinning reserve. They support voltage-frequency regulation at the point of common coupling (PCC) and also act as storage for off-peak wind and solar power generation. Apart form that, energy storage are used for peak load shaving, to facilitate black-start as well.

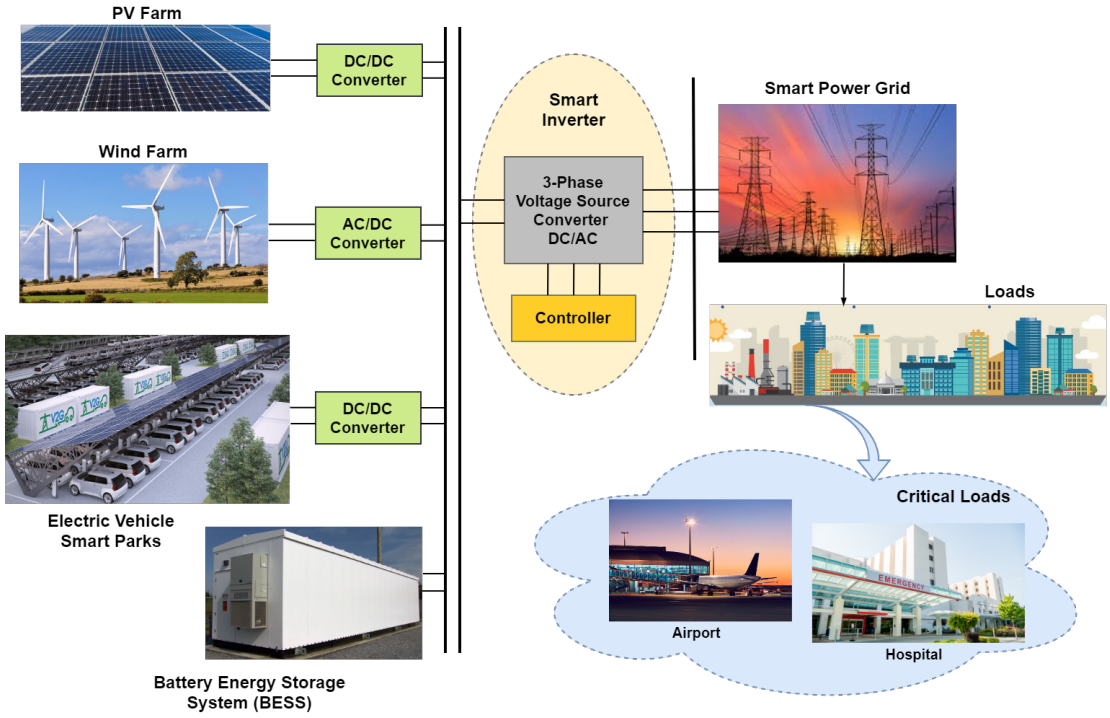

Figure 1.1: Overview of the modern power distribution network.

Battery energy storage systems (BESS) have proven to be a viable solution in addressing such challenges since they can react fast to balance-out the dynamic variations in electricity consumption and production with their capability to operate in very high power ramp rates. Therefore, BESS can play an important role in the power quality management, autonomous grid forming and maintaining grid stability. Further, the aggregated electric vehicles (EVs) (e.g., smart EV parks) have the potential to act as energy storages as well as energy sinks with bidirectional power transfer capability [3]. Hence, with the increased use of EVs, the EV parks can used for current harmonic compensations, active and reactive power control. All these DG resources are called as distributed energy resources (DERs) and they are connected to the network through smart inverters (SIs) as shown in Figure 1.1.

The aforementioned functionalities of DERs are achieved through advance power electronics and controls implemented in the smart inverter [4]. Unlike with the conventional power generation, SI-connected DERs are capable of fast dynamic control over distribution network parameters. Specially when it comes to energy storage system integration, the SI controllers should facilitate bidirectional power flow control considering both grid conditions and state of the charge (SOC) of the storage. The IEEE 1547-2018 standard [5], has mandated a set of functionalities for grid integrated DERs which includes Volt-Var control, Volt-Watt control, fault-ride-through etc. These stipulated functionalities are implemented by incorporating proper control techniques in the SI. For better performance of SI-based DERs, advanced control techniques become highly imperative.

Another serious challenge faced by the modern distribution network is extreme weather events which triggers long outages, equipment failures and large economic loss. This has become a serious issue more than ever now since the frequency of extreme events such as hurricanes, wildfire, floods etc. has increased dramatically in recent years due to the climate change. The resilience topic has gained much attention in power systems area due to frequent intensified extreme weather events, increasing digitization of society and shifting consumer expectations, increasing vulnerability to cyber attacks, vulnerability due to increased dependence on natural gas for electric power etc [6].

There are several definitions of power system resilience, including those given by the U.S. Department of Energy (DOE), the Industrial Control Systems- Computer Emergency Readiness Team (ICS-CERT), and federal labs such as the National Renewable Energy Laboratory (NREL) and the Pacific Northwest National Laboratory (PNNL) [7–10]. In the context of the energy system, resilience indicates the strength of the system against high-impact, low-frequency events such as natural

disasters or cyber-attacks, human-physical activities. In this work, we refer to such events as extreme events. More explicitly, the resilience can be defined as system's ability to anticipate, prepare for, and adapt to changing conditions and withstand, respond to, and recover rapidly from disruptions through sustainable, adaptable, and holistic planning and technical solutions [11].

The impact of power interruptions is severe specially at critical load (CL) nodes of the network. The functioning of critical loads in the network is essential for the well being of society and economy e.g., hospital, airport, police etc. The definition adopted in this paper measures resiliency of a PDN as its ability to provide continuous power supply to at least one of its CL nodes during the occurrence of an extreme event. Power system fails even during normal weather due to progressive degradation of system components, human factors amongst many others [12]. But the impact on power system due to extreme events is severe as it is mostly unpredictable, progresses so fast and can cause faults in several locations simultaneously. It also can be hard to physically access the fault locations in order to start the restoration process while the event progresses.

As the distribution network is vulnerable to natural disasters, it is necessary to develop control and operation methods and planning strategies to restore the power quickly and effectively at least for the critical loads. There are various such techniques are proposed in the literature including system hardening methodologies and restoration schemes [13,14] which are further discussed in the section 1.2. Since DERs are dispersed across the PDN, proper DER placement also has the potential to enhance the grid resilience by creating islands to provide continuous power supply to the critical loads. Before the implementation of these resilience enhancement techniques in the system, it is required to assess their impact on the system and to justify them technically and financially. To do that there should be some resilience

quantification scheme. Therefore, it's highly important to develop resiliency metrics and evaluation methods to compare planning and operation alternatives.

1.2 Literature Review

The conventional control of voltage source converter (VSC) with proportional-integral (PI) control can be disadvantageous in highly dynamic systems with constant perturbations. This is because conventional PIs are pre-tuned to certain system parameters and they might not provide the same expected performance under different dynamic conditions. Also PI controllers are characterized with slow transient response [15]. The direct power control (DPC) technique was introduced as an alternative and it uses a lookup table with predefined switching states [16]. Although DPC can outperform PI controllers with its high dynamic performance, it is disadvantaged with higher power and current ripples since the control is based on a finite switch table. But there are various developments of DPC addressing its weaknesses including the design to operate in constant switching frequency including grid voltage modulated direct power control (GVM-DPC) and sliding-mode direct power control (SM-DPC) [17].

The model predictive control (MPC) for converter control has gained a huge popularity in power electronic research community with the evolution of powerful and fast microprocessors. MPC is a promising control technique for power converters due to it's desirable features such as ability to handle multiple inputs/ outputs, easily handle system constraints and non-linearities and fast dynamic response [18]. There are two divisions of MPC used for grid connected converters; model predictive direct power control (MPDPC) [19,20] and model predictive current control (MPCC) [21, 22]. In MPCC, the grid current is used as the state variable to be controlled.

And in MPDPC the active and reactive power injected and/or absorbed by the converter is controlled. Therefore, MPDPC is well suited for bidirectional control of grid connected converters.

Among two major variants of MPC which are finite control set model predictive control (FS-MPC) and continuous control set model predictive control (CCS-MPC), FS-MPC is the most commonly used technique for power converters [23]. The reason is that, the converter systems have well known mathematical models and can easily identify the finite number of switching states as the finite control set. FS-MPC uses the mathematical model of the converter to predict the behaviour of the state variables at each sampling period for all control inputs in the finite control set.

In conventional FS-MPC, the optimal candidate from the finite control set is chosen by performing a brute-force search. This can exhaust the processes specially if the control set is large, as it could involve a huge number of computations. Therefore, research has been carried out to develop techniques to reduce the computational complexity involved in FS-MPC with a bigger voltage set. The state-of-the-art of the research on this regard is extensively analyzed in Section 2.2.

As mentioned before, MPC is a promising control technique and is applicable to systems that has precise mathematical models [24, 25]. The operation of a typical VSC can be replicated by a linear mathematical model which makes it more suitable for MPC. In contrast, fuzzy logic control (FLC) based on fuzzy decision making (FDM) involves human knowledge for defining control objectives and commands and does not require a mathematical model. Most real-world scenarios are hard to model mathematically and they operate based on approximations or estimations due to high parameter variations and lack of required data. FLC requires a good qualitative understanding about the plant and the objective of the controller is to emulate the human thinking patterns and the logic. There are recent developments

towards deriving fuzzy inference through data clustering and artificial intelligence based evolving rules as well.

In order to amalgamate the benefits of different control techniques, consensus controllers are being developed combining two or more control techniques depending on the system [26]. In [27], a fuzzy gain scheduling scheme is proposed for a PID controller to improve the transient performance of a PV farm.

As discussed in the section 1.1, DERs have the potential to solve multitude challenges emerged in the modern PDN. With the increasing number of grid-connected DERs on distribution feeders, there are studies focused on leveraging the DERs for grid resilience enhancement during extreme weather [28, 29]. These resilience enhancement methods can be divided into two, based on the time of action. They are hardening or preparation at pre-event and corrective actions or restoration at on-event. The articles [30–32] are focused on developing restoration and reconfiguration algorithms. Authors of [30] proposes a scheme to self-heal the system by sectionalizing the network into self-supplied microgrids. The development of impact assessment model and optimal restoration model for a PDN with DERs is done using non-sequential Monte Carlo simulation for a modeled probabilistic extreme event in [32]. In [31], an optimal scheduling model for microgrids to enhance resiliency during an outage is presented. Deployment of networked microgrids to achieve higher level of resilience is extensively analyzed in [33].

Optimal DER hosting and placement is a grid hardening technique at pre-event and is an important area of research but little of this concept have been studied and reported in literature. Optimal DER hosting (sizing) and placement of the DER is typically constrained by the PDN's power flow, voltage measurements, cable ampacity, thermal limits as well power quality. But when considering the resilience

enhancement, other conditions and constraints also needs to put into the optimization problem.

As discussed in the Section 1.1, it's necessary having a resilience quantification technique for the process of resilience enhancement in power network. Various metric schemes for resilience evaluation can be found in literature, but a standardized metric scheme to measure the resilience of power network is not currently available. Based on the metrics of resilience proposed in literature, the metric formulation approaches can be categorized into attributes-based and performance-based. Different entities identify and name these approaches differently. The grid modernization lab consortium metrics analysis project, identifies that metric can either be performance based or multi-criteria decision analysis (MCDA) based [34]. And the IEEE power & energy society (PES) industry technical support leadership committee task force defines the same as qualitative and quantitative frameworks [35].

Attribute based metrics evaluate system properties and their availability in the system for measuring the resilience. This approach provides a qualitative understanding of the system's current resilience based on system properties such as resourcefulness, redundancy, network configuration, adaptivity etc. Generally, the metric is obtained by performing a series of calculationsimplementing an evaluation technique such as analytical hierarchical process (AHP), numerical scoring, checklists etc. to aggregate the impact of each attribute [35]. Some of the attribute based metrics use topological properties of the system as attributes. One such assessment scheme is defined in the paper [36], where Choquet integral is used to aggregate the network topology based measures. The paper [37] proposes a similar attribute based scheme where they've applied AHP to combine six system configuration attributes to quantify the resilience. Both of these metric schemes reflect the resilience

enhancements only due to network positioning of load, generation nodes, switches, lines etc.

The performance based approach quantitatively assess the resilience of power system through historical data of past events, or using estimates or simulating potential scenarios through computational models of grid operations, disruption, and recovery. These metrics provide quantitative information of the reaction of the system and infrastructure in the event of specified disruptions. In this way, it's possible to evaluate the system performance associated with proposed resilience enhancements and investments. This approach basically use the parameters such as outage time, time to recover, cost of recovery etc. and few examples for performance based metrics are expected number of lines on outage, loss of load probability, expected demand not served, difficulty level of grid recovery [38], network performance indices [39] etc.

The attribute based metrics have a simpler data requirement, but might not that informative. In contrast, the performance based metrics can be highly informative and ideal for cost-benefit and planning analyses, but it comes with a significant data requirement. Therefore, performance based metrics are ideal for cost-benefit and planning analyses. The grid modernization lab consortium metrics analysis project, has proposed a combined approach where they have MCDA metrics for high-level characterization and performance metrics to deepen the resilience assessment by integrating economic and regional considerations [34].

1.3 Research Objectives and Original Contributions

The main objective of the proposed research is to resolve some of the challenges in performance enhancement in modern distribution grid as discussed in Section 1.1. The research approaches are viewed along two broader areas; development of

control strategies for smart inverters that interlinks DERs to the grid, and the PDN resilience enhancement and quantification. The work was conducted along two main objectives given below:

1. **Objective 1: Develop advance control techniques for the smart inverters that interlinks DERs to the grid.**

   Research carried out for this objective includes two studies with several original contributions. The conventional finite control set model predictive control (FS-MPC) has a degraded performance due to the finite candidate vector set and when the voltage set extended using discrete space vector modulation it increases the computational complexity due to the inherent brute-force search. First study is to develop a complexity reduced finite set model predictive direct power controller (FS-MPDPC) for grid-connected converters which has the capability of bidirectional active-reactive power flow control. The second work is focused on developing a consensus controller which combines fuzzy logic control with model predictive control for autonomous operation of SIs that interlink BESSs to the grid. This controller addresses grid conditions at the point of common coupling (PCC) as well as the constraints at BESS side. The key contribution of this work is the introduction of the concept of FDM based MPC for control of grid connected converters and investigation of its viability in controlling SI to manage dynamic system conditions and constraints of BESS integration.

2. **Objective 2: Develop resilience enhancement and quantification techniques for power distribution network.**

   Research efforts are twofold for this objective. A unique algorithm has been developed which leverages the benefits of DER sizing and placement to ensure

continued power supply to the maximum possible number of critical load (CL) nodes with minimum power losses during an extreme event. The algorithm incorporates a ranking scheme to prioritize the CL nodes for the DER placement. The algorithm is based on the feeder's voltage sensitivity which allows more PV integration by pushing the maximum nodal voltages close to the overvoltage limit. Unlike other PV-integrated resiliency improvement algorithms, this algorithm applies complete power flow constraints including the operation of the voltage control legacy devices. Secondly, a metric scheme is formulated to quantify the enhancements done for the PDN resilience. Further, the developed metrics are validated in a IEEE test system by implementing test cases of resilience enhancement.

1.4 Dissertation Organization

The rest of this dissertation is organized as follows: Chapter 2 proposes a computational complexity reduction technique for finite control set model predictive control (FS-MPC) for converter control with extended voltage vector set. The developed controller is specifically designed for active-reactive power control of a grid-connected converter that interlinks an energy storage system to the grid. The controller technique is simulated in MATLAB Simulink environment and the performance is analyzed in all four active-reactive bidirectional power flow modes. Results validate the performance of the controller both in steady-state and transient conditions.

Chapter 3 presents a fuzzy decision making (FDM) assisted model predictive direct power controller (fuzzy-MPDPC) that is derived for a three-phase grid-connected converter which interlinks battery energy storage system (BESS) to the grid. The controller combines fuzzy logic and MPDPC theories to control bidirec-

tional active, reactive power flow of the inverter based on grid requirements and state of BESS. The operability of the proposed controller is verified using Matlab Simulink simulation models.

Chapter 4 introduces an algorithmic formulation for optimal PV hosting and placement of DER for network resiliency enhancement. The algorithm incorporates a unique critical infrastructure (CI) ranking scheme to prioritize the CI nodes for the DER placement while ensuring maximum hosting of the DER. The developed multi-objective non linear programming formulation is validated on an IEEE 34 bus feeder with different outage scenarios caused by a hurricane event.

Chapter 5 provides a development of a new metric scheme for resilience quantification which incorporates critical load prioritization. The developed metrics are validated on an IEEE 123 bus feeder before and after implementing resilience enhancement. Further, the impact of the intensity of hurricane wind profiles on the metrics is also analyzed.

Chapter 6 summarizes the research outcomes, concludes the insights, and provides recommendations for the future works.

CHAPTER 2

A LOW COMPLEXITY FCS-MPDPC WITH EXTENDED VOLTAGE SET FOR GRID CONNECTED CONVERTERS

2.1 Overview

Large scale integration of the renewable energy generation in modern power grids is highly desired in order to address the growing energy demand and environmental concerns. However, the increased levels of penetration of DERs (which are mainly from renewable energy) can weaken the rigidity and stability of the grid. Energy storage systems has the potential to address many of these challenges of renewable energy-based DERs. These energy storage systems operates in all four power quadrants (absorbing and injecting active and reactive power), therefore can play an important role in the power quality management, autonomous grid forming and maintaining grid stability of distribution networks. These functionalities of classically controlled DERs are achieved through advance power electronics and controls [40]. Grid supporting smart inverter-connected (SI) DERs are being used to maintain grid voltage and frequency within the acceptable range with active and reactive power control (P-Q control) [41].

In this work FS-MPDPC based controller is designed for grid connected converters to control the bidirectional active-reactive power flow. To improve the performance of FS-MPDPC, the discrete space vector modulation (DSVM) is integrated and a novel technique is developed to reduce the complexity associated with DSVM. The developed controller will be referred as low complexity-FS-MPDPC (LC-FS-MPDPC) hereinafter. The comparative advantages of this controller compared to the state-of-the-art and the novelty of this work is presented in the Section 2.2.

2.2 The State-Of-The-Art of Computational Complexity Reduction Algorithms for FCS-MPDPC

In FS-MPC, the voltage chosen as the optimal vector is applied to the whole control cycle. For a three-phase two-level converter, the operable voltage vector set without employing any modulation technique is limited to seven. The size of the converter voltage vector set is one of the major disadvantages of FS-MPC for three-phase power applications which causes power ripples and current harmonics. For multi-phase systems this issue is not that critical since the finite voltage vector set is larger and can emulate a more continuous behaviour [42, 43]. Although, employing a higher switching frequency for conventional FS-MPC alleviates this issue, it can increase switching losses.

To circumvent this limitation, the DSVM based FS-MPC techniques have been proposed in the literature. This generates a bigger vector set for the optimization [44, 45]. DSVM-FS-MPC applies multiple voltage vectors in a single switch cycle therefore creating a virtual vector space which can effectively suppress the harmonic content in current waveforms. But, again when the vector set gets bigger, the brute-force search of FS-MPC becomes computationally expensive. Variable switching frequency is another complication that comes with virtual vector synthesis [46]. And there are other constrains as well, such as maintaining a minimum switching frequency to reduce losses and reducing the common mode voltage. In the light of above concerns, different techniques have been developed and proposed in the literature to address these issues [47].

Several significant approaches that have been proposed in literature to reduce the computational complexity are comprehensively discussed here with their respective references. First one is the deadbeat technique, in which the desired converter volt-

age vector for the next state is calculated based on line current predictions [48–50]. Then the calculated desired voltage is used as a reference to narrow down the search area in the vector space which reduces the number of candidate vectors. Since the desired voltage is calculated using system model equations, the deadbeat technique based MPC is heavily depends on system parameters. Hence, the deadbeat technique is not robust for system perturbations and requires higher sampling frequency to achieve a better performance. And also this method involves an additional computational load for reference voltage calculations in each cycle. The paper [49] proposes a deadbeat DSVM-FS-MPC for a grid connected VSC. There, the converter reference voltage is calculated and its magnitude and phase angle is used to reduce the search area in the vector space. This technique hugely reduces the number of voltage vectors used for the optimization, but still the drawbacks mentioned earlier persists.

The authors of [51] have proposed the extended model predictive-sliding mode control (EMP-SMC) technique for grid connected converters. They have applied sliding mode theory for d-q axis currents which is used as the basis to narrow-down the search area in the vector space. A pre-calculated lookup table is used to select the candidate vectors for the optimization at each case identified by the sliding mode theory. In this work, a vector set of 19 is considered and the proposed method has reduced number of candidates to 10 for the optimization. In this method, the lookup table formulation consumes considerable computation power and the complexity of formulation increases as the size of the vector set increases. A bigger vector set increases the size of the look table as well. Therefore, EMP-SMC can be almost impractical when the size of the vector set increases.

The modified FS-MPC proposed in [52] uses a technique that has a pre-selection stage and two optimization stages for voltage vector selection process in the vector

space to reduce computations in DSVM-FS-MPC. Initially, a pre-selection process is executed to reduce the size of the vector set to half. In the first optimization stage, only the real vectors in the pre-selected region is considered for the optimization. Then the virtual vectors closest to the optimal real vector produced in the first stage is selected for the second stage optimization. This technique cut down unnecessary voltage vectors for the optimization. But, the complicated process with several optimization stages in each switching cycle make the technique computationally expensive.

Another technique proposed in literature to improve the performance of conventional FS-MPC is duty cycle control method [53, 54]. Rather than extending the voltage set, the duty cycles of the real vectors are controlled to obtain the optimal vector. In [55], the duty cycle control is applied for a double vector optimization scheme. Here, the first optimum voltage is calculated similar to conventional FS-MPC and then the second vector is selected adjacent to the first one to reduce the number of switching. Then, the duty cycles of two vectors were calculated minimizing the cost function. One of the key contributions of this work is that, it avoids the use of zero voltage vectors in order to reduce the common-mode voltage. Although this method has a lower computational complexity and reduced common mode voltage, the current harmonic distortion is higher compared to other techniques discussed earlier. Also, the duty cycle control technique is highly disadvantaged due to inherent variable switching frequency. An improved dual-vector-based predictive duty cycle control strategy is proposed in [56], which states that it eliminates the time consuming procedure of duty-cycle optimization. The proposed controller in [56] utilizes the cost function for both best vector selection and duration derivation. Another duty cycle control based MPC is proposed in [57], and this strategy

determines the mapping between variables by exploring the dual relationship of vector synthesis and duty cycles.

In contrast to the above discussed literature, the key contributions proposed in this work can be highlighted as follows.

1. *Constant switching frequency.*: The proposed technique has a constant switching frequency ($3f_s$) for space vector generation.
2. *Bidirectional power control and consideration of grid constraints in objective function.*: Almost all the publications discussed previously (and others) focused on uni-directional power flow (either rectifier or inverter operation). The proposed technique is designed and validated for bidirectional active and reactive power control. And there are many practical operational constraints affecting the controller operation of a grid connected converter. But, none of the works discussed earlier contemplate these constraints and this work incorporates the operational constrains in to the objective function.
3. *Improved computational efficiency.*: Unlike other methods in literature, the proposed approach is formulated based on MPDPC. Hence the control problem is in the stationary reference frame avoiding additional steps needed to compute the park transformation. In addition to the contributions mentioned above, a computational complexity comparison of the proposed technique is presented in section. 2.6.3.

2.3 Grid-connected BESS as a Case Study

The grid network used for the study is illustrated in Fig.2.1. An energy storage system is connected to the distribution grid through a three-phase two-level VSC. Also the system is equipped with a simple inductor (L) filter and a resistor for

passive damping. The controller generates necessary gate control signals for the converter.

As stipulated in the IEEE 1547-2018 standard [5], grid-connected DERs' SIs should be capable of providing grid supporting ancillary services such as P-Q control for voltage and frequency regulation. Therefore, converters that interlinks energy storage systems to the grid should be able to operate in all four quadrants of the P-Q power flow and should smoothly transit between these operation modes seamlessly.

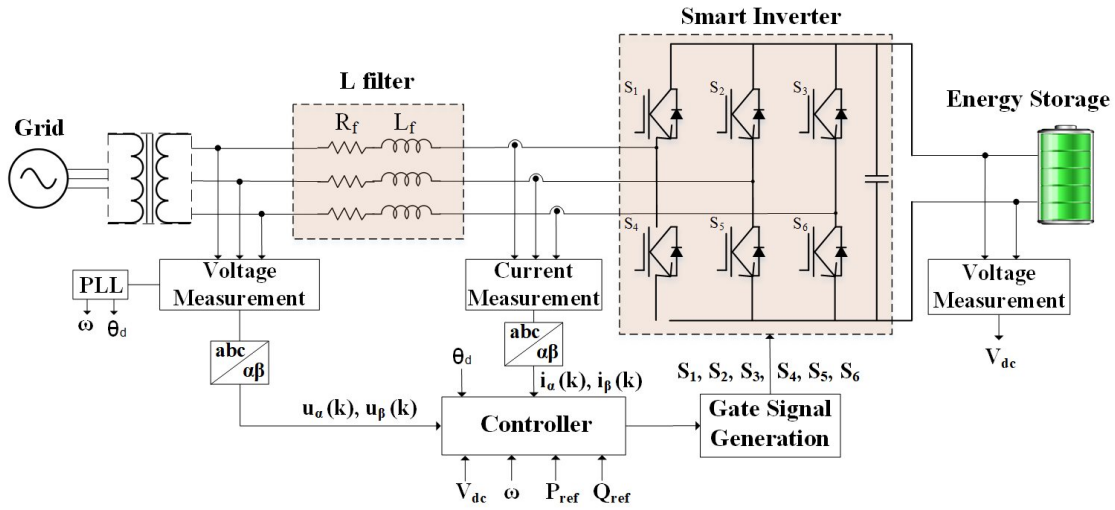

Figure 2.1: The system used for the study: the energy storage connected to the grid via a three-phase two-level voltage source converter and a L filter.

The are two basic functionalities expected from the controller. Firstly, the converter should inject or absorb, active and reactive power to/from the grid according to the grid requirements and dynamics. Secondly, the controller should maintain the permissible charge limits of the energy storage by feeding active power to the energy storage. Therefore, the instantaneous reference power (P_{ref} and Q_{ref}) is fed to the controller based on the magnitude of grid voltage, frequency fluctuations, smart inverter settings and the charge state of energy storage. The sign convention used in this work as the power flow from energy storage to the grid is positive, and

negative otherwise. The power flow is constrained by the maximum apparent power of the converter, S_r.

2.4 Conventional FCSMPC for a Grid-connected Converter

MPC is a model based control strategy and the system under study can be simply modeled by (2.1). Here, $u_{abc},\ e_{abc},\ i_{abc}$ are three-phase grid-end voltages, converter-end voltages and grid currents respectively. R_f and L_f are the filter damping resistance and the filter inductance.

$$e_{abc} = R_f i_{abc} + L_f \frac{di_{abc}}{dt} + u_{abc} \tag{2.1}$$

The time-varying nature of sinusoidal voltage-current components complicates the implementation of control algorithm. To reduce this complexity, the voltage and current measurements are converted to stationary reference frame using Clarke transformation ($abc\,to\,\alpha-\beta$). The $\alpha-\beta$ transformed system model can be expressed as eq. (2.2).

$$e_{\alpha\beta} = R_f i_{\alpha\beta} + L_f \frac{di_{\alpha\beta}}{dt} + u_{\alpha\beta} \tag{2.2}$$

To apply FS-MPC, the system equations are converted to discrete time domain using forward Euler transformation. The discrete state space representation of the system [58] is given in eq. (3.2)

$$X(k+1) = AX(k) + BU(k) + M \tag{2.3}$$

where,

$$X = [i_\alpha, i_\beta]^T, U = [e_\alpha, e_\beta]^T, A = \begin{bmatrix} \left(1 - \frac{T_s R_f}{L_f}\right) & 0 \\ 0 & \left(1 - \frac{T_s R_f}{L_f}\right) \end{bmatrix}$$

$B = \begin{bmatrix} \frac{T_s}{L_f} & \frac{T_s}{L_f} \end{bmatrix}, M = \begin{bmatrix} \frac{-T_s u_\alpha}{L_f} & \frac{-T_s u_\beta}{L_f} \end{bmatrix}, T_s$is the sampling time.

According to instantaneous power theory, active and reactive power at the point of common coupling (PCC) is $P = \frac{3}{2}(u_\alpha i_\alpha + u_\beta i_\beta)$ and $Q = \frac{3}{2}(u_\beta i_\alpha - u_\alpha i_\beta)$ respectively. The grid voltages can be approximated as $u_\alpha(k+1) = u_\alpha(k), \;\; u_\beta(k+1) = u_\beta(k)$, since the sampling frequency is relatively much higher compared to the grid frequency. Therefore, the active and reactive power for the next state can be simplified as expressed in eq. (3.3).

$$\begin{aligned} P(k+1) &= 1.5(u_\alpha(k) i_\alpha(k+1) + u_\beta(k) i_\beta(k+1)) \\ Q(k+1) &= 1.5(u_\beta(k) i_\alpha(k+1) - u_\alpha(k) i_\beta(k+1)) \end{aligned} \tag{2.4}$$

Then, by substituting eq. (3.2) in to eq. (3.3), the predictive model for system is derived and is as expressed in eq. (3.6). In this model, the prediction horizon is extended to two in order to compensate the delay in the actual digital control.

$$\begin{aligned} \begin{bmatrix} P(k+2) \\ Q(k+2) \end{bmatrix} = & \begin{bmatrix} \left(1 - \frac{T_s R_f}{L_f}\right) & -T_s\omega \\ T_s\omega & \left(1 - \frac{T_s R_f}{L_f}\right) \end{bmatrix} \begin{bmatrix} P(k+1) \\ Q(k+1) \end{bmatrix} \\ & + \frac{3T_s}{2L_f} \begin{bmatrix} |\vec{u_{\alpha\beta}}|^2 - Re(\vec{u_{\alpha\beta}} \vec{e_{\alpha\beta}}^*) \\ -Im(\vec{u_{\alpha\beta}} \vec{e_{\alpha\beta}}^*) \end{bmatrix} \end{aligned} \tag{2.5}$$

In FS-MPDPC a finite set of converter voltage vectors are considered to predict the next state power using the eq. (3.6). Without any modulation technique in use, the converter AC side voltages correspond to the possible switching states which is eight in number for a three-phase two-level converter. The eight switch states generate seven unique voltage vectors as given in eq. (2.6) in which n is the

switching state and V_{DC} is the DC link voltage.

$$e_n = \begin{cases} \frac{2}{3} V_{dc} e^{jn\frac{\pi}{3}} & n = 1, 2, ..., 6 \\ 0 & n = 0, 7 \end{cases} \tag{2.6}$$

2.4.1 Objective Function Formulation and Optimization

The active power reference (P_{ref}) and reactive power reference (Q_{ref}) values are provided to the control system as mentioned in section 2.3. The objective function given in eq. (2.7) consists of two conditions and a constraint. The two conditions are designed with quadratic norm to minimize the power error. λ_1 and λ_2 are the weights of each component in the objective function. The maximum apparent power limitation of the converter is applied as a constraint.

$$\begin{aligned} Min : \{J(k+2) = \lambda_1 (P(k+2) - P_{ref})^2 + \\ \lambda_2 (Q(k+2) - Q_{ref})^2 \} \end{aligned}$$

$$Subjected \;\; to : P(k+2)^2 + Q(k+2)^2 < S_r^2 \tag{2.7}$$

The objective function is solved for all predicted power values that corresponds to candidate voltage vectors of the converter. Then the voltage vector that generates the minimum cost is selected as the input for the next state operation.

2.5 Virtual Vector Synthesis and Proposed Low Complexity FCS-MPDPC Algorithm

As discussed extensively in section 2.2, the use of a finite voltage set as the control input in FS-MPC can degrade the performance, leading to a more discrete and

variable output with lot of ripples in the current and power waveforms. A near-continuous flow can be obtained by increasing the number of elements in the voltage set. Therefore, to address this issue an extended voltage vector set can be used with virtual vector synthesis. This concept was proposed in [59] which uses 37 distinct voltage vectors that are uniformly distributed in the vector space.

In this work, the converter voltage vector space (CVVS) is divided creating three concentric hexagons on which 37 voltage vectors are placed in equidistant. Among them, 7 are the real switch voltages of a three phase two level converter and the rest are virtual voltages. The same vector distribution in the CVVS is considered in this work and it is given in Fig. 2.2 (a) in which green square markers indicate the real switch states. The virtual vectors (VV) are synthesized using DSVM technique in which VVs are formulated as vector summations of real voltages. The three elements of a switch state represent the turn-on ratio of the switches of three phases. For example,

$$Z\ Z\ 0 \Longrightarrow ZT_s * V_1 + ZT_s * V_3 + 0T_s * V_5 + ZT_s * V_7$$

$$0\ 2Z\ Z \Longrightarrow 0T_s * V_1 + 2ZT_s * V_3 + ZT_s * V_5 + 0T_s * V_7$$

Here, the VV related to ZZ0 switch state is composed by applying V_1, V_3 and V_7 voltages for time periods of ZT_s each. The turned-on time of phase C switch is zero for this case and V_7 is the zero vector. The variable $Z = 1/3$ and T_s is the sampling period. The significance of the selected set is that the VV generation doesn't lead to a variable frequency switching and it increases to $3f_s$. The switching states and their relevant voltage vectors used in this analysis is given in the Table.2.1.

Table 2.1: Converter voltage vectors

Switching state			Voltage	Switching state			Voltage
0/1	0/1	0/1	0	Z	2Z	0	$\frac{2}{3\sqrt{3}}V_{dc}e^{\frac{\pi}{2}j}$
Z	0	0	$\frac{2}{9}V_{dc}e^{0j}$	Z	1	0	$\frac{2\sqrt{7}}{9}V_{dc}e^{\frac{4\pi}{9}j}$
2Z	0	0	$\frac{4}{9}V_{dc}e^{0j}$	2Z	1	0	$\frac{2\sqrt{7}}{9}V_{dc}e^{\frac{5\pi}{6}j}$
1	0	0	$\frac{2}{3}V_{dc}e^{0j}$	0	Z	0	$\frac{2}{9}V_{dc}e^{\frac{2\pi}{3}j}$
2Z	Z	0	$\frac{2}{3\sqrt{3}}V_{dc}e^{\frac{\pi}{6}j}$	0	2Z	0	$\frac{4}{9}V_{dc}e^{\frac{2\pi}{3}j}$
1	Z	0	$\frac{2\sqrt{7}}{9}V_{dc}e^{\frac{\pi}{9}j}$	0	1	0	$\frac{2}{3}V_{dc}e^{\frac{2\pi}{3}j}$
1	2Z	0	$\frac{2\sqrt{7}}{9}V_{dc}e^{\frac{2\pi}{9}j}$	0	2Z	Z	$\frac{2}{3\sqrt{3}}V_{dc}e^{\frac{5\pi}{6}j}$
Z	Z	0	$\frac{2}{9}V_{dc}e^{\frac{\pi}{3}j}$	0	1	Z	$\frac{2\sqrt{7}}{9}V_{dc}e^{\frac{7\pi}{9}j}$
2Z	2Z	0	$\frac{4}{9}V_{dc}e^{\frac{\pi}{3}j}$	0	1	2Z	$\frac{2\sqrt{7}}{9}V_{dc}e^{\frac{8\pi}{9}j}$
1	1	0	$\frac{2}{3}V_{dc}e^{\frac{\pi}{3}j}$	0	Z	Z	$\frac{2}{9}V_{dc}e^{\pi j}$
2Z	0	1	$\frac{2\sqrt{7}}{9}V_{dc}e^{\frac{-4\pi}{9}j}$	1	0	1	$\frac{2}{3}V_{dc}e^{\frac{-\pi}{3}j}$
Z	0	Z	$\frac{2}{9}V_{dc}e^{\frac{-\pi}{3}j}$	2Z	0	Z	$\frac{2}{3\sqrt{3}}V_{dc}e^{\frac{-\pi}{6}j}$
2Z	0	2Z	$\frac{4}{9}V_{dc}e^{\frac{-\pi}{3}j}$	1	0	Z	$\frac{2\sqrt{7}}{9}V_{dc}e^{\frac{-\pi}{9}j}$
0	2Z	2Z	$\frac{4}{9}V_{dc}e^{\pi j}$	0	0	2Z	$\frac{4}{9}V_{dc}e^{\frac{-2\pi}{3}j}$
0	1	1	$\frac{2}{3}V_{dc}e^{\pi j}$	0	0	1	$\frac{2}{3}V_{dc}e^{\frac{-2\pi}{3}j}$
0	Z	2Z	$\frac{2}{3\sqrt{3}}V_{dc}e^{\frac{-5\pi}{6}j}$	Z	0	2Z	$\frac{2}{3\sqrt{3}}V_{dc}e^{\frac{-3\pi}{2}j}$

Switching state			Voltage	Switching state			Voltage
0	Z	1	$\frac{2\sqrt{7}}{9}V_{dc}e^{\frac{-8\pi}{9}j}$	Z	0	1	$\frac{2\sqrt{7}}{9}V_{dc}e^{\frac{-5\pi}{9}j}$
0	2Z	1	$\frac{2\sqrt{7}}{9}V_{dc}e^{\frac{-7\pi}{9}j}$	1	0	2Z	$\frac{2\sqrt{7}}{9}V_{dc}e^{\frac{-2\pi}{9}j}$
0	0	Z	$\frac{2}{9}V_{dc}e^{\frac{-2\pi}{3}j}$				

2.5.1 Proposed Algorithm to Constrict the Optimal Vector Search

As mentioned earlier, a total of 37 voltage vectors are used as the finite vector set to solve the optimization problem. To reduce the number of computations required in each switch cycle, a simplification strategy for the vector search is proposed in this section.

The basis of DPC theory is utilized here to reduce the complexity involved in virtual vector integrated FS-MPDPC. The instantaneous active and reactive powers are the final deliverable that needs to be regulated by the grid connected converter for this case and they are analogous to the role of the torque and flux amplitude in direct torque control (DTC) of induction motor. Inspired by DTC applied to the induction motor in [60], an algorithm is developed to reduce the vector selection area from the virtual vector space.

In conventional DPC, offline switching tables are used to determine the inverter voltage vector to be applied based on the desired active and reactive power variations and the information of the grid voltage at PCC [61]. As stated by the DPC theory, each switching voltage vector of the converter in the CVVS has different influence on the change of instantaneous active-reactive powers and this influence varies with the angular position of the changing grid voltage, $V_{\alpha\beta}$ [62, 63]. There-

fore, optimal switching functions can be applied systematically based on power injection/absorption requirements under different angular positions of $V_{\alpha\beta}$.

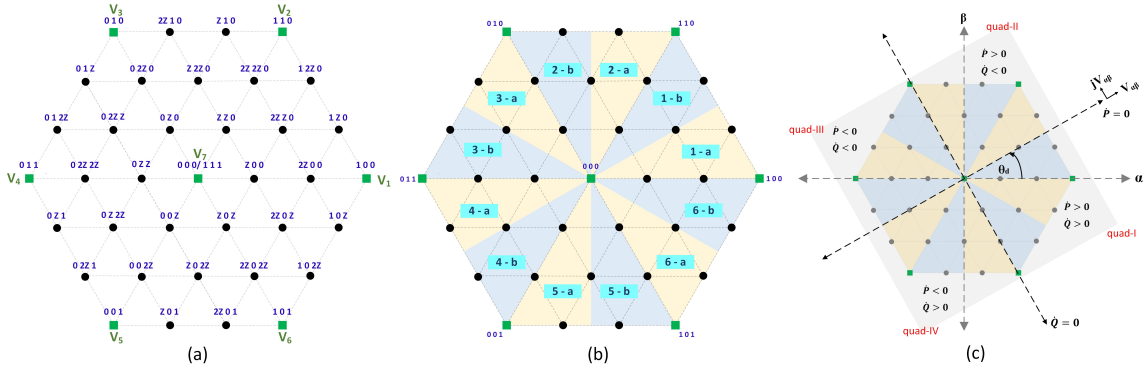

Figure 2.2: (a) Locus of the considered real and virtual switching vectors in CVVS, (b) Division of the CVVS into 12 sectors (1-a, 1-b, ...), (c) Approximated behavior of $\dot{P}$ and $\dot{Q}$ in the GVVS.

In this work the DPC concept is incorporated in developing the algorithm to simplify the vector search. As presented in [63], two perpendicular planes are defined on the CVVS which are aligned along the grid voltage vector, $V_{\alpha\beta}$ and $jV_{\alpha\beta}$. Hereinafter we refer these planes as grid voltage vector space (GVVS). The GVVS is shifted from $\alpha - \beta$ plane by the angular position θ_d which rotates in synchronous speed. The approximated behaviour of the instantaneous active power first derivative, $\dot{P}$ and the instantaneous reactive power first derivative, $\dot{Q}$ with respect to the planes are as given in the Fig. 2.2 (c) [64]. Therefore, the converter voltage vectors in each quadrant of the GVVS steer the active and reactive power in different directions as illustrated in the Fig. 2.2 (c). At some positions of θ_d, there are at most three real voltage vectors that provide the same behaviour of $\dot{P}$ and $\dot{Q}$. In this work a single real vector for each quadrant is selected following the modified Eloy-Garcia approach which provides a better tracking of both P and Q towards their references [64].

Table 2.2: Optimal switching table for converter when grid voltage vector at sector k

	$\dot{P}$	$\dot{Q}$	Converter voltage vector @ sector k-a	Converter voltage vector @ sector k-b
quad-I	>0	>0	e_k	e_k
quad-II	>0	<0	e_{k+1}	e_{k+1}
quad-III	<0	>0	e_{k-2}	e_{k-1}
quad-IV	<0	<0	e_{k+2}	e_{k+3}

The developed controller algorithm can be explained in three steps. The first step is obtaining the relevant real converter voltage vector, based on the position of $V_{\alpha\beta}$ in CVVS and the quadrant of operation in GVVS. In order to determine the quadrant of operation in the GVVS, $\dot{P}$ and $\dot{Q}$ are calculated as expressed in eq.(2.8).

$$\begin{aligned} &\dot{P} > 0 \rightarrow P(k) < P_{ref}, \quad \dot{P} < 0 \rightarrow P(k) > P_{ref} \\ &\dot{Q} > 0 \rightarrow Q(k) < Q_{ref}, \quad \dot{Q} < 0 \rightarrow Q(k) > Q_{ref} \end{aligned} \tag{2.8}$$

As GVVS rotates in synchronous speed, it is necessary to locate the quadrants in converter vector space at each control cycle to determine candidate voltage vector set. Therefore, the converter vector space is divided into 12 sectors, which combines the six main sectors each divided into two as shown in Figure. 2.2 (b) and the position of $V_{\alpha\beta}$ is determined with respect to the sectors. Then based on the sector of $V_{\alpha\beta}$ and the quadrant of operation in GVVS, the suitable real converter voltage vector is selected using Table. 2.2. For an example, if V_d is at sector 1-b and if both $\dot{P}$ and $\dot{Q}$ needs negative, the real voltage vector for converter is chosen as the voltage of '011' switch state which is $\frac{2}{3}V_{dc}e^{\pi j}$.

Then the candidate vector set connected to the obtained real voltage vector needs to be identified. Each real vector is neighboured by six virtual voltage vectors. The real vector, the six neighboring virtual vectors and the zero vector are chosen as

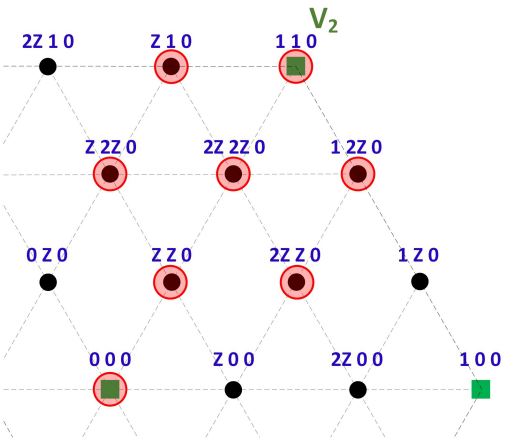

Figure 2.3: Selection of the candidate voltage vector set: the vector set connected to V_2 real vector.

the candidate vector set to solve the optimization problem. The selection of the vector set is illustrated in Figure.2.3 which circles-out the vector set related to '1 1 0' switch state. In this way the size of the candidate vector set is reduced from 37 to 8 for the optimization.

Finally, the process follows the conventional MPC technique explained in section 2.4 for the constricted candidate voltage vector set. The optimal voltage vector that minimizes the objective function is selected for the next state operation and duty ratios are calculated for that. The controller algorithm is completely illustrated in a block diagram in Figure. 2.4.

2.6 Results and Discussion

To analyze and validate the performance of the proposed control algorithm the system is modeled in MATLAB/Simulink. The system parameters used for modeling are given in Table 2.3. The system is designed with a L filter only, to highlight the performance comparisons of different controllers.

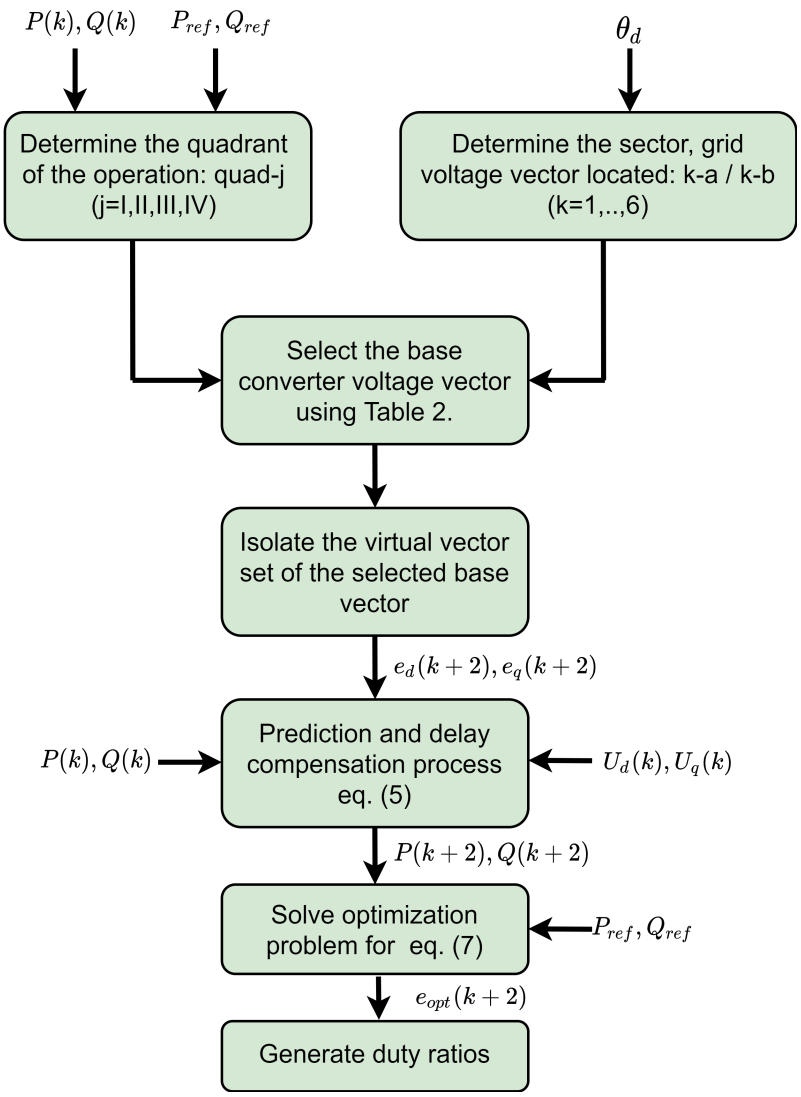

Figure 2.4: Block diagram of controller operation.

Table 2.3: Parameters used for Simulations

Parameters	Values
Converter rated power (S_r)	7.5 kVA
DC link voltage (V_{dc})	500 V
Filter resistance (R_f)	0.2 Ω
Filter inductance (L_f)	15 mH
Sampling time (T_s)	0.000002 s
Fundamental frequency	60 Hz
Grid voltage	120V
Weights λ_1, λ_2	1, 1

2.6.1 Steady-state Performance Analysis

Simulations were carried out under steady state conditions to compare the performance of the conventional FS-MPDPC, FS-MPDPC with extended voltage set and LC-FS-MPDPC with extended voltage set. Fig. 2.5 shows the grid voltage, line current and FFT analysis of line current for each method. It can be clearly observed that the conventional FS-MPDPC with the seven element vector set has a higher harmonic content compared to other two methods with extended voltage sets. The total harmonic distortion (THD) in line current has a striking reduction from 10.75% in conventional FS-MPDPC to 4.02% in FS-MPDPC with the extended voltage set (specially in 5^{th} and 7^{th} harmonics). However, the quality of line current has slightly reduced from Fig. 2.5 (b) to Fig. 2.5 (c). But, this slight increase in THD in the LC-FS-MPDPC is almost insignificant when considering the computational simplification achieved. Therefore, unlike the conventional FS-MPDPC, the proposed technique guarantees a better performance with a lower harmonic content.

To further analyze, in Fig. 2.6 the line current in stationary reference frame ($I_{\alpha\beta}$) is plotted for a steady-state conditions to highlight the performance improvement achieved by introducing virtual vectors to the candidate voltage set. Fig. 2.6 (a) shows the $I_{\alpha\beta}$ plot for the conventional FS-MPC while Fig. 2.6 (b) shows the $I_{\alpha\beta}$ plot using the the proposed controller. It can be seen that the line currents perform better using the the proposed controller.

A comparison of active and reactive power ripples for both conventional FS-MPDPC and LC-FS-MPDPC is simulated and shown in Fig.2.7. The standard deviation function is applied to calculate the active and reactive power ripples at two different reference points. The active and reactive power ripples are calculated at the two scenarios of $P_{ref} = 4000\ W$, $Q_{ref} = 3000\ var$ and $P_{ref} = 2000\ W$, $Q_{ref} = 1000\ var$. A quantitative analysis of ripple percentages are illustrated in

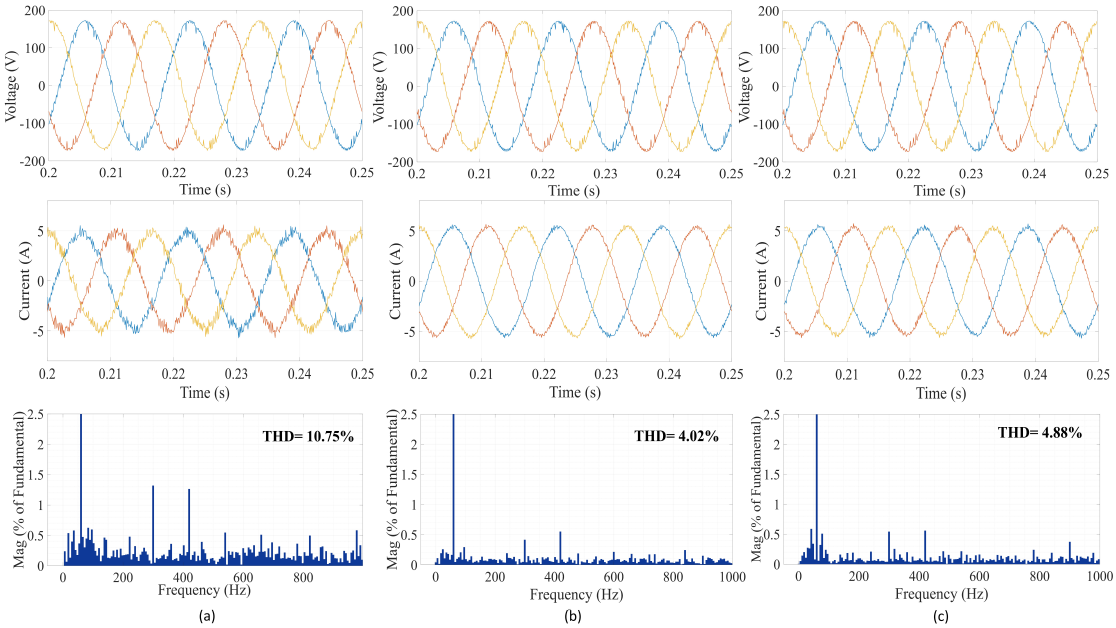

Figure 2.5: Steady state performance of grid voltage, line current and FFT analysis of line current for (a) conventional FS-MPDPC, (b) FS-MPDPC with extended voltage set, (c) LC-FS-MPDPC with extended voltage set.

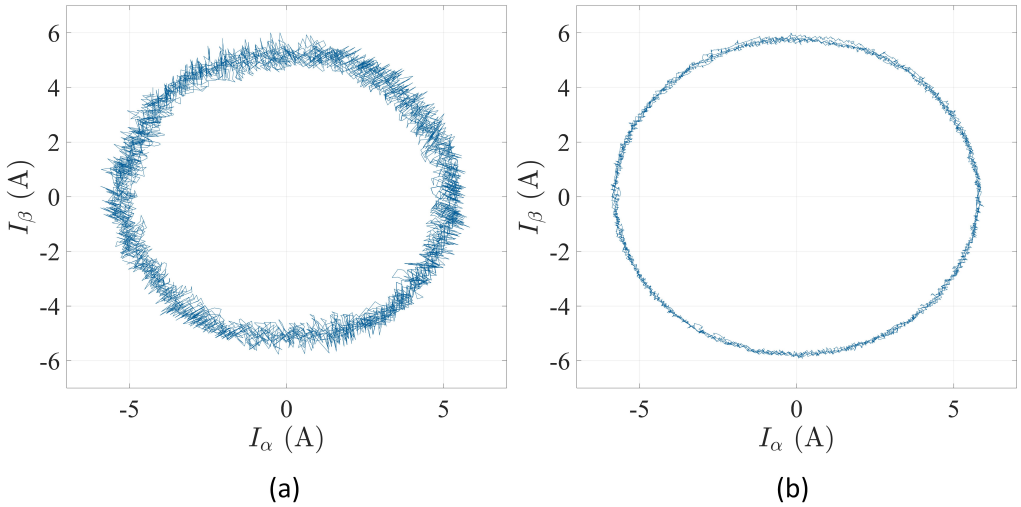

Figure 2.6: Plot of $I_{\alpha\beta}$ at steady-state for (a) conventional FS-MPDPC, (b) LC-FS-MPDPC with extended voltage set.

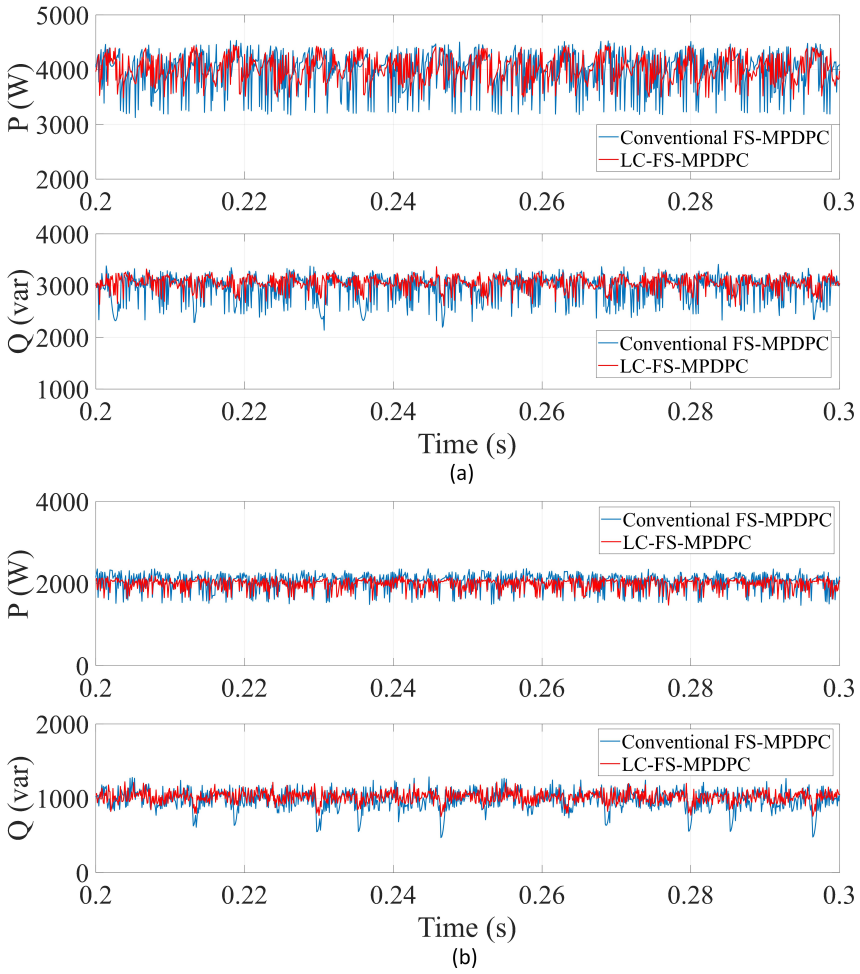

Figure 2.7: Active power and reactive power wave forms for conventional FS-MPDPC and LC-FS-MPDPC with extended voltage set at (a) $P_{ref} = 4000\ W$, $Q_{ref} = 3000\ var$, (b) $P_{ref} = 2000\ W$, $Q_{ref} = 1000\ var$.

Fig. 2.8. The ripple percentages are significantly for LC-FS-MPDPC compared to the conventional FS-MPDPC in all scenarios. Also, from the figure it is evident that the percentage ripple reduction is higher at the light power reference point ($P_{ref} = 2000\ W$, $Q_{ref} = 1000\ var$). This validates that the VV implementation improves the power performance in a wider range.

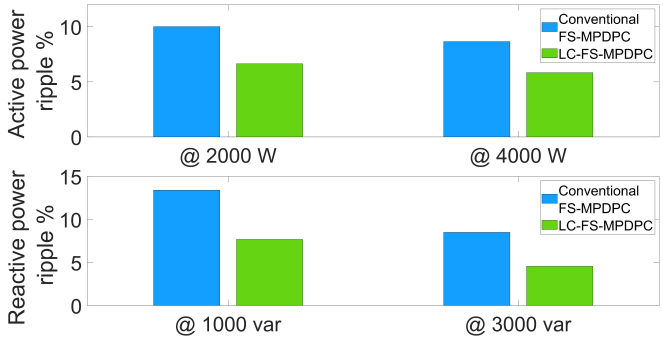

Figure 2.8: Comparisons of the active and reactive power ripples for conventional FS-MPDPC and LC-FS-MPDPC with extended voltage set.

2.6.2 Transient Performance Analysis

To further validate the performance of the LC-FS-MPDPC, simulations are carried out for several transient situations. In the first case, P_{ref} and Q_{ref} are varied so that the active power and reactive power linearly vary with time. Four scenarios were simulated to demonstrate the operation in all four quadrants of GVVS. The controller perfectly tracks the linear variations of the power references as depicted in Fig. 2.9. The figure provides the performance in all four quadrants, quad-I: $\dot{P}$ ¿ 0, $\dot{Q}$ ¿ 0, quad-II: $\dot{P}$ ¿ 0, $\dot{Q}$ ¡ 0, quad-III: $\dot{P}$ ¡ 0, $\dot{Q}$ ¡ 0 and quad-IV: $\dot{P}$ ¡ 0, $\dot{Q}$ ¿ 0 in Fig. 2.9 (a), (b), (c) and (d) respectively. The line current behaviour is also shown for each condition.

The second transient simulation was to test the capability of controlling bidirectional power flow. A grid connected converter operates in four power flow modes; capacitive-power source (P¿0, Q¿0), capacitive-load (P¡0, Q¿0), inductive-power source (P¿0, Q¡0) and inductive-load (P¡0, Q¡0). Active power and reactive power commands were varied to test the transition performance between two power modes. In Fig. 2.10, a smooth transition between capacitive-power and capacitive-load modes can be observed and the transition time is around 0.8 mS for both active

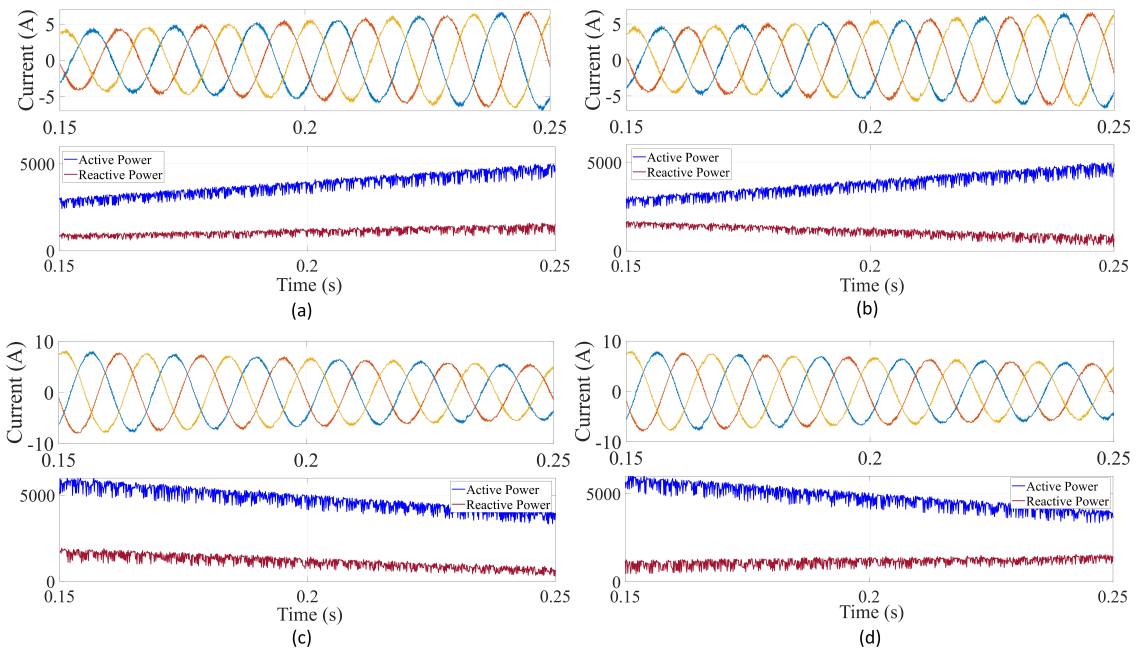

Figure 2.9: Transient performance: grid current, active power and reactive power for (a) quad-I ($\dot{P} > 0$, $\dot{Q} > 0$) operation, (b) quad-II ($\dot{P} > 0$, $\dot{Q} < 0$) operation, (c) quad-III ($\dot{P} < 0$, $\dot{Q} < 0$) operation, (d) quad-IV ($\dot{P} < 0$, $\dot{Q} > 0$) operation.

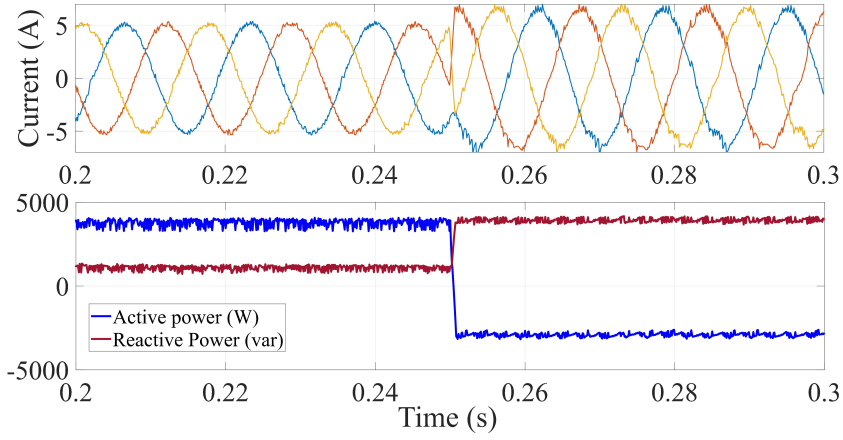

Figure 2.10: Transient performance: transition between capacitive-power source and capacitive-load modes.

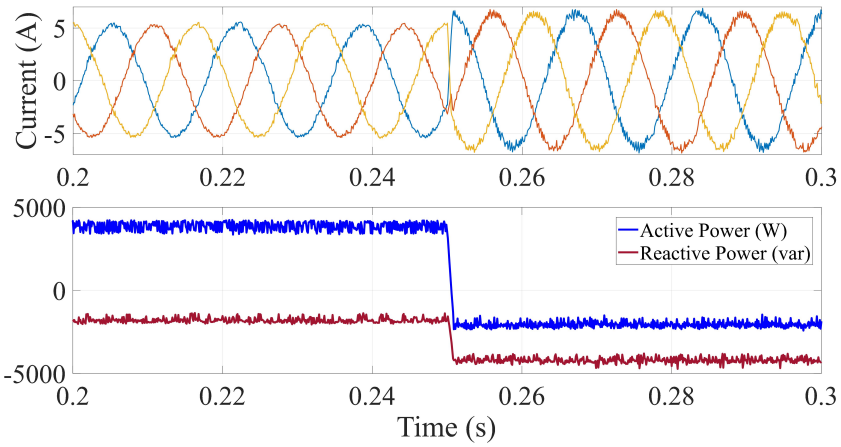

Figure 2.11: Transient performance: transition between inductive-power source and inductive-load modes.

and reactive power. A fast and accurate convergence to the commanded power values are observed for inductive-power source and inductive-load modes as well which is shown in Fig.2.11. After the transient condition, a good steady-state operation is observed in all the four power modes and the ripples in both active power and reactive power are within the acceptable range.

2.6.3 Computational Complexity Comparisons

One of the main objectives of this work is to propose a technique that reduces the hardware execution time by simplifying the optimal vector search of the controller. FS-MPDPC has several processing steps which include, P-Q predictions, delay compensations and optimization of the objective function. Each of this step involves a certain number of computations which includes multiplications and additions. When quantifying the number of computations, it directly depend on the number of candidate voltage vectors. The number of computations involved in these steps for conventional FS-MPDPC, FS-MPDPC with extended voltage set and LC-FS-MPDPC with extended voltage set are quantified and shown in Table.2.4. Other

Table 2.4: A comparison on number of computations.

Technique	Number of Additions	Number of Multiplications	Total Computations
Conventional FS-MPDPC	101	118	219
FS-MPDPC with extended voltage set	491	538	1029
LC-FS-MPDPC with extended voltage set	118	139	257

Table 2.5: A comparison on timing performance.

Technique	Execution time (μs)
Conventional FS-MPDPC	30
FS-MPDPC with extended voltage set	68
LC-FS-MPDPC with extended voltage set	36

than aforementioned processing steps, the proposed technique involves additional computations for the constriction algorithm which are added to the total given in the Table.2.4.

A striking reduction in computations can be observed due to the constriction algorithm which is almost a reduction of 70 %. The computations are a little high in the LC-FS-MPDPC compared to the conventional FS-MPDPC method. However, when consider in-terms of the improvement in performance attained due to virtual vectors which is indicated in Fig.2.5, this increment in computations can be deemed negligible.

The execution time of an algorithm is another measure of efficiency, but it depends on implementation details such as hardware and software configuration, parallel processors etc. of the computer. Since this is a comparison between three algorithms, simulations are done in the same processor platform under similar conditions to avoid the dependence to the platform. Therefore, the minimum execution time out of 100 executions has been reported here as it provides the closest approximate execution time for the algorithm with minimal overhead time. The timing performance of the proposed algorithm and the conventional schemes are given in Table 2.5.

Four state-of-the-art techniques to reduce the computational complexity that were discussed in the Section 2.2 are comparatively analyzed in Table. 2.6. One publication from each of the technique is considered here. It is quite difficult to execute a comprehensive performance comparison between the considered publications because their results were generated under dissimilar conditions and settings. Therefore, a general comparison based on certain features are considered for the evaluation.

2.7 Conclusion

This work proposes a complexity reduction technique to reduce the computational load involved in FCS-MPC with extended voltage vector set. The controller is designed for bidirectional active-reactive power flow control of a converter that interlinks an energy storage system with the grid. The algorithm is developed inspired by the DPC theory in which predetermined switching combinations are used for power flow control based on the desired active and reactive power variations and

Table 2.6: Comparison between the existing and proposed schemes.

	Deadbeat FS-MPC [49]	EMP-SMC [51]	Two-stage optimization [52]	Duty-cycle control [55]	LC-FS-MPDPC
Park transformation	Not required	Required	Required	Not required	Not required
PLL	Not required	Required	Required	Not required	Required
Switching frequency	Constant	Constant	Constant	Variable	Constant
Robustness for parameter variations	Low	High	High	High	High

the instantaneous angular position of grid voltage. This constriction algorithm has reduced the size of the candidate voltage vector set for optimization from 37 to 8.

The effectiveness of the controller is evaluated both under steady-state and transient conditions. The harmonic analysis of line current at steady-state exhibits a huge improvement in the proposed controller compared to the conventional FC-MPDPC in which the THD has reduced from 9.7% to 3.89%. Further, the number of computations is significantly reduced from 1029 in FC-MPDPC with extended voltage set to 257 after apply the proposed algorithm. The controller performance in all power flow stages is analyzed and smooth transitions between different power stages is observed. The system is also tested for operation in all four quadrants of GVVS. The obtained results verify that the proposed controller provides almost similar performance of extended voltage set FC-MPDPC but requiring lesser computations.

CHAPTER 3

FUZZY DECISION MAKING ASSISTED MODEL PREDICTIVE DIRECT POWER CONTROLLER FOR A GRID-INTERLINKING CONVERTER OF A BATTERY ENERGY STORAGE SYSTEM

3.1 Overview

Consensus controllers combines the benifits of each individual control technique, therefore much suitable for performance improvement of complex systems. MPC make control predictions based on the mathematical model of the system while FLC/ FDM applies the qualitative understanding of the plant emulating the human thinking patterns and the logic. In this chapter, the concept of FDM assisted MPC is discussed and then is applied for a grid connected BESS to facilitate it's complex functionalities. Then the constructed system is validated in Matlab Simulink environment.

3.2 Literature Review

Fuzzy-MPC consensus control integrates conventional MPC with FDM to apply for dynamic and complex control systems [65, 66]. Fuzzy-MPC controllers can be used for systems with non-linerar models [67] or can be used to design the objective function of MPC with multi criteria FDM [68]. The authors of [69] propose a fuzzy based duty cycle modulation technique for improved model predictive direct power control (MPDPC). In some systems it requires to have individual control over the components of objective function, so that the degree of impact can change dynamically based on human knowledge backed by experience. This additional flexibility can be obtained by applying fuzzy goals and fuzzy constraints as proposed

in [70, 71]. The concept of fuzzy goal / constraint integrated objective function is illustrated in Fig. 3.1.

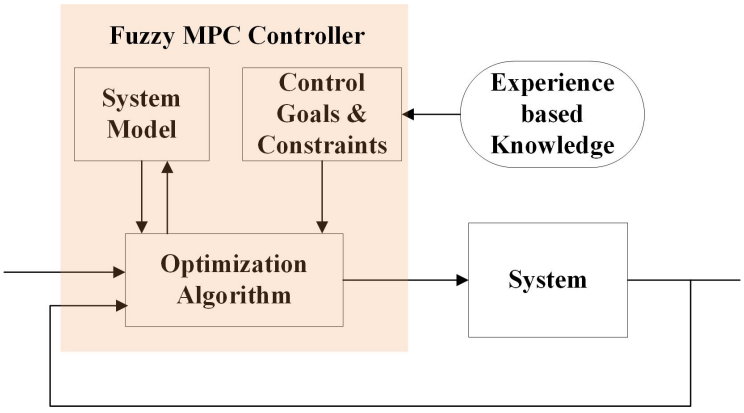

Figure 3.1: Fuzzy logic based decision making in MPC.

For the SI in BESS integration, facilitating grid-support mode with frequency and voltage control is not sufficient. The controller should switch to charging mode when the state of charge (SOC) level of the battery goes below a predefined threshold. Dynamic active and reactive power allocation between the grid and BESS is determined based on human knowledge based guidelines. Since this operation has a complex, fuzzy behaviour, FLC is ideal for battery dispatch scheduling [72,73]. But, none of the approaches used fuzzy-MPC integrated into converter level automatic operation for different grid and storage conditions.

The key contribution of this study is the introduction of the concept of FDM based MPC for control of grid connected converters and investigation of it's viability in automatic control of SI to manage bidirectional power flow of a BESS according to dynamic system conditions. A fuzzy-MPDPC framework is proposed and the operability is analytically proved in MATLAB Simulink environment.

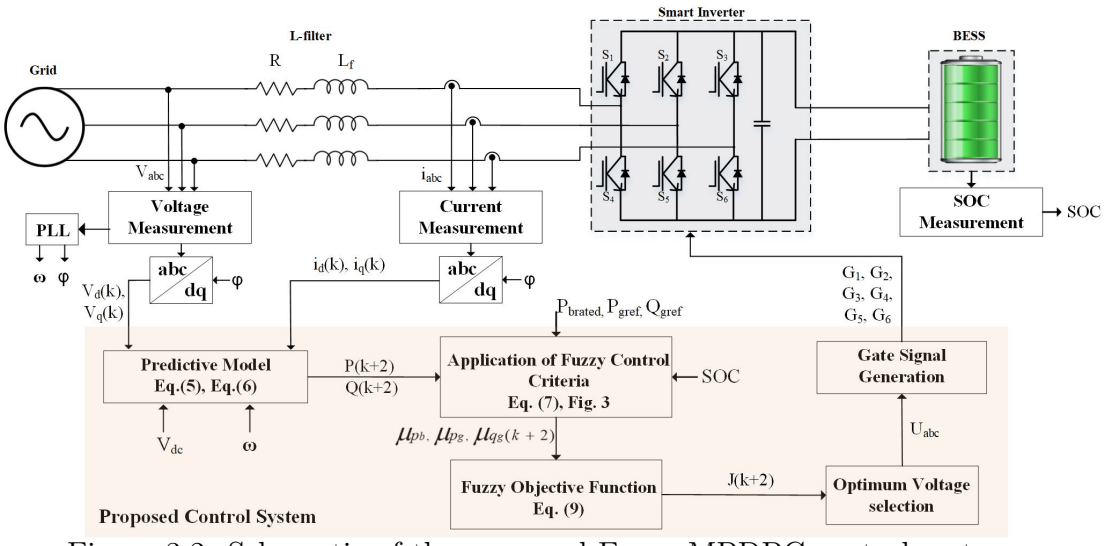

Figure 3.2: Schematic of the proposed Fuzzy-MPDPC control system.

3.3 Proposed Fuzzy-MPDPC Controller

3.3.1 Design of MPDPC

The system under study is shown in the Fig.3.2 which consists of a BESS connected to the grid through a three-phase VSC and a L-type filter. In the figure, V_{abc}, i_{abc} and U_{abc} correspond to phase voltages, phase currents and converter-end voltages, respectively. Also, L_f and R represent filter inductance and the equivalent system resistance. The converter voltage is controlled by seven voltage vectors, $U_n = \begin{cases} \frac{2}{3}V_{dc}e^{jn\frac{\pi}{3}} & n = 1, 2, ..., 6 \\ U_0 & n = 0, 7 \end{cases}$ where V_{dc} is the DC link voltage.

The system voltage equations are converted to synchronous reference frame (3.1) using power invariant Clarke and Park transformations to avoid the complications in control. Here, U_{dq}, V_{dq} and i_{dq} are d-q components of converter-end voltage, grid voltage and grid current in synchronous reference frame respectively.

$$U_{dq} = V_{dq} + Ri_{dq} + L_f \frac{di_{dq}}{dt} \tag{3.1}$$

The system equation (3.1) requires to be in discrete domain for digital implementation of MPC. Therefore, differential equations are converted to difference equations

using forward Euler transformation. The discrete state space representation of the system is given in (3.2) where state variable $x = [i_d, i_q]^T$, input $u = [V_d, V_q]^T$, state matrix $A = \begin{bmatrix} \left(1 - \frac{T_s R}{L_f}\right) & T_s\omega \\ -T_s\omega & \left(1 - \frac{T_s R}{L_f}\right) \end{bmatrix}$, input matrix $B = \begin{bmatrix} -\frac{1}{L_f} & -\frac{1}{L_f} \end{bmatrix}$ and $M = \begin{bmatrix} \frac{U_d}{L_f} & \frac{U_q}{L_f} \end{bmatrix}$.

$$x(k+1) = Ax(k) + Bu(k) + M \tag{3.2}$$

According to the instantaneous power theory, active power P and reactive power Q of $(k+1)^{th}$ state at PCC can be determined by (3.3).

$$\begin{aligned} P(k+1) &= 1.5(V_d(k+1)i_d(k+1) + V_q(k+1)i_q(k+1)) \\ Q(k+1) &= 1.5(V_q(k+1)i_d(k+1) - V_d(k+1)i_q(k+1)) \end{aligned} \tag{3.3}$$

Since the sampling frequency is much higher than the grid frequency, it is approximated that the change in grid voltages is negligible: $V_d(k+1) = V_d(k)$, $V_q(k+1) = V_q(k)$. Active and reactive powers are further reduced to (3.4) since V_d is set on the d-axis of d-q reference frame in phase-locked technology.

$$\begin{aligned} P(k+1) &= 1.5(V_d(k)i_d(k+1)) \\ Q(k+1) &= -1.5(V_d(k)i_q(k+1)) \end{aligned} \tag{3.4}$$

Subsequently, (3.5) can be derived from (3.3) and (3.4).

$$\begin{bmatrix} P(k+1) \\ Q(k+1) \end{bmatrix} = \begin{bmatrix} \left(1 - \frac{T_s r}{L_f}\right) & -T_s\omega \\ T_s\omega & \left(1 - \frac{T_s r}{L_f}\right) \end{bmatrix} \begin{bmatrix} P(k) \\ Q(k) \end{bmatrix} + \frac{T_s}{L_f} \begin{bmatrix} U_d(k+1).V_d(k) - V_d^2(k) \\ -U_q(k+1).V_d(k) \end{bmatrix} \tag{3.5}$$

To compensate the delay in an actual digital implementation of control, the prediction horizon is extended to two and modified model for $(k+2)^{th}$ state is given

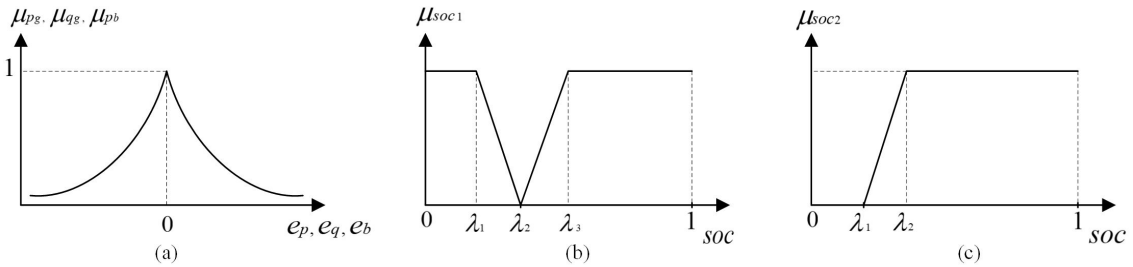

Figure 3.3: Membership functions for (a) active, reactive power errors at PCC and BESS, (b) SOC constraint for active power (c) SOC constraint for reactive power.

in (3.6).

$$\begin{bmatrix} P(k+2) \\ Q(k+2) \end{bmatrix} = \begin{bmatrix} \left(1 - \frac{T_s r}{L_f}\right) & -T_s\omega \\ T_s\omega & \left(1 - \frac{T_s r}{L_f}\right) \end{bmatrix} \begin{bmatrix} P(k+1) \\ Q(k+1) \end{bmatrix} + \frac{T_s}{L_f} \begin{bmatrix} U_d(k+2).V_d(k+1) - V_d^2(k+1) \\ -U_q(k+2).V_d(k+1) \end{bmatrix} \tag{3.6}$$

The active and reactive power values are predicted for seven converter voltage vectors mentioned before using (3.6) and the switching state relevant to the voltage vector that results the minimum cost for a predefined objective function is chosen to apply to the converter in next control cycle. The conventional objective function is generally a quadratic function when L-2 norm applied and there are weights assigned to each goal and constraint for control errors and control actions respectively. But, in this work a fuzzy based Objective function is designed as given in section 3.3.2 for which doesn't require to tune weight parameters to get the appropriate output since the use of membership functions introduce direct normalization.

3.3.2 Fuzzy Control Criteria for MPDPC

The significance of fuzzy control is it can integrate the notions of human perception into control criteria through a set of rules. Normally, this set of rules is specified by an operator or a design engineer who's familiar with the system.

The controller of SI manages the active, reactive power inflow, outflow appropriately according to the system conditions. The power flow conditions for BESS integration is quite complicated as it depends on several factors. As discussed in Section 3.1, to address grid conditions at PCC such as power deficits, voltage fluctuations etc. active and reactive power outflows from the BESS respectively. But, in case of lower SOC levels of the battery, the active power outflow from BESS should stop immediately and start recharging the battery regardless of the grid power requirements.

The control criteria defined for the fuzzy-DPMPC is as follows. A proper power control is required to get the maximum benefits out of expensive BESS and also to have a longer life expectancy. Therefore, a minimum SOC threshold λ_1 is defined for the discharge of battery. Battery starts to charge when level of SOC reaches λ_2 and it is possible to discharge reactive power till the level reaches λ_1. Above SOC level of λ_3 the battery can freely serve for grid conditions. Membership functions are designed to satisfy these design criteria and acceptable SOC range for the operation of the BESS is defined in this work as hard constraints as given in Fig. 3.3 (b), (c).

Lets consider $P_{g_{ref}}$ and $Q_{g_{ref}}$ as the active and reactive power outflow requirements at the PCC and $P_{b_{rated}}$ is the rated power of the battery. These requirements are constrained by SOC level of the battery. The error functions are defined as eq.(3.7).

$$\begin{aligned} e_p(k+2) &= (P(k+2) - P_{g_{ref}} * \mu_{soc1}) \\ e_q(k+2) &= (Q(k+2) - Q_{g_{ref}} * \mu_{soc2}) \\ e_b(k+2) &= (P(k+2) - P_{b_{rated}} * \mu_{soc1}) \end{aligned} \tag{3.7}$$

Here, e_p, e_q, e_b are the error values of active, reactive and battery power respectively. And their relevant membership functions, μ_{p_g}, μ_{q_g} and μ_{p_b} are represented

in exponential form as given in Eq. 3.8. K_p, K_q and K_b are the normalization factors used to tune the μ variation with respect to the errors of active, reactive and battery power. The exponential form is chosen to provide an increased effect on objective function when the error is small. All these fuzzy criterion and the parameter settings should defined by the design engineer based on system characteristics and performance requirements. Some of the parameters to consider are SOC threshold of the battery, ramp rate thresholds of battery and the inverter. Integration of aforementioned fuzzy control rules to the objective function is explained in the section. 3.3.3.

$$\mu_{p_g,\ q_g,\ p_b} = \begin{cases} exp(\frac{e_{p,q,b}(k+2)}{K_{p,q,b}}) & -\infty < e(k+2) < 0 \\ exp(-\frac{e_{p,q,b}(k+2)}{K_{p,q,b}}) & 0 \leq e(k+2) < \infty \end{cases} \tag{3.8}$$

3.3.3 Integration of Fuzzy Criteria into the Objective Function

In a state space system, fuzzy goals and constraints can be defined to manage state variables and control actions. Let $G_i : i = 1, .., n$ be the control goals and $C_j : j = 1, ..m$ fuzzy constraints for a given system. According to fuzzy control theory, G_i and C_j can be mapped to a space with an interval [0,1] using membership functions μ_{G_i} and μ_{C_j}. The membership functions of goals and constraints have to be aggregated appropriately for the whole control sequence π as given in (3.9) [70, 71]. Here, N_p is the prediction horizon and $\odot_A$ is a general representation of the aggregation operator. Aggregation operators are defined for each goals, constraints appropriate to the problem.

$$
\begin{aligned}
J =&(\mu_{G_{11}} \odot_A ... \odot_A \mu_{G_{1n}}) \odot_A (\mu_{C_{11}} \odot_A ... \odot_A \mu_{C_{1m}}) \odot_A \\
&... \\
&(\mu_{G_{N_p1}} \odot_A ... \odot_A \mu_{G_{N_pn}}) \odot_A (\mu_{C_{N_p1}} \odot_A ... \odot_A \mu_{C_{N_pm}})
\end{aligned} \tag{3.9}
$$

Since J represents the complete decision criteria, maximization of it provides the fuzzy based objective function. With the capability of applying various aggregation operators, this technique has provided a high flexibility in designing the objective function. Assimilating the same concept, the objective function for the VSC control for integration of BESS is designed based on the fuzzy goals and constraints in section. 3.3.2 and is given in Eq. 3.10.

$$
\begin{aligned}
Max :\{&J(k+2) = \mu_{p_b}(e_b(k+2)) + \\
&\mu_{p_g}(e_p(k+2)) + \mu_{q_g}(e_q(k+2))\}
\end{aligned} \tag{3.10}
$$

Aggregation operators are selected appropriately; the sum operator is applied between each goal.

3.4 Analytical Validation

In-order to validate and analyze the performance of the proposed controller the system given in 3.2 is modeled in MATLAB / Simulink environment. The system parameters used for modeling are given in Table 3.1. The normalization factors, K_p, K_q and K_b were determined empirically based on typical error variations. The SOC thresholds, λ_1, λ_2 and λ_3 which originally should be determined based on

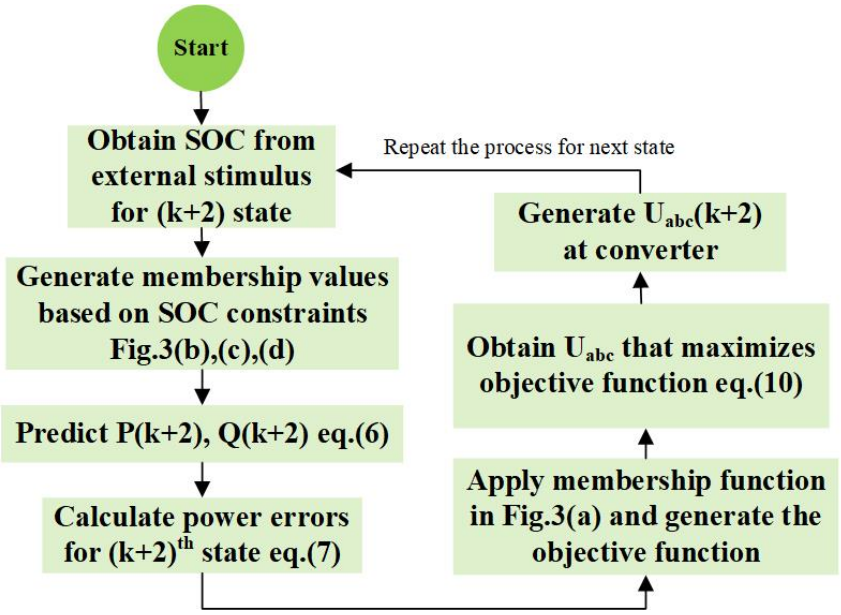

Figure 3.4: Flowchart of the validation procedure.

Table 3.1: Parameters used for Simulations

Parameters	Values
Inverter rated power	1.5 kVA
DC link voltage	185 V
Phase voltage	120 V
Equivalent resistance (R)	0.0019 Ω
Filter inductance	0.25 mH
Normalization factors (K_p, K_q, K_b)	1, 2, 1
SOC thresholds ($\lambda_1, \lambda_2, \lambda_3$)	0.2, 0.3, 0.5
Sampling time (T_s)	0.000002 s

actual system requirements were selected randomly here for the controller validation purpose. The simulation procedure is illustrated in Fig. 3.4 as a flowchart.

Since the change of the SOC level in batteries is very small relative to the simulation time, it was emulated by providing an external stimulus for the controller. In the stimulus the level of SOC was varied from 100% to 0% during the simulation time and tested the controller performance for all possible scenarios. The applied external stimulus and the change of μ_{soc1} and μ_{soc2} during the simulation is shown in Fig.3.5.

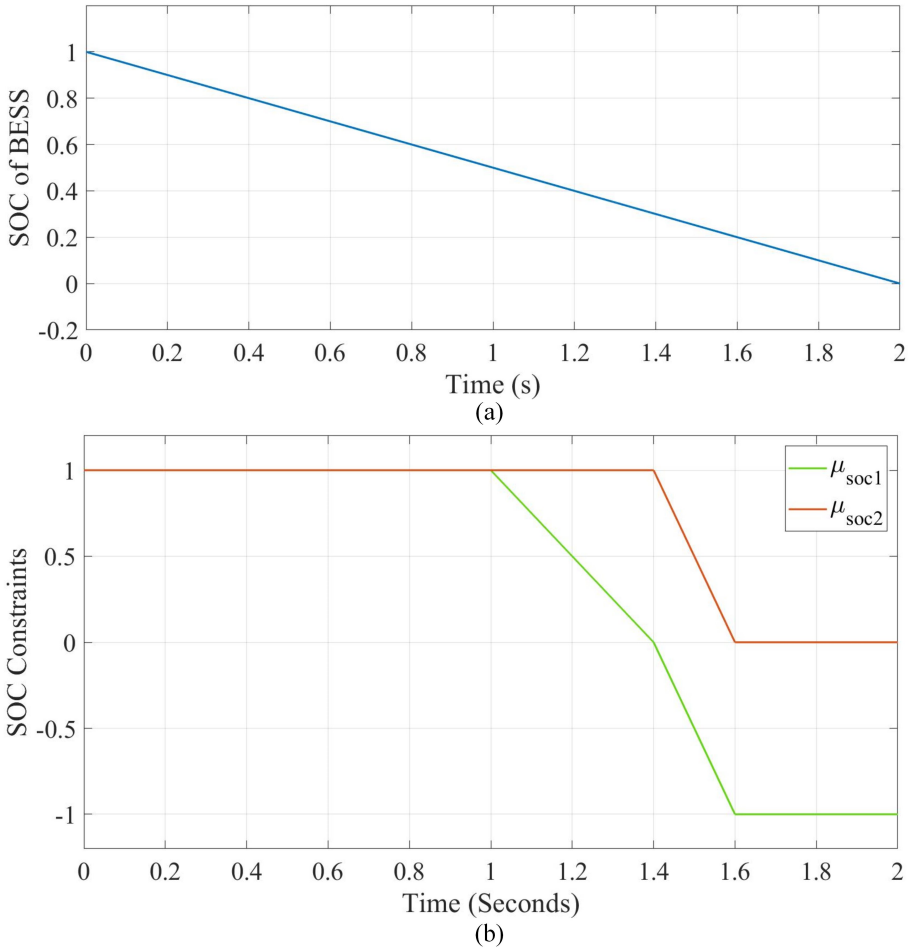

Figure 3.5: (a) External stimulus used in the simulation to emulates the SOC level, (b) Change of μ_{soc1} and μ_{soc2} with change of SOC level during simulation.

To analyze the steady state performance of the controller, Initially, $P_{g_{ref}}$ and $Q_{g_{ref}}$ were set to 60 kW and 40 kW respectively. And the rated battery power, $P_{b_{ref}}$ was set to 50 kW. With the change of SOC level, the provided power references are constrained according to membership functions and these variations are illustrated in Fig.3.6. Therefore, actual power references get limited by the SOC of battery before fed to the MPC.

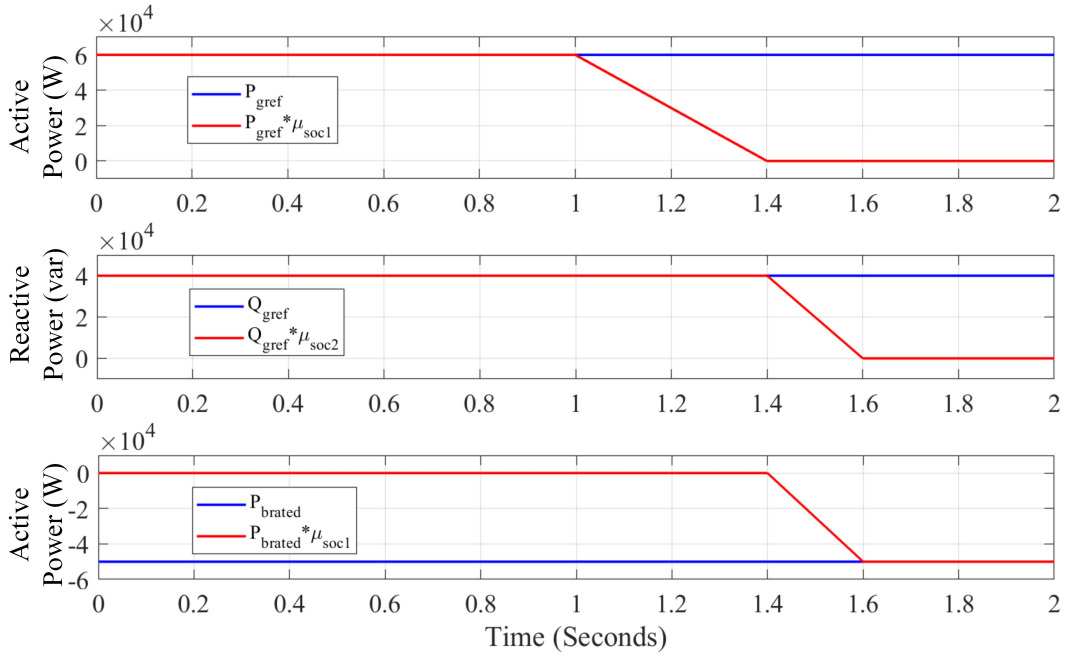

Figure 3.6: Power requirements and power references to MPC constrained by SOC limitations.

The change of active power flow from the inverter over the time is illustrated in Fig. 3.7 (a). Initially, 100% of the active power requirement at PCC is supplied by the inverter. At time = 1 s, the SOC reaches λ_3 threshold and the active power feed to the grid starts to decrease. At λ_2 it becomes zero and the active power starts to inflow to charge the battery at that SOC as expected. When SOC reaches the minimum threshold (λ_1), the battery starts to get charged with full rated power since μ_{soc1} is 1 that point on-wards.

The reactive power feed from the inverter is illustrated Fig. 3.7 (b). According to the criterion of the design, reactive power starts to decrease at λ_2 and completely stops the generation at λ_1. After that point of SOC level, the total apparent power capacity of the inverter is used to generate active charging power for the battery. Fig. 3.8, shows the dq axis current and voltage variation with time while the SOC level varies during the simulation. i_d and I_q variations are proportional to active, reactive power variations respectively. V_q goes to zero due to grid synchronization and V_d stays constant throughout.

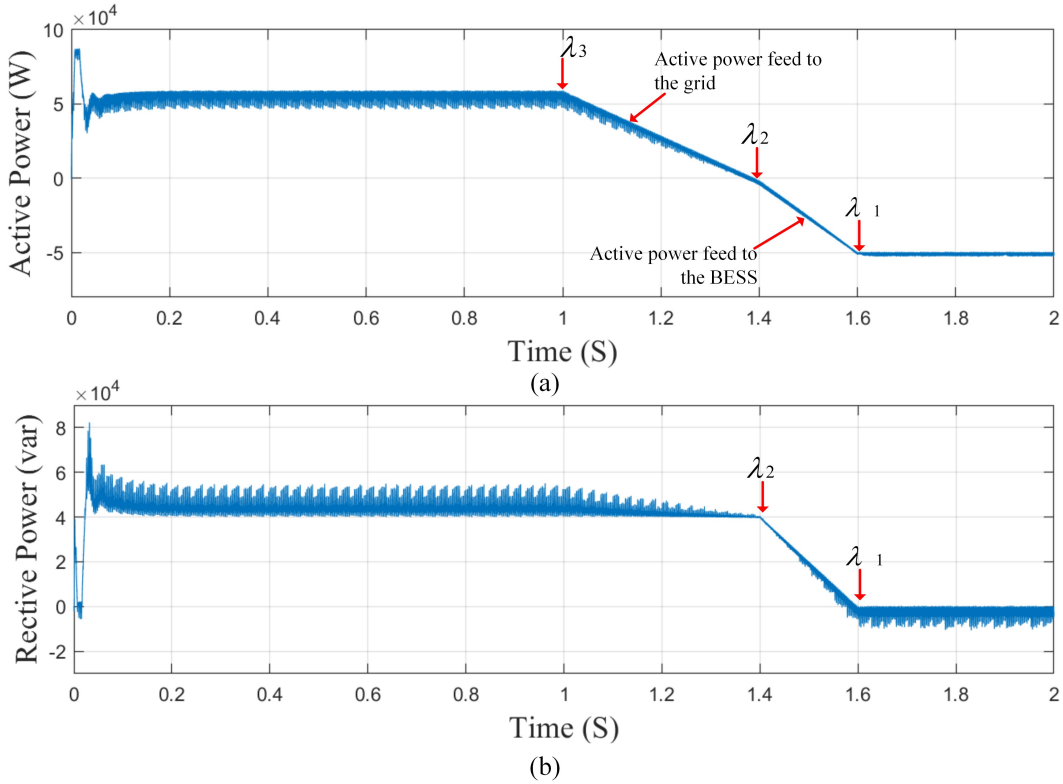

Figure 3.7: Variation of (a) active power (b) reactive power feed from the inverter for steady state situation.

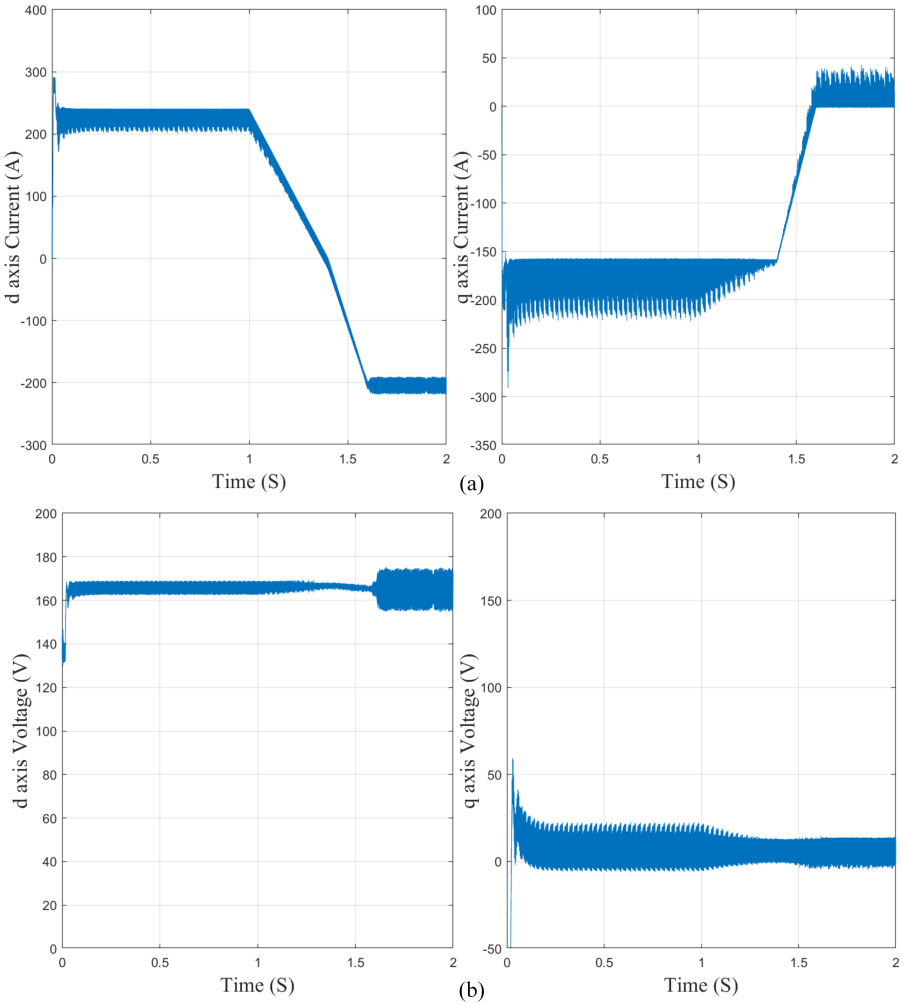

Figure 3.8: Change of d-q axis (a) currents and (b) voltages with time for steady state situation.

3.5 Conclusion

The work proposes a novel control technique for BESS interlinking SI. The proposed controller capable of integrating the experience based knowledge in to the objective function of classical DPMPC as fuzzy goals and constraints. Active, reactive power for grid services and active power to charge the battery are used to calculate projected errors for next states of operation using DPMPC. Then, membership functions were obtained for error magnitudes and for the SOC level, by applying fuzzy control criteria. The objective function is designed aggregating these

membership functions. A defuzzification step is not required for the design as this objective function provides a normalized performance measure of each converter voltage vector. In contrast of having layered control architecture with primary and secondary control levels, this technique has reduced the complexity by dynamically adjusting the objective function according to system changes. The operation of the proposed controller has been validated using MATLAB/Simulink models and the obtained results are presented.

CHAPTER 4

ALGORITHMIC FORMULATION FOR NETWORK RESILIENCE ENHANCEMENT BY OPTIMAL DER HOSTING AND PLACEMENT

4.1 Overview

Studies on the resilience of PDN have gained much attention recently, partly due to more frequent occurrence of extreme weather events. As mentioned in the 1.1, this work defines the resilience of PDN by prioritizing the CLs. During an extreme event it is important to prevent loss of critical services such as medical services, fire rescue etc. Therefore, it's crucial to prioritize those CL nodes when enhancing PDN's resiliency. The developed algorithm prioritizes the CLs in the system when hosting the DERs. CL prioritization is mostly a cognitive decision in existing literature [74]. In contrast to that, this work proposes a clear and consistent mathematically formulated ranking scheme for CLs and it is presented in section 4.3.

The developed algorithm aims to significantly enhance the resiliency of a distribution network by installing DER systems strategically with respect to the network's CL nodes such that these DER systems and their corresponding local control systems can be treated as individual power plants. This concept illustrated in Figure.4.1. The lowest layer of the figure shows the entire PDN prior to identifying the CIs. The CI's are identified and prioritized in the middle layer while the DER are optimally sized (based on maximum DER hosting) and strategically located to enhance the PDN's resilience.

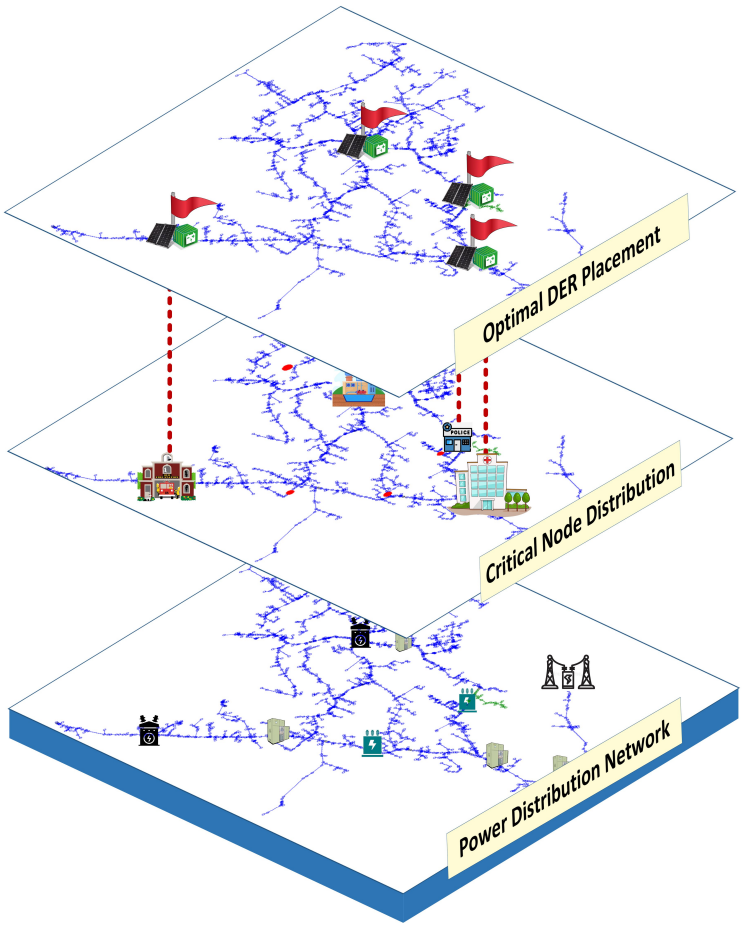

Figure 4.1: Resilience enhancement of power distribution network through optimal DER hosting prioritizing the critical nodes.

4.2 Literature Review

Proper DER placement can consider as a grid hardening technique at pre-event and there are only few previous studies carried out on strategical DER placement and sizing for resilience enhancement. An extensive review on different approaches of optimal energy storage and microgrid allocation to face extreme weather conditions is presented in [75]. The state-of-the-art on this regard is reviewed and a summary is tabulated in the Table.4.1. The general DER hosting calculations involve physical constraints of the system such as power flow voltage limits, generation limits

and thermal limits of the PDN. One of the first papers that incorporates resilience constraints in to the DER hosting algorithms is [76] in which mixed-integer linear programming has used for optimal size and locate microgrids in the power transmission line to maximize the system resilience. Here, the objective function is defined to minimize the cost of unserved energy following hurricanes.

The paper [77] has also presented a strategy for optimal allocation of distributed generation to minimize the cost and emission and improve the transmission line resilience. Optimal sizing and siting scheme for energy storage and PV is proposed in [78] to increase the reachability and accessibility of power in the face of an extreme event. Similar to previous studies the objective of the optimization includes the economic cost factor. Also a new parameter, the capacity accessibility is introduced there to represents the state of the resilience. The paper [79] has proposed an algorithm to identify the optimal microgrid placement to improve the resilience index of the system but doesn't do the sizing. Diesel generators with fixed capacities are used as DERs here and the optimal locations are identified by simulating for all possible candidates rather than using any optimization technique.

None of the aforementioned articles have prioritized critical loads in their formulations of DER hosting. The only paper found in literature that have prioritized critical loads when placing DERs for resilience enhancement is [80]. There they have incorporated the unmet demand penalty costs of different load types in the objective function which prioritize them according to a ranking scheme. So, the power outage levels or the unmet demand is used here to represents the resilience measure. Further, they have performed a sensitivity analysis for different budget options. But, still this paper doesn't do the optimal sizing and assumes the generation power and electricity outputs of DERs are known.

Table 4.1: A summary of state-of-the-art articles in DER locating and allocating for resilience enhancement.

Author, Year	Technique	Highlights	Significance	Weaknesses
Eskandarpour et al., 2016 [76]	Mixed-integer linear programming	• Microgrid optimal placement model that optimally size and locate microgrids to maximize system resilience. • Focused on transmission line resilience. • Resilience of the system is viewed as the cost of unserved energy.	Simulated hurricane passing through three hypothetical paths for validation.	Not clearly specified a methodology the microgrid sizing and placement has done and doesn't do the sizing of DERs and doesn't do critical load prioritization.
Shirazi et al., 2021 [77]	Multi-objective Gray Wolf optimization	• Objectives for optimization are minimizing the economic costs and greenhouse gas emissions, and maximize the system resilience. • Focused on transmission line resilience. • Resilience is viewed as the optimal resilience cost.	Considers reduction of greenhouse gas emissions as one of the objectives.	Doesn't do the sizing of DERs and doesn't do critical load prioritization.

Author, Year	Technique	Highlights	Significance	Weaknesses
Zhang et al., 2019 [78]	Multi-objective optimization	• Optimal sizing and siting scheme for battery storage and PV in the transmission network. • Objectives for optimization are investment and operation costs, capacity accessibility for demand and capacity accessibility for non-blackstart units.	Validated for events of different intensities.	Doesn't do critical load prioritization.
Widiputra et al., 2019 [79]	By simulating each candidate DER placement.	• Resilience index is used to quantify the resilience. • Bus injection to bus current (BIBC) matrix is used to find the islanded buses due to the disaster.	Validated for three storm situations.	Doesn't do the sizing of DERs and a fixed capacity diesel generators are used as DERs.

Author, Year	Technique	Highlights	Significance	Weaknesses
Kizito et al., 2020 [80]	Single-source capacitated facility location coverage problem	• Resilience is viewed as power outage levels due to extreme event. • Objectives for optimization are minimize total investment costs, operation and maintenance cost, distance traveled for electricity distribution, power outage levels, and levels of excess renewable penetration.	• Sensitivity analysis is performed for different budget options. • Unmet demand penalty cost is arbitrarily assigned for each building type to prioritize the critical loads.	• DER sizing isn't optimized. • Generation power is kept fixed for optimization. • Power flow conditions are not evaluated.

To the best of the authors knowledge, till date no paper has integrated PV hosting capacity problem as a holistic approach to distribution feeder resiliency improvement. Also several individual PV hosting algorithms have been proposed in literature [81–84] which are not formulated to improve distribution feeder's resiliency. The PV hosting algorithms in literature usually iteratively or sequentially increases the sizes of PV on the nodes where the PVs are connected. This work uses a voltage sensitivity approach to increase the PV across the optimal PV nodes for maximum PV hosting capacity. In order to achieve this, voltages across all the nodes are monitored and the sizes of the PVs are increased based on their optimal locations up to the over-voltage limit according to the ANSI C84.1 standard. It is also worthy of note that most resiliency improvement algorithms in literature that integrates PVs, do not use the complete PV hosting capacity constraints which include the power flow, and the constraints of the legacy device operations.

Different to the discussed literature, this algorithm optimizes the DER sizing and placement with the objective of improving the PDN resiliency prioritizing the CLs of the system incorporating system limitations as well. The key contributions of the work are listed below.

1. Uniquely proposes an algorithmic formulation which leverages the benefits of DER sizing and placement to ensure continued power supply to the maximum possible number of CL nodes with minimum power losses during an extreme event.
2. Prioritizes the CLs in the network for PV sizing and placement with a developed ranking scheme.
3. Formulation of PV hosing capacity algorithm that is based on the feeder's voltage sensitivity which allows more PV integration by pushing the maximum

nodal voltages close to the overvoltage limit. Unlike other PV-integrated resiliency improvement algorithms, this algorithm applies complete power flow constraints including the operation of the voltage control legacy devices.

4. Application of probabilistic time series tools to emulate an extreme weather event to validate the proposed algorithm.

4.3 Identifying and Ranking the CI Nodes

A node within the grid whose loss or degradation poses a significant threat to the safety, health, environmental, economical, technological, or functional aspects of a society can be defined as a critical node. According to the U.S. Department of Homeland Security, these nodes are belong to one of the 16 CIs that include, but not limited to, energy, food and agriculture, emergency services, transportation systems, healthcare and public health, communications, government facilities, and water and wastewater systems [85]. But it is to be understood that this whole set of infrastructure does not have the same level of criticality when prioritizing the power continuity in the case of an extreme weather event.

During an extreme event it's highly required to power up the CIs which are directly connected to the safety of human life. The ranking of infrastructure criticality is heavily dependent on that particular system. Some of the utility networks may have one or several critical loads such as hospitals, fire stations, police stations, air ports etc. and some may have none. Also, priorities change subjective to the extreme weather events frequent to that specific area. For an example hurricane is the most common extreme weather event in Florida while it is wildfires in California. During a wildfire, the electricity supply to the residential buildings in the affected area is cut off (public safety power shutoffs) while it's the opposite for the

hurricane. Unlike during a hurricane, transportation systems get a higher priority during a wildfire.

The approaches to identify and rank CI nodes involves risk assessment strategies that can be either qualitative or quantitative, and are typically bounded by the CI protection (CIP) guidelines of the North American Electric Reliability Corporation (NERC). Many methods exist in the literature to rank CI systems and subsystems [86–91]. The work in [89] proposes a graph theory-based formulation to model the robustness of interdependent CI networks, where interdependencies were modeled as directed graphs, with critical nodes identified using graph centrality indices. Stochastic ordering techniques such as the Copeland scores have been used to rank CI nodes [88]. Economic impacts on CI nodes have been separately considered in [90, 91]. The work in [87] presents a development of a national CI priority inventory for Germany. They proposes critical proportion, critical time and critical quality as properties of the criticality.

The work in [86] contrast the monocriteria and multicriteria techniques to rank CI nodes. The monocriteria model considers the interdependencies between CI nodes and evaluates the impacts of cascading failures. It creates a dependence matrix that represents the likelihood of each node in the network to be disrupted as a consequence of the disruption in another network. However, this model does not quantify the impacts and relies on the uncertainty of its decision-makers to rank the nodes. A multicriteria model, on the other hand, uses a scoring methodology where the net score depends on six specific criteria- the density of people and assets in the network, the financial impact, the nature of the CI sector, the degree of interdependency, the quickness of service delivery, and public confidence. This model, however, does not assign weights to these criteria, thereby giving them all equal importance, which is impractical. Almost all of these studies have focused on developing national

CI priority schemes and they do not capture the specifics related to power system. Most of these studies measure the criticality based on the position of the node in the network and its likelihood to trigger cascaded failures. But, failure propagation due to the disruption of a node is most unlikely in the context of CI that we consider in this study. One among the very few studies found in literature which ranks CIs in distribution network resilience studies is [74]. Other than the CI ranking, this work introduces the term critical loads (CL) which represents the critical portion of a CI that needs emergency power supply. Although it has proposed applying different weights for each customer type according their criticality, it's a random weight assignment and does not provide any exact methodology.

The cost of the power loss should be considered when ranking the CIs for power continuity. In this work we consider three criteria that contributes to the cost of power loss. First one is the social importance of the infrastructure, R_i^{SI}. Ranking based on the social importance is more of a cognetic decision and is specific to the particular event and to the system. The simplest example is a hospital load which is essential to power up during a hurricane. This is because the cost of human life is invaluable and evaluated at the highest cost. Losing power of a bigger load create a bigger economic loss as well as a higher impact to the stability of the grid. Therefore the next criteria is selected as the apparent power rating of the power load, S_i^L. During an extreme event the loads furthest away from the substation are more vulnerable as there is more chance they loose power due to damages to the incoming power line. Therefore, the proximity to the substation, D_i is selected as a criteria for CI ranking.

As multiple criteria involved in decision making, analytic hierarchy process (AHP) is applied and the criteria are compared pairwise using the semantic scale of Saaty. The relative importance of criteria are obtained through pairwise com-

parison as 0.724, 0.193 and 0.083 for R_i^{SI}, S_i^L and D_i respectively. Assuming $\mathcal{N}_{CI}$ as the set of all CIs, $\forall i \in \mathcal{N}_{CI}$, R_i^{SI} is the normalized social importance ranking of each CI, S_i^L is the normalized apparent power rating of each CI, and D_i is the normalized distance between each CI from the substation transformer. And they can be expressed as (4.1) , (4.2) and (4.3) respectively.

$$\mathbf{R}_{N,i}^{SI} = \frac{2}{|\mathcal{N}_{CI}|}\left(1 - \frac{R_i^{SI}}{|\mathcal{N}_{CI}|+1}\right) \tag{4.1}$$

$$\mathbf{S}_{N,i}^{L} = \frac{S_i^L}{\sum\limits_{i\in\mathcal{N}_{CI}} S_i^L} \tag{4.2}$$

$$\mathbf{D}_{N,i} = \frac{D_i}{\sum\limits_{i\in\mathcal{N}_{CI}} D_i} \tag{4.3}$$

Then, the net score (weight) for each node $i \in \mathcal{N}_{CI}$ is expressed in (4.4).

$$\omega_i = 0.724 \cdot \mathbf{R}_{N,i}^{SI} + 0.193 \cdot \mathbf{S}_{N,i}^{L} + 0.083 \cdot \mathbf{D}_{N,i} \tag{4.4}$$

A set ω_i weights are developed for the given network. The weights of CI nodes are arranged in descending order such that the node with the highest weight gets a rank of 1 (most critical), and the node with the least weight gets a rank of $|\mathcal{N}_{CI}|$ (least critical) where $|\mathcal{N}_{CI}|$ is the cardinality of $\mathcal{N}_{CI}$.

4.4 Developed Network Resiliency Enhancement Algorithm

The developed optimal DER placement algorithm for network resiliency enhancement is illustrated in the Figure. 4.2. The DER considered in this work is a photovoltaic (PV) system. The proposed algorithm is formulated as a multi-objective

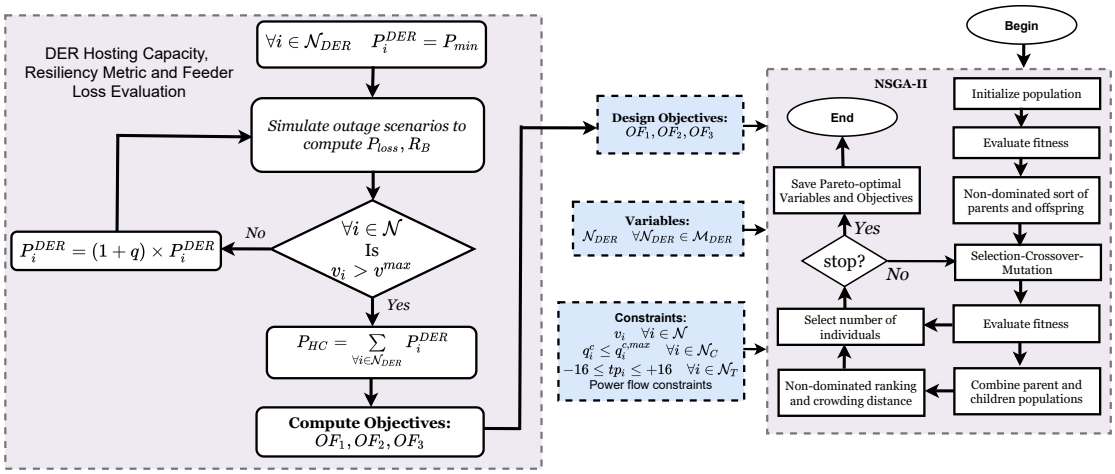

Figure 4.2: Flowchart of the proposed optimal DER location and hosting algorithm for resilience enhancement.

non-linear programming optimization problem in which three objectives are considered. Other than the optimal DER hosting and placement of DERs, maximizing the resilience and minimizing the overall power loss are formulated as the objective functions for the optimization problem. In order to measure the level of resilience, the resiliency metric used is expressed as (4.5) [74].

$$OF_1 := \max|R_B| = \max\left|\frac{\sum_{i=1}^{N_{CI}} \omega^{(i)} T_{U,i}}{\sum_{i=1}^{N_{CI}} (T_{U,i} + T_{D,i})}\right| \tag{4.5}$$

where, $T_{U,i}$ is the the up time of the CI on node i and $T_{D,i}$ is the down time of CI on node i.

In this work, a PV hosting algorithm based on the feeder's voltage sensitivity at the point of common coupling is developed to ensure a high PV penetration in the distribution feeder. While optimally locating the PVs, proposed method tries to increase the size of the PV until the system reaches the overvoltage limit (v^{max}). Depending on the x/r of the feeder at the point of interconnection (POI), more

active power from the PV can be integrated into the feeder. The maximum voltage at the POI of a PV for $\Delta P_i^{pv,max}$ and $\Delta Q_i^{pv,max}$ injection can be expressed as (4.6).

$$v^{max} = v_i - \left\{ \frac{\Delta P_i^{pv,max} - \mathbf{j}\Delta Q_i^{pv,max}}{v_i \angle \delta_i} \right\} (R_i^{eq} + \mathbf{j} X_i^{eq}), \quad \forall i \in \mathcal{N} \tag{4.6}$$

where R_i^{eq} and Q_i^{eq} are the thevenein equivalent resistance and reactance at the POI of the PV, v_i and δ_i are the voltage and voltage angle at the POI while $\mathcal{N}$ is the set containing all the nodes in the network.

In order to maximize the DER hosting capacity of the network, the second objective of the optimization problem is expressed as (4.7).

$$OF_2 := \max|DER_{HC}| = \max\Big| \sum_{i \in \mathcal{N}_{pv}} P_i^{pv} \Big| \tag{4.7}$$

where $\mathcal{N}_{pv}$ is the set containing all the PV systems used as DER in the network and P_i^{pv} is the kW rating based on DER hosing capacity of the PV at node i.

The third objective of the problem formulation is to minimize the average hourly power loss as expressed in (4.8)

$$OF_3 := \min\Big| \frac{1}{T} \sum_{t=1}^{T} P_{loss,t} \Big| \tag{4.8}$$

where

$$P_{loss,t} = \sum_{(i,j) \in \mathrm{L}} r_{ij} \times \frac{P_{ij}^2 + Q_{ij}^2}{v_i}$$

t is the hourly time index [1,... T], L is the set of all branches in the network. $\forall ij \in \mathrm{L}$, P_{ij} and Q_{ij} are the active and reactive power flow from node i to j, r_{ij} is the resistance between branch ij while v_i is the nodal voltage at node i.

The optimization constraints include the power flow constraints expressed in (4.9) and (4.10) ; the capacitor banks reactive power and voltage regulator tap constraints expressed in (4.11) and (4.12) ; and nodal voltage constraint is expressed as (4.13)

$$\begin{aligned} P_i^G =& P_i^L + v_i^d \sum_{k=1}^{n} \left(\mathbf{G}_{ik} v_k^d - \mathbf{B}_{ik} v_k^q\right) \\ &+ v_i^q \sum_{k=1}^{n} \left(\mathbf{B}_{ik} v_k^d + \mathbf{G}_{ik} v_k^q\right) \forall i \in \mathcal{N} \end{aligned} \tag{4.9}$$

$$\begin{aligned} Q_i^G =& Q_i^L + v_i^d \sum_{k=1}^{n} \left(-\mathbf{B}_{ik} v_k^d - \mathbf{G}_{ik} v_k^q\right) \\ &+ v_i^q \sum_{k=1}^{n} \left(\mathbf{G}_{ik} v_k^d - \mathbf{B}_{ik} v_k^q\right) \forall i \in \mathcal{N} \end{aligned} \tag{4.10}$$

$$q_i^c \leq q_i^{c,max} \quad \forall i \in \mathcal{N}_C \tag{4.11}$$

$$-16 \leq tp_i \leq +16 \quad \forall i \in \mathcal{N}_T \tag{4.12}$$

$$v^{max} \geq |v_i| \geq v^{min} \tag{4.13}$$

where $\mathcal{N}$ is the set containing all the nodes in the network, $\mathcal{N}_C$ is the set containing all the capacitor banks, $\mathcal{N}_T$ is the set of nodes with voltage regulators/load tap changers, $\forall i \in \mathcal{N}$; $P_i^L + \mathbf{j}Q_i^L$ is the active and reactive load at bus i, $v_i = v_i^d + \mathbf{j}v_i^q$ is the complex voltage phasor, $\mathbf{Y} = \mathbf{G} + \mathbf{jB}$ is the network admittance matrix, q_i^c and $q_i^{c,max}$ are the reactive and maximum reactive power injection by the capacitor banks at node i, tp_i is the voltage regulator/ load tap changer tap position at node i while v^{max} and v^{min} are the maximum and minimum nodal voltage usually set at $1.05pu$ and $0.95pu$ respectively

The algorithm starts by using the NSGA-II to generate the initial population of variables which is the set of nodes $\mathcal{N}_{pv}$ from the candidates set of notes $\mathcal{M}_{pv}$ (which are all three-phase nodes in the network) which are used to evaluate the fitness of the objective functions (OF_1, OF_2 and OF_3 as expressed in (4.5), (4.7), and (4.8) respectively). The DER considered in this algorithm is a photovoltaic (PV) system. In order to obtain the PV hosting capacity, R_B and the average hourly power loss, based in the $\mathcal{N}_{pv}$, algorithm starts by setting the PV kW rating to a minimum set value of $P_i^{pv,min}$. The outage scenarios are simulated as explained in detail in the section 4.5 and the power loss and resilience metric are calculated for that particular scenario. Then the system nodes are checked for any voltage constraint violations and if the voltage stays within the limits the power level of each PV is increased by a factor q for the next PV hosting capacity iteration. The kW rating of the PVs are increased and the outage scenarios simulated until the first nodal voltage violation occurs. The values of OF_1, OF_2 and OF_3 are computed while the NSGA-II generates the new set of off-springs and the process is continued until stop criteria is met and the Pareto Optimal Solutions (POS) are saved.

4.5 Simulation Results and Analysis: A Test Case

When performing the resiliency study, it is required to simulate the extreme weather event over the PDN. In order to emulate the failure bunching phenomenon due to extreme weather, [92] and [13] applied a sequential Monte-Carlo-based probabilistic tool. They have used a probability distribution of a wind profile and weather dependent fragility curves of the components to replicate the stochastic power system failure events across space and time during a hurricane. Adopting the same concept, this work uses a fragility curve for power lines which is acquired from [93]. A

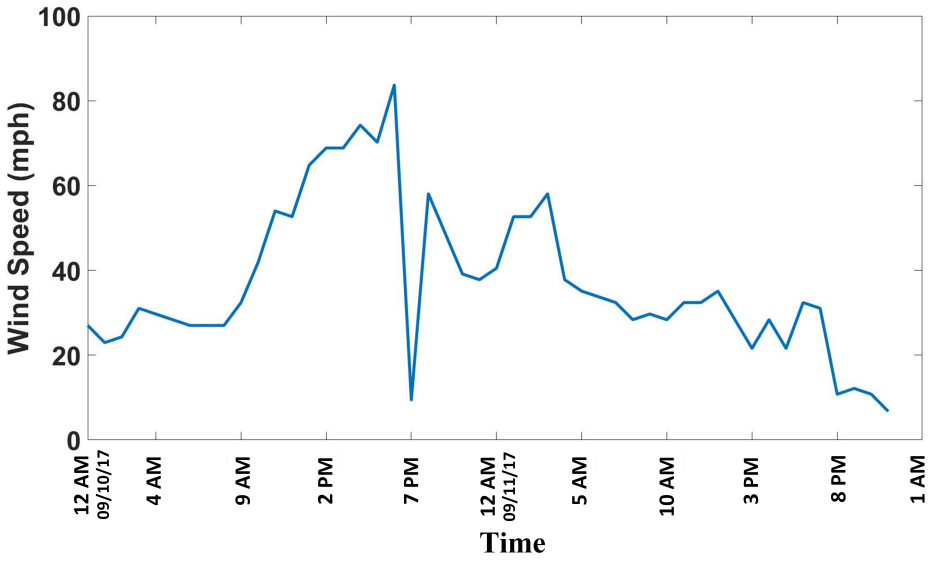

Figure 4.3: Wind profile of Hurricane Irma at Fort Myers, FL on 09/10/2017 and 09/11/2017.

wind profile of the hurricane Irma for the Fort Myers area in Florida is used for the analysis. The total simulation is done for a 48 hour time period starting at 12 am on 10^{th} September 2017 with a 1-hour time resolution as shown in Figure.4.3. The wind speed is assumed to be constant during the one hour period. The probability of failure of lines during the event is not only dependent on the wind intensity but also on the age and wear of each of the line. Therefore, to provide this randomness in failure, the failure probability of line k, $P_c^k(\omega)$ is compared with a uniformly distributed random number, r at every simulation step. If $P_c^k(\omega) > r$ then the line k will trip and otherwise the line will continue to operate. This method is implemented to provide different deterioration levels for different lines.

In the considered test case, the wind storm progresses, reaching almost category-1 winds for that area. It is assumed that the damage assessments and line restorations begin as soon as the disastrous winds are over. The mean time for damage assessment and line restoration process is assumed as 12 hours and again this time is randomized for different lines by multiplying by a random number [39]. The obtained

line failures are simulated at each simulation step and necessary measurements are obtained by performing the power flow analysis.

4.5.1 Network Description

To validate the effectiveness of the proposed DER hosting and optimal placement algorithm for resiliency improvement, the IEEE 34 is modeled in the OpenDSS platform as a PDN as shown in Fig. 4.4. Five PVs are modeled as DERs and integrated into the PDN for the proposed algorithm. The global horizontal irradiance (GHI) profile and temperature (both ambient as well as module temperature) for the PV systems were collected from an actual 1.4 MW PV system located on the Engineering campus of Florida International University. Since the PVs are assumed to be utility scale PV, all the 3-phase nodes are selected as candidate nodes which means $\mathcal{M}_{pv} = 25$ from which the optimal five locations for the PVs $\mathcal{N}_{pv}$ will be selected.

The nominal voltage rating of the feeder is $24.9kV$. The feeder has two voltage regulators between nodes $814 - 850$ and $852 - 832$. The substation transformer upstream of node 850 is a $2.5MVA$, $69/24.9kV, \Delta Y$. The combined rating of the load (modified) on the feeder is approximately 3.1 MW (active) and 0.689 MVAr (reactive). Node 838 is the farthest distance and its approximately 59 km away from the substation transformer.

The IEEE feeder contains of 31 loads and 10 out of them are chosen as CI nodes for this study. Ten three-phase loads that are distributed across the network are randomly selected as the CI nodes as shown in the Figure.4.4. The chosen CIs are ranked according to the load prioritization scheme proposed in the Section 4.3 and is illustrated in the Table.4.2. RES_1 and RES_2 are residential loads on nodes mid858 and 850 respectively, HOS is a hospital load on node mid834, FR is fire rescue on

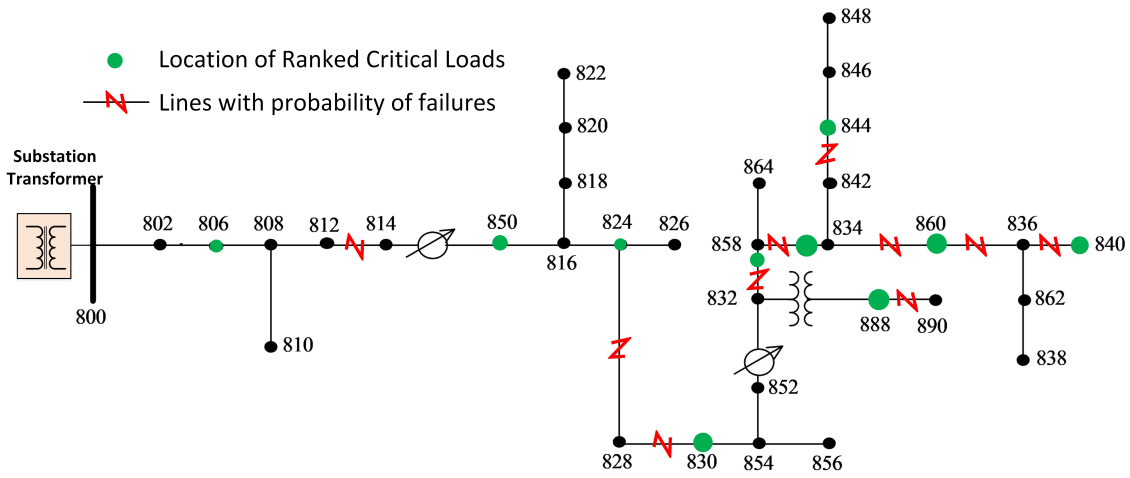

Figure 4.4: IEEE 34 bus network with CI nodes and lines with probability of failure marked on it.

node 860, CH is city hall on node 840, SM is shopping mall on node 844, SUP_1 and SUP_2 are supermarket loads on node 824 and 806 respectively, WPS is the water pump station on node 888 while POL is the police station on node 830.

Table 4.2: Ranking of the CI nodes.

Load Type	R_i^{SI}	$\mathbf{R}_{N,i}^{SI}$	S_i^L (kVA)	$\mathbf{S}_{N,i}^L$	D_i (km)	$\mathbf{D}_{N,i}$	ω_i
RES_1	5	0.109	107.7	0.071	53.5	0.121	0.103
HOS	1	0.182	151.3	0.100	55.1	0.125	0.161
FR	2	0.164	76.8	0.051	56.6	0.128	0.139
CH	7	0.073	34.2	0.022	57.7	0.131	0.068
SM	10	0.018	513.1	0.337	56.5	0.128	0.089
SUP_2	9	0.036	76.8	0.051	34.8	0.079	0.043
WPS	4	0.127	458.9	0.302	52.7	0.119	0.160
POL	3	0.145	50.2	0.033	41.3	0.094	0.119
R2	6	0.091	17.9	0.012	31.6	0.072	0.074
SUP_1	8	0.055	33.5	0.021	1.3	0.003	0.044

4.5.2 Results and Analysis

The developed algorithm as described in section 4.4 is scripted in Matlab and coupled with OpenDSS through its COM interface. The simulation is run on a computing machine with Intel® Core i5-7400 @ 3.0GHz processor and 24GB RAM. The multi-objective optimization algorithm generated 18 Pareto optimal solutions (POS) for the considered test case as tabulated in Table 4.3. Each POS gives the nodes for optimal DER placement based on the set objectives (OF_1, OF_2, OF_3). Based on the objective of highest priority, the corresponding set of nodes for optimal placement of the DER can be selected from the table.

Table 4.3: POSs obtained for the test case

POS	DER placement					Objective function		
	$\mathcal{N}_{pv}$					OF_1	OF_2	OF_3
1	816	852	814	834	830	0.89	0.61	77.15
2	832	828	860	816	834	0.94	1.91	138.83
3	858	840	860	842	806	0.86	2.55	137.59
4	834	844	854	814	812	0.86	0.98	104.79
5	824	830	852	814	812	0.77	3.08	42.51
6	824	848	816	834	830	0.84	1.58	121.84
7	816	830	848	850	814	0.84	0.74	98.12
8	816	852	814	834	830	0.89	0.61	77.15
9	850	816	846	828	824	0.84	1.19	116.83
10	846	840	842	858	832	0.87	2.32	143.50
11	854	828	846	824	850	0.89	0.89	114.53
12	806	828	812	830	854	0.72	4.10	61.72
13	846	828	830	824	854	0.89	0.74	110.04
14	824	848	850	858	830	0.88	1.31	125.78
15	824	830	852	814	812	0.77	3.08	42.51
16	832	830	860	850	834	0.94	1.74	134.96
17	830	834	842	816	854	0.89	1.08	125.53
18	848	844	814	806	832	0.86	1.44	129.68

The POS values (POS-2, POS-5 and POS-12) that produces the best of the three objectives is highlighted in gray as shown in Table 4.3. These solutions are selected for performance analysis of the proposed algorithm. The optimal DER locations

and sizes achieved from POS-2 produces the highest resilience base (OF_1) value of 0.94. The DER locations and sizes achieved from POS-5 has the least power loss (OF_3) of 42.51kW while that achieved from POS-12 provides the highest DER hosting capacity (OF_2) of 4.10MW. All the POS values can be used to size and site the DERs based in the priorities set by the distribution planning engineers. Trade-offs can be made in the selection of the DER sizes and location based on the objectives of priority. Rather than focusing only on maximizing a single objective, it is possible to select a POS in the middle ground according to the requirements of the distribution system. From the POS solution, Figure. 4.5 shows the 3-D plot the three set objectives. The plot clearly shows the interaction between the set optimization objectives.

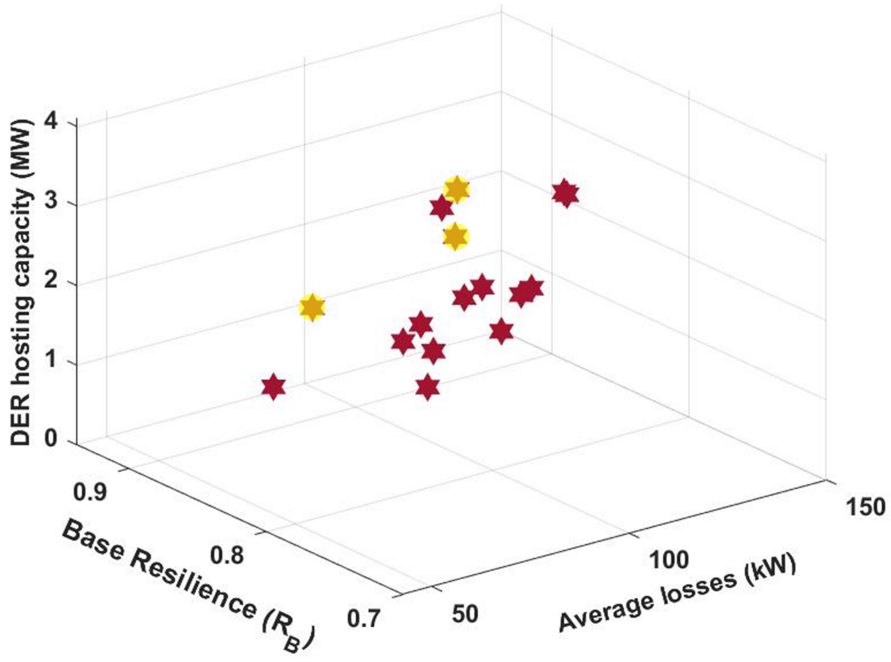

Figure 4.5: Pareto front with dominated solutions highlighted for further analysis.

Figure.4.6 shows the resilience trapezoids of the optimal DER (PV) placements and location for each of the POSs in contrast to the resilience trapezoid of without DER (PV) placement.

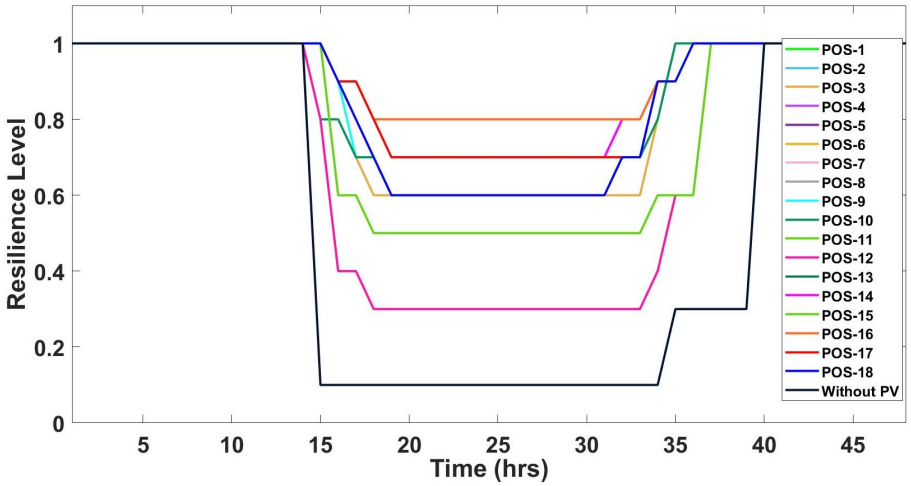

Figure 4.6: Resilience trapezoids for different Pareto optimal solutions.

The plot (Figure.4.6) shows the percentage availabilities of CIs which are indicated as the measure of the network's resilience. Typically, the resilience trapezoid provides information on the level of resilience degradation, the rate of system degradation, rate of restoration and the outage time. From the figure, we can see POS-12 (of all the POS solutions) has a steep resilience degradation, a long outage time and lowest resilience level of 0.3 (which is the lowest of the POS values). POS-12 has the largest trapezoid area. Compared to POS-12, the lowest resilience level which POS-2 dropped to is 0.8 and its area of the trapezoid the smallest of all the POS. This correlates with the values obtained from the POS which shows that POS-12 and POS-2 generates the lowest (0.72) and highest (0.94) R_B values respectively (as seen from table 4.3). The resilience trapezoids also show that the trapezoid area without DERs (PV) is the largest compared to all the POS solutions with DERs integrated. The lowest value the resilience level drops is 0.1. For this scenario (without DER) the R_B value is 0.51. This further shows the benefit of DER (PV) integration and further optimizing their location and sizes for improved PDN's resiliency.

Figure.4.7 shows the voltage profile of the CI nodes without DER (PV) integration and it can be seen that nine out of ten CI nodes experiences outages during the

hurricane. The zero voltage on the CI nodes during the simulated hurricane further

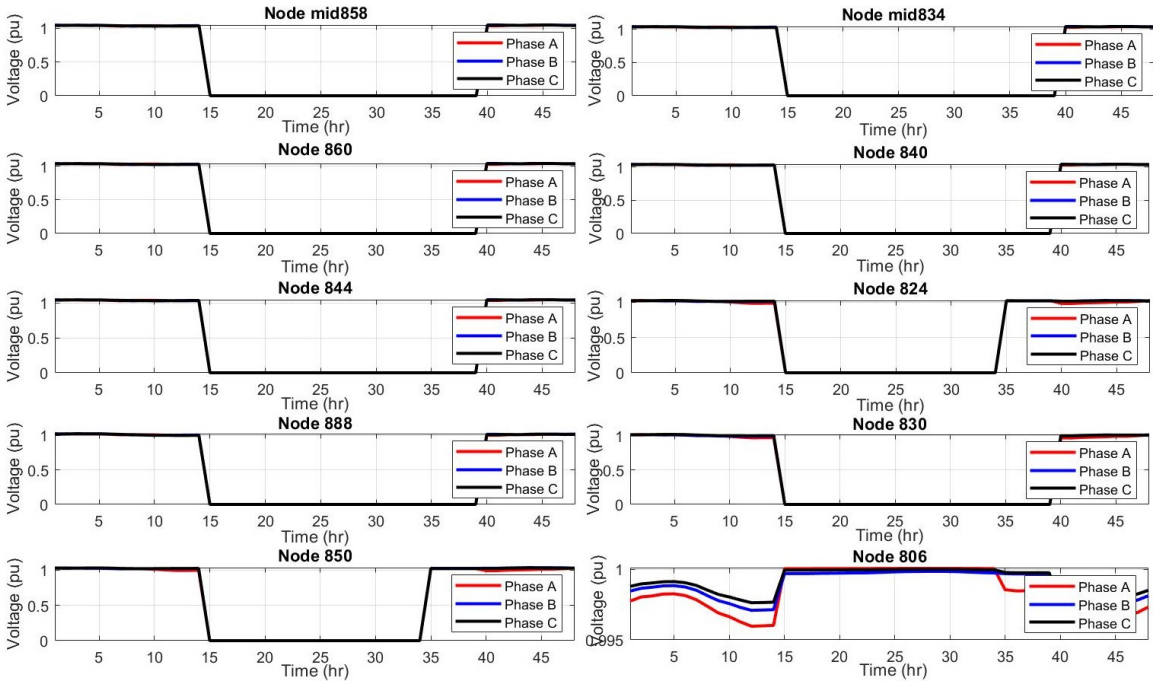

Figure 4.7: Voltage performance at CI nodes for without PV integration.

highlights the importance of using DER to improve the availability of power to the CI nodes which is the measure of the network's resiliency as defined in this work. The sizing and locating the DER (PV) can be achieved by the POS in Table 4.3 as previously discussed.

Figures 4.8, 4.9 and 4.10 show the voltage profile of each of the critical node loads for POS-2, POS-5 and POS-12 respectively. The nodal voltages at a given time goes to zero whenever a power outage occurs due to the hurricane event. Comparing the voltage profiles of POS-2, POS-5, and POS-12, it can been that the higher base resilience value of POS-12 ($OF_1 = 0.94$) compared to POS-5 ($OF_1 = 0.77$) and POS-12 ($OF_1 = 0.72$) lead to lesser impact of the hurricane event on the outages on the critical infrastructure. This choice of POS-2 solution for the DER (PV) location and sizes gives the highest up time for the CI nodes and can be selected if the base

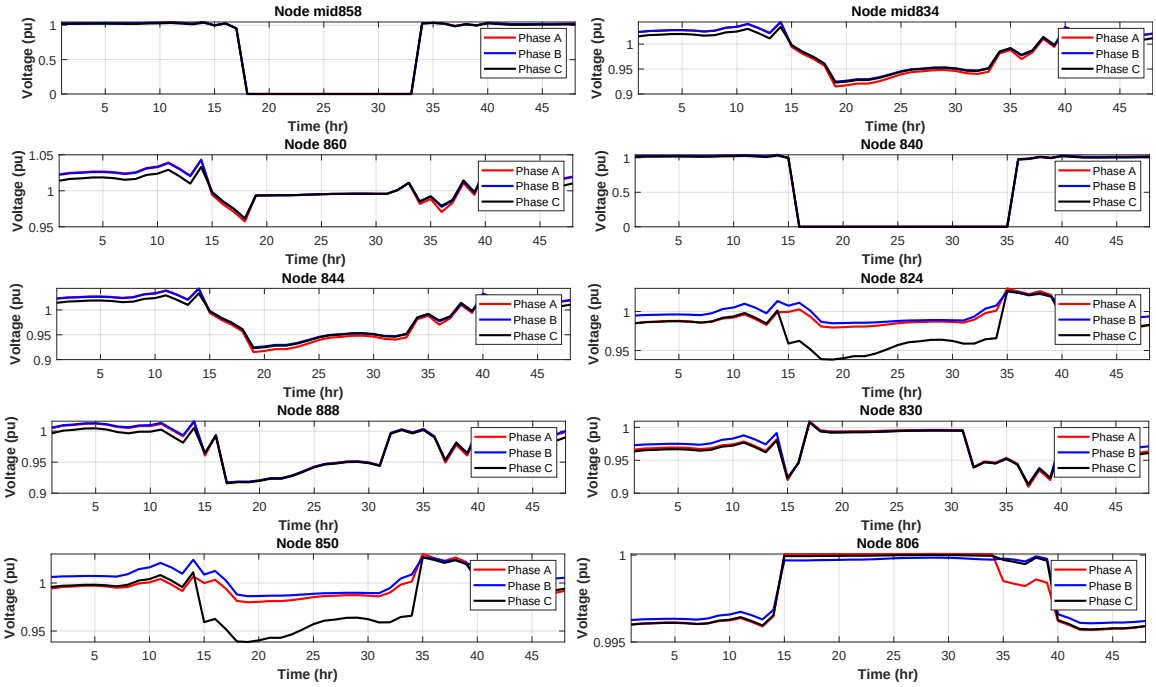

Figure 4.8: Voltage profile at CI nodes for POS-2.

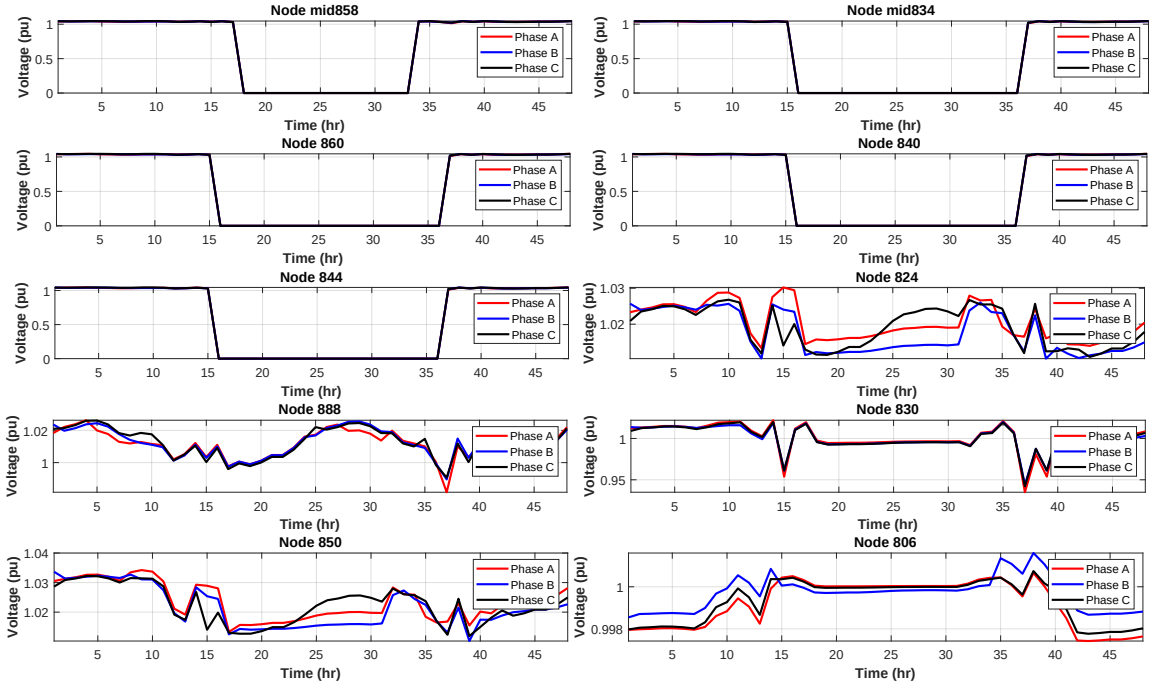

Figure 4.9: Voltage profile at CI nodes for POS-5.

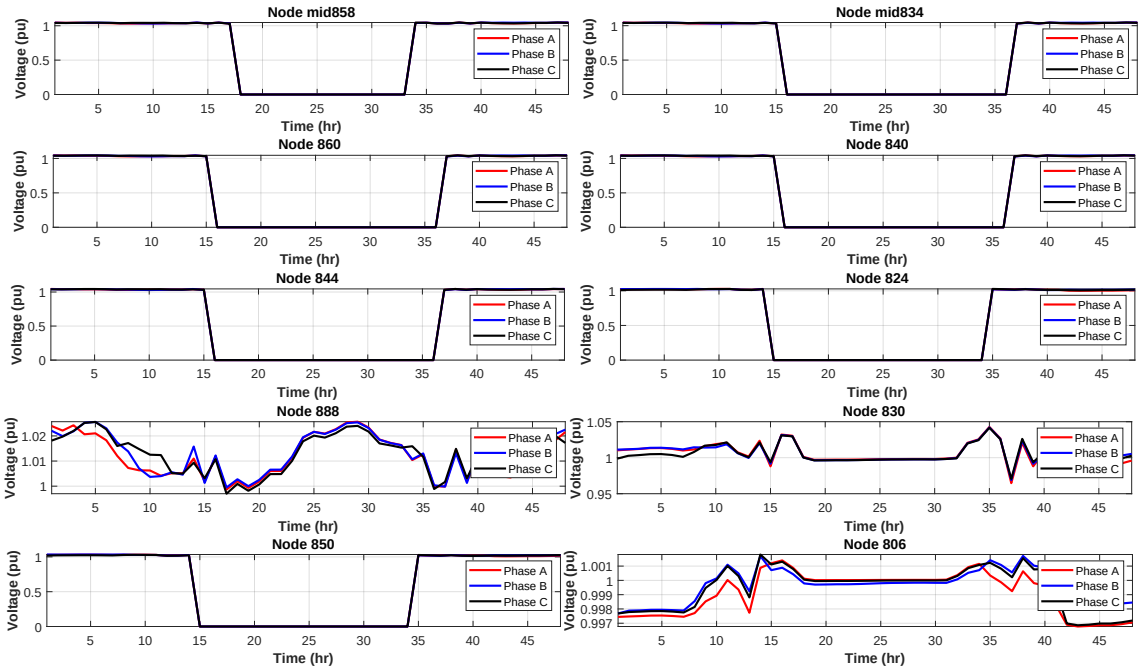

Figure 4.10: Voltage profile at CI nodes for POS-12.

resilience is of most importance to the distribution planning engineers. The trade-off of this solution (POS-2) is the lesser value of its DER (PV) hosting capacity value (1.91 MW) and higher active power loss value (138.83 kW) compared to that of POS-5 (DER (PV) hosting capacity value=3.08 MW and active power loss= 42.51 kW) and POS-12 (DER (PV) hosting capacity value = 4.10 MW and active power loss= 61.72 kW).

We further investigated how the up times of the CI nodes are improved based on their level of criticality. The up times of the CI nodes for the selected POSs are analyzed in comparison to the priority weights applied to those CI nodes. This analysis is as shown in Figs. 4.11 , 4.12 and 4.13. It can be seen that the three most critical CIs, water pumping station, hospital and fire station all have highest up times with POS-2 (which has the highest base resilience). This shows the effectiveness of the proposed ranking scheme. Although POS-5 and POS-12 generates the highest up time for water pumping station, the hospital and fire station CI loads have lower

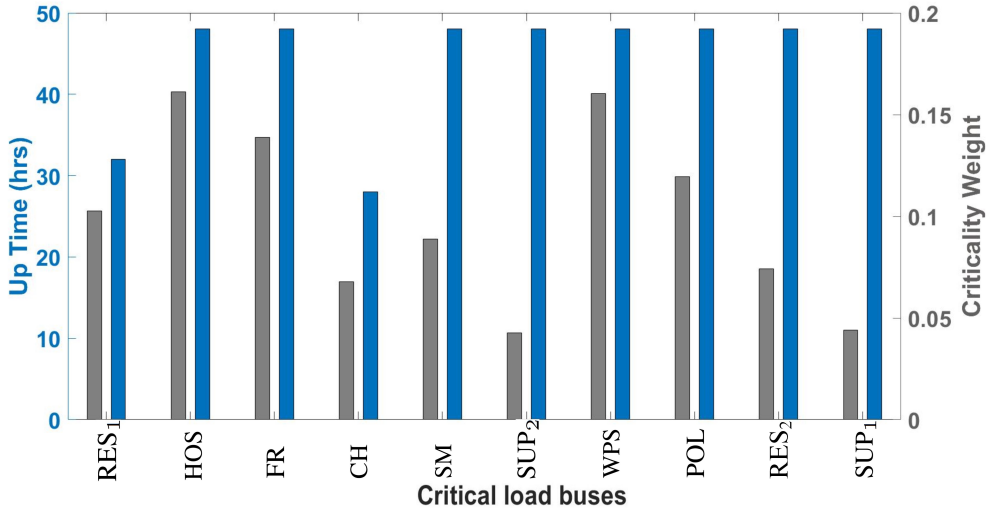

Figure 4.11: The priority levels of CI vs. the up time with POS-2.

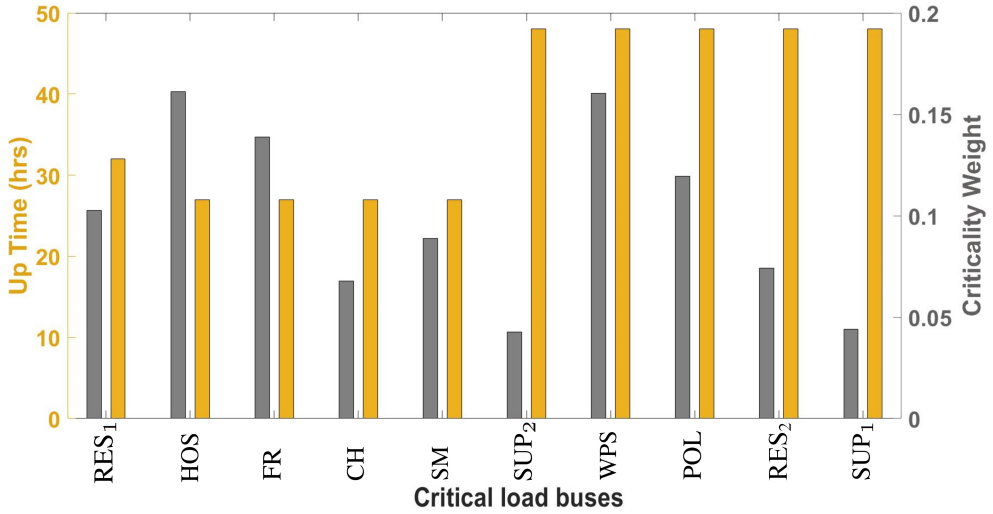

Figure 4.12: The priority levels of CI vs. the up time with POS-5.

up time values. This is due to the fact that POS-5 and POS-12 achieves the least power losses and the most PV hosting capacity values respectively moreover does not achieve a higher base resilience value (compared to POS-2).

The developed algorithm is further evaluated in comparison to a benchmark algorithm that has been created based on the existing studies presented in Section 4.2. Most of the studies don't prioritize critical loads in their DER placement algo-

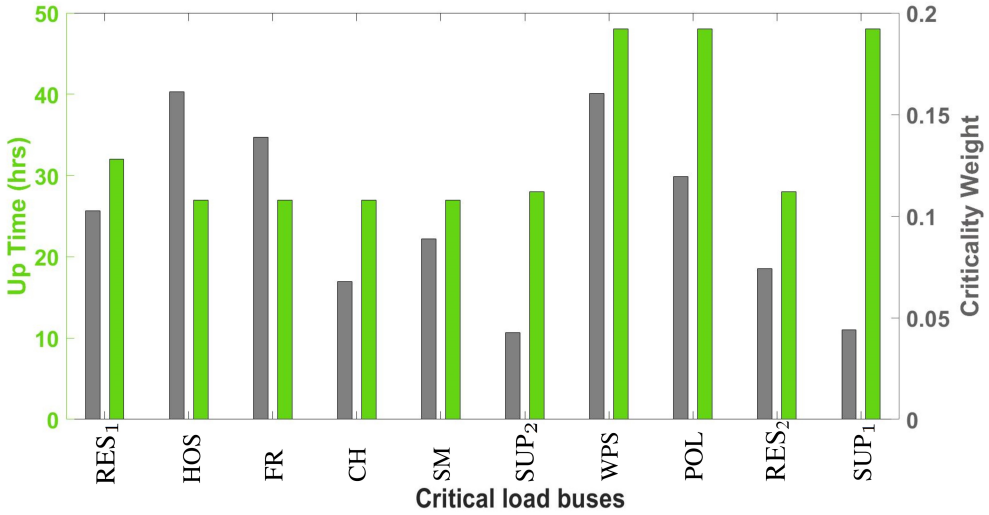

Figure 4.13: The priority levels of CI vs. the up time with POS-12.

rithms [76, 77, 79]. Also, these studies either don't apply PV hosting as part of their algorithm for PV placement which evaluates the existing system's capacities and capabilities ([80]) or they apply the system limits as constraints in the optimization algorithm [76, 77, 79]. Therefore, the benchmark algorithm was developed without critical load prioritization and without incorporating PV hosting. The Figure. 4.14 shows the up times of each critical load with the benchmark algorithm and it can be observed that the magnitudes of up times of the critical loads are not in priority order. When compared with Figure. 4.11, the FR which stands in second place of the priority order has a lower up time while low priority loads like CH and RES_1 have high up times. Furthermore, not incorporating the power flow and the legacy devices constraints in the PV hosting formulation for resiliency enhancement could result in practically infeasible solution. This further validates the superiority of the proposed algorithm compared to the benchmark models that exists in literature.

A sensitivity analysis has been carried out to see how the changes in the input parameters of the optimization problem, the PV placement and sizing would change the objectives of the optimization. First, the size of the PVs are kept constant

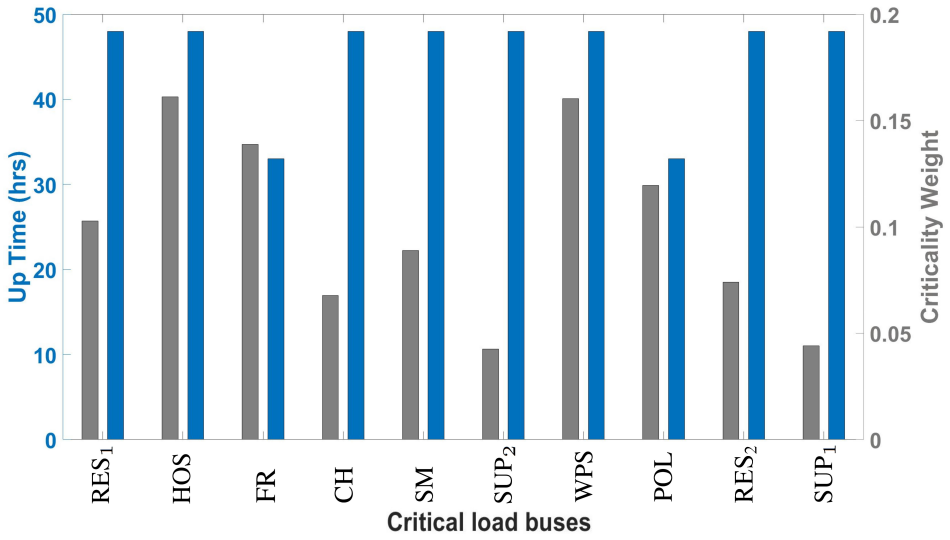

Figure 4.14: The priority levels of CI vs. the up time for the benchmark algorithm.

and varied the placements. Since there are ${}^{25}C_5 = 53130$ number of possibilities of PV placement in this test case, the analysis is carried out only for selected PV placements. To begin with, the placements and sizes of POS-2 which is the highest resilience POS has been selected and one out of five PV placements of it changed at a time. Figure. 4.15. displays the sensitivity of R_B for those variations and R_B at POS-2 is highlighted in yellow. It can be observed that R_B is sensitive to the placements of PVs with an average change of 0.031 for a change in single placement. Similarly, the sensitivity of the power losses for PV placement is investigated using POS-5 placements. The obtained power loss variations for minimum changes to the placement is depicted in Figure. 4.16 and the average variation in there is 12.04 kW.

Then the sensitivity to the size of PVs is evaluated by keeping the placements constant at POS-2 and POS-5 and varying the sizes. As per the results obtained, the change in R_B due to varying sizes is almost negligible. This might be due to composition of R_B and the way it views the resilience. But, as given in Figure. 4.17

the power losses vary with the sizes of PVs and can quantify it as 15 W of average change per 1 KW change in size.

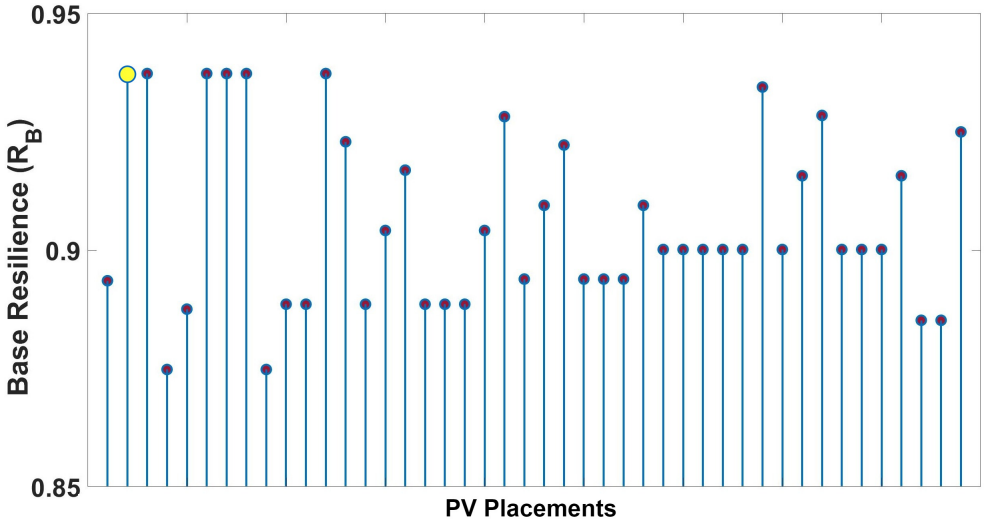

Figure 4.15: The sensitivity of R_B for changes in PV placement.

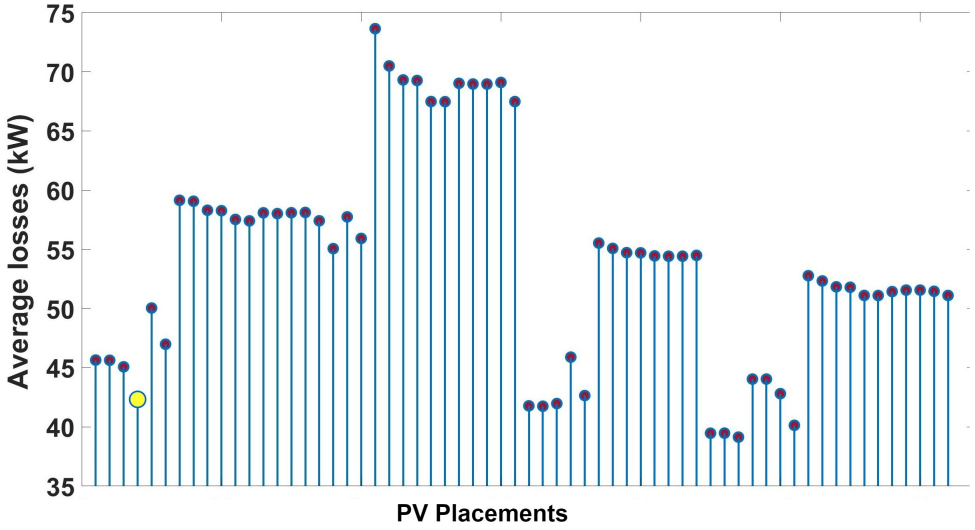

Figure 4.16: The sensitivity of power loss for changes in PV placement.

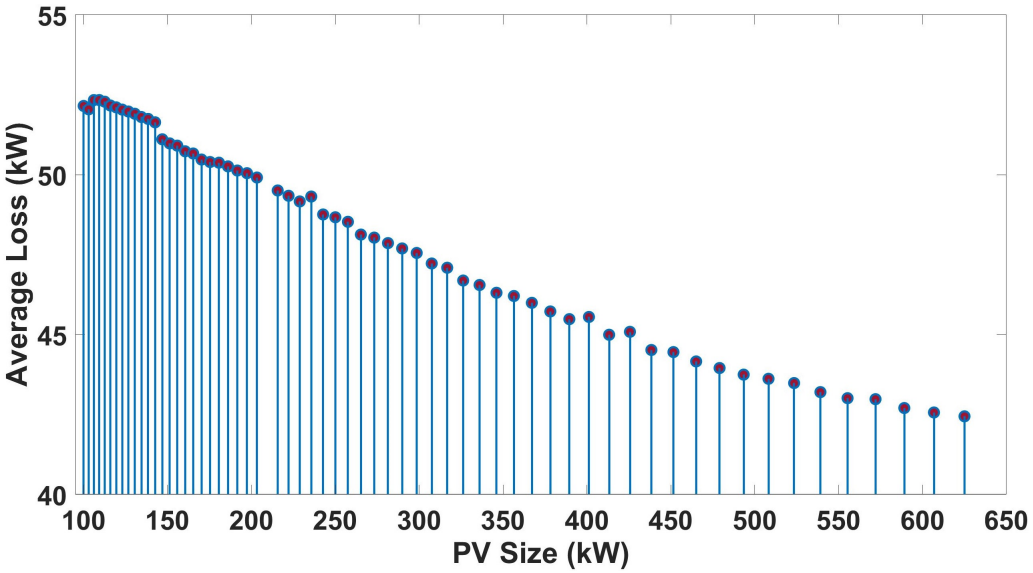

Figure 4.17: The sensitivity of power loss for changes in PV size.

4.6 Conclusion and Future Work

In this work an optimal DER hosting algorithm to enhance the resilience of power distribution network is proposed. Here, the resilience of PDN is measured in the perspective of critical loads. Therefore, critical loads are prioritized according to a unique ranking scheme developed in this work. The problem is formulated as a multi-objective optimization where NSGA-II is applied to obtain Pareto optimal solutions for the three objectives: enhance base resilience, maximize PV hosting capacity and minimize power losses.

The developed algorithm is validated in a simulated environment in where a hurricane is emulated for two days time period applying probabilistic tools. The simulation results provide several options of DER (PV) sizes and placement which have different trade offs between the three objectives. The three dominated POSs are further analyzed for their impact on PDN. Conclusions can be drawn based on the results of the case study that:

1. critical load ranking scheme provides the required level of load prioritization in where hospital load ranked one and the water pumping station with the highest power consumption is ranked the second
2. the resilience of the PDN is enhanced by the optimal DER (PV) hosting and placement using the proposed algorithm from a minimum $R_B = 0.51$ to maximum $R_B = 0.94$
3. the algorithm was also able to maximize the DER (PV) hosting capacity from the least value of $0.61MW$ to the highest value of $4.10MW$

CHAPTER 5

METRIC FORMULATION FOR QUANTIFICATION OF POWER DISTRIBUTION NETWORK RESILIENCE

5.1 Overview

As in any development plan, it requires to set investment priorities for the resilience enhancement planning. For that, the anticipated resilience enhancement due to the investments need to be quantified and then should be able to justify the actions technically and financially. This process requires an accurate and effective resilience quantification scheme for the power system. Such resilience metric scheme provides a benchmark for operational and policy making decisions.

Resilience is a broad concept, hence formulation of a comprehensive resilience metric in one shot is hard to achieve. Therefore, every progressive step is important for accumulating different aspects associated with the resilience concept. In this study a new metric scheme is developed with critical load prioritization integrated to them. In this work, the performance based approach is chosen since it is more informative for planning analyses as discussed in the Chapter 1. Since performance based metrics are event dependent, the impact of event severity on the developed metrics is also analyzed. The proposed metric scheme is designed for distribution network resilience evaluation and in this work the resilience of a distribution network is viewed as its ability to provide continuous power supply to at least one of its critical loads during the occurrence of an extreme event.

5.2 Literature Review

Resilience of the power system is starting to receive much recognition from the research community and resilience metric development is one of the areas that gained much attention recently. Up to date there is no standardized metric for resilience, but many research are carried out towards that. Several selected publications which can be considered as milestones in the evolution of resilience metrics are extensively discussed this section and also tabulated in the Table. 5.1.

As discussed in Chapter 1 there are two variations of metrics, attribute based and performance based and among them attribute based metrics are not able to provide the full functionality expected from a resilience metric. In the Table. 5.1 there are two attribute based metrics are listed [36, 37] and they considers only the network configurations or topological characteristics of the system. Therefore, they are not able to reflect all four emergency management phases that should be there as stated in [34]. According to [34], the MCDA metrics can provide only a baseline understanding of the current state of the system. But the resilience metrics should quantify the consequences of the power disruption caused due to extreme event.

The paper [94] introduces several resilience metrics as given in the Table. 5.1 and one of it's metric 'resistance' has the variable intensity of the event incorporated to it. This is the only paper found in literatire with the intensity variable in the metric. Although it has been used, the variable is not properly defined ir derived stating that it is out of scope for that study. Two metrics among this metric set, base resilience and outage incidence are selected and further improved in [74] by applying critical load prioritization. This is one of the very few first papers that integrated load criticality in to the metric. But again they don't provide any formulation for ranking or prioritization.

Table 5.1: A summary of state-of-the-art articles in resilience metric formulation.

Year, Ref.	Approach	Metrics	Significance & Drawbacks
2016, [94]	Performance	• Base resilience • Disruption speed • Restoration speed • Resistance • Brittleness	Introduces the variable, intensity of the event in one of the developed metrics. But the method of calculating the variable has not provided. No critical load prioritization. Metric calculation and analysis done with actual data of hurricane and earthquake.
2016, [37]	Attribute	• Critical fraction • Diameter of network • Length of the graph • Betweenness centrality • Clustering coefficient • Algebraic connectivity AHP applied to choose weights	Topological characteristics are aggregated to calculate the metric.
2017, [38]	Performance	• Modified LOLP • Modified EDNS	Probabilistic metrics, hence provide the essence of uncertainty. Metrics doesn't incorporate critical load prioritization or the event intensity.
2017, [13]	Performance	Φ, Λ, E, Π	Measurements are based on the resilience trapezoid. Metrics are constructed for the transmission network. Metrics doesn't incorporate critical load prioritization or the event intensity.

Year, Ref.	Approach	Metrics	Significance & Drawbacks
2018, [95]	Performance	Code based metric	The impact is assessed by the time duration taken by a system to recover.
2020, [93]	Performance	• Value-at-risk • Conditional value-at-risk	Two probabilistic metrics are presented.
2018, [36]	Attribute	• Branch count effect • Overlapping branches • Switching operations • Source repetition • Path redundancy • Probability of source availability and penalty • Aggregated central point dominance with Choquet Integrals computation	The parameters that depict the resourcefulness are measured and aggregated. Critical loads are prioritized.
2020, [35]	Performance	• Storm resilience metric • Non-storm resilience metric	The two metrics represent the black sky and gray sky operations.
2020, [34]	Combined Performance, Attribute	Integrated MCDA and performance based metric	MCDA based metrics are used for high-level alternative overview while performance based metrics are used for cost benefit analysis. Adopts concepts from the national emergency preparedness paradigm for the MCDA metrics.

Year, Ref.	Approach	Metrics	Significance & Drawbacks
2021, [74]	Performance	• Augmented base resilience • Augmented outage incidence	Critical loads are prioritized. Critical load categorization is also presented.
2022, [96]	Combined Performance, Attribute	• Anticipate • Withstand • Recover	Integrates system characteristics of blue sky, black sky, and gray sky operations the extreme event. Adopts concepts from the national emergency preparedness paradigm.

The metric scheme of Φ, Λ, E, Π in [13] is constructed based on the characteristics measured in the resilience trapezoid such as the speed resilience dropped, the lowest level of resilience etc. In [95], a code based metric scheme presented and it measures the resilience based the time duration needs the system to recover irrespective of the event. The metrics value-at-risk, conditinal value at risk [93] and modified loss of load probability (LOLP), expected demand not served (EDNS) [38] are probabilistic reasilience metrics. As [34] stated the resilience metrics should reflect the uncertainties that comes with extreme events. These metrics suits well in that sense.

A combination of both attribute and performance based approaches are proposed in several articles. The article [34] formulated MCDA metrics adopting the concepts from national emergency preparedness platform and applied them for baseline resilience evaluation. Then performance based are applied for selection of resilience enhancement investments. The metrics presented in [96] also implements the combined approach and captures the concepts from national emergency preparedness paradigm. Also, those metrics represent the system characteristics of the three

phases of an extreme event; blue sky, black sky and gray sky. Blue sky indicates pre-event atmosphere in where the system is with normal operating conditions. Then black sky refers to the system state when it is subjected to catastrophic event and the recovery phase is represented as the gray sky.

As per the above discussion, most metric formulations found in literature have not incorporated critical load prioritization or have not analyzed the impact of the intensity of extreme event for the performance based metrics. That research gap is addressed through this study.

5.3 Analysis on the Intensity of Extreme Events

The level of destruction the grid assets are anticipated to subject are clearly depend on the intensity of the weather event. When it comes to performance based metrics they have the downside of being event dependent if not the event intensity factor is removed. For an example the resiliency measure obtained for category 1 hurricane can be higher than the measure for category 4 hurricane. This doesn't provide a fair evaluation of the resilience of the system since it is a measurement for two different scenarios. Therefore, it's important to equalize measures from different severity categories and take metrics into a homogenized platform. In this study the impact of intensity of extreme event on the developed performance based metrics are analyzed.

Saffir-Simpson wind scale is currently in use to quantify the intensity of hurricanes and it solely depends on the wind speed. The longer that wind lasts, the longer it exerts force on an object and the higher the potential to cause damage. According to [97] the hurricane actions that influence power outages are storm surge, wind speed, coverage area and the duration under at least tropical wind speed. The

article [98] presents the hurricane severity index which is defined to quantify the destructive capability of a hurricane. This index incorporate the intensity of the wind and the size of area covered as parameters. Actually it's the kinetic energy of the wind that exert force on objects and create failures. But it's quite hard to mathematically model the severity of a hurricane exactly as it depends on various parameters.

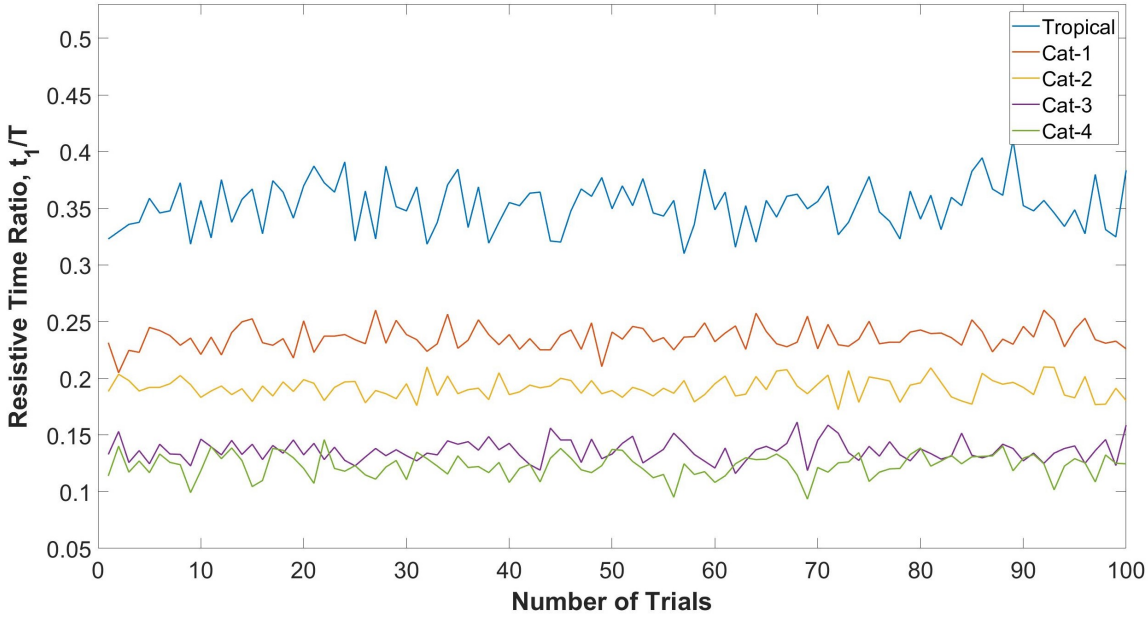

Figure 5.1: Resistive time ratio for wind profiles of different intensities.

One of the parameter used for the metric scheme is resistive time ratio, t_1/T. So in fig. 5.1, the variation of time ratio for different hurricane intensities is analyzed. Six hurricane wind profiles of different hurricane categories were used for this analysis. Hundred simulation trials were carried out for each hurricane wind profile since the threat modeling of this study use probabilistic measures to create failure scenarios. From this graph we can see each scenario has almost constant time ratios in all the trials. The average for tropical storm winds is 0.352, for category-1 0.236, category-2 0.181, category-3 0.138 and category-4 0.123. Other-than the small vari-

ation in category-1 and 2 it can be observed that time ratio is reducing when the intensity increases as expected. It needs to be noted that the critical load weightings are not applied for the analysis since the objective is to view the impact of intensity only.

5.4 Resilience Metrics Formulation

Extreme events progresses so fast and cause longer power outages as it can be hard to physically access the fault locations in order to start the restoration process. With this nature of extreme events, the power system resilience can be evaluated in three temporal phases. Starting with pre-event and then event progression and post-event. This post-event can further classify as immediate post-event which involves recovery and restoration, and the long term post-event. These information are depicted in the resilience trapezoid in fig. 5.2. The focus of this study is only on the distribution network and it is assumed that there are no distribution network power outages occur due to failures of the feeding transmission lines.

For this study the start of extreme event is marked when the wind speed reaches the tropical storm speed threshold and event ends when the speed is less than that threshold. The knee point speed at which the first critical load failed is considered as the breaking wind speed. Here, T indicates the total event duration while t_1^i is the time between start of event to failure of load i. In this work the level of resilience is considered as the availability of critical loads. After the end of extreme event it takes a certain amount of time to do the damage assessment and the maintenance crew to reach to the location. In this study it is assumed that the mean time to start recovery process is 10 hours. This value is again randomized with uniform random

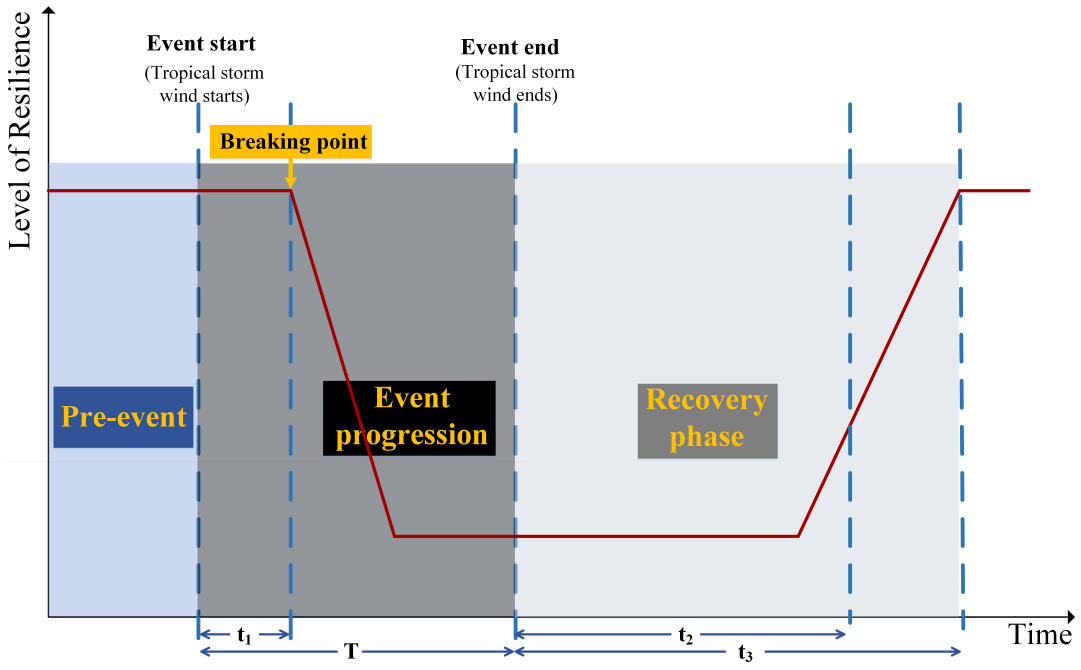

Figure 5.2: Basic resilience trapezoid with temporal phases of an extreme event marked.

distribution for each critical load. Therefore, the time it takes for restoration of load i is marked as t_2^i here. The complete restoration at time t_3.

If the unavailability of a certain load put the safety, health or economy of a society at a huge risk then it can be identified as a critical load. There can be several such loads identified in a certain portion of PDN and all these doesn't have the same level of criticality to prioritize the criticality during an extreme weather event. For this study, the load prioritization scheme presented in [99] has been used.

5.4.1 Developed Metrics

In this work a three-dimensional metric scheme is proposed in where each dimension captures a phase to get the complete picture of resilience of a system. The metric scheme can represent as $< \alpha, \beta, \gamma > @\sigma$. Rather than providing the area under

the curve, these 3 metrics provides an understanding of the three progressive steps separately, hence delivers an insight that which areas should be improved. The designed metrics are given in eq. (5.1), eq. (5.2) and eq. (5.3). The α is an attribute-based metric and presents the concept of preparedness of the system during the pre-event while β is a performance-based metric and represent the quality of absorption during event progresses. And the γ is also a performance-based metric and provide restoration capabilities in post-event.

$$\alpha = \sum_{i=1}^{5} c_i A_i \tag{5.1}$$

$$\beta = \frac{1}{T} \sum_{i=1}^{N_{Cl}} W_i t_1^i \tag{5.2}$$

$$\gamma = \delta R.t_3 \sum_{i=1}^{N_{Cl}} \frac{W_i}{t_2^i} \tag{5.3}$$

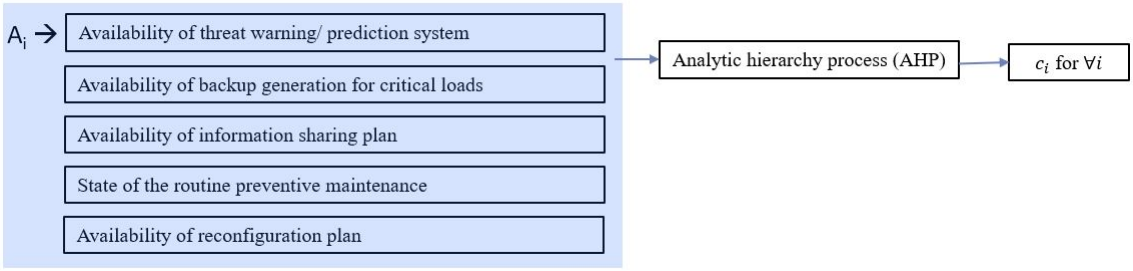

Figure 5.3: The composition of metric α.

The attributes that composes the metric α is given in fig. 5.1. The relative importance of each criteria is calculated using analytic hierarchy process and those values are represented as c_i for all i attributes in the eq. (5.1). W_i is the weight given to each load depending on it's criticality and it's a value between 0 and 1 where the sum of all W_is is one. Here, N_{Cl} is the number of critical loads in the

system. In eq. (5.3), $deltaR$ is the change of resilience level and it is represented as a percentage value. Since the metrics β and γ are performance-based metrics, the event intensity is indicated in the metric scheme as σ. The value of σ is considered as the peak wind speed for the hurricane situation. Although, a hurricane scenario is emulated for validation of the developed metric scheme, it is applicable for any type of extreme weather event.

5.5 Threat Modeling

Resilience quantification process of performance based metrics is done with either historical data sets or estimated data sets or with computer models that emulate grid operations, disruption, and recovery. In this work, computer models are used for threat modeling to perform the metric validation. Extreme weather events inherit uncertainties at every stage starting from wind speed, wind spread to time required for response and restoration. To reflect this uncertainties probability measures and randomization are incorporated in the process of threat modeling. In-order to emulate the impact of extreme weather over PDN, component level fragility curves are used for determining failure probability of each component. Fragility curves are developed either analytically, with empirical data or with professional judgment. Since this study is focusing on hurricanes as extreme weather, fragility curves for wind speed is obtained from the article [100]. For the simplicity, distribution lines and towers are considered as the only components in the system that are susceptible to failure during extreme weather. The failure probability of the lines and towers are obtained applying the wind speed of that hour to the fragility curve and the system failure probability is calculated as the union of failure probability of each component separately as given in the eq. (5.4).

$$P_F = P_{F,poles} + P_{F,lines} - P_{F,poles}.P_{F,lines} \tag{5.4}$$

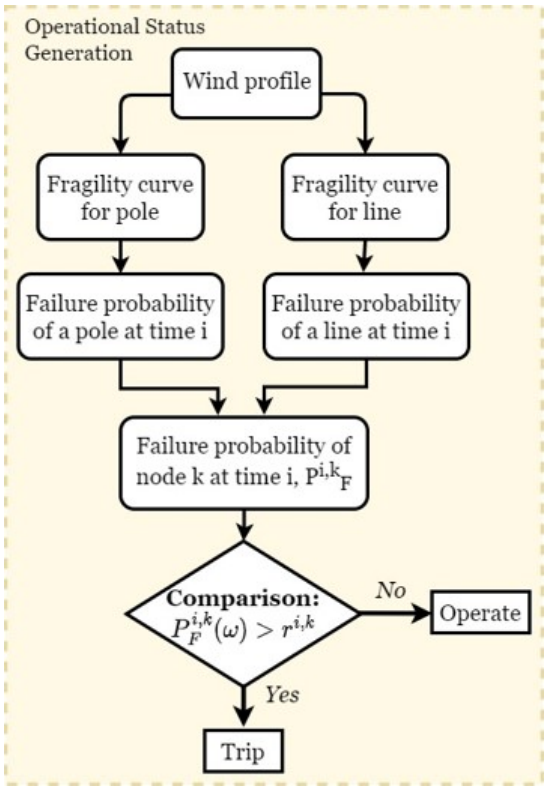

Figure 5.4: Process flow of operational status generation.

For this analysis five wind profiles with different wind intensities are used to replicate the stochastic power system failure events across time during hurricanes. The simulation is done for 48 hour time duration and maximum sustained wind speed data over 10 min is used. Therefore, time resolution of the simulation is also used as 10 minutes. The failure probability of lines and towers are depend on the age and wear of the component as well. Therefore, to provide different deterioration levels for different lines and towers, the failure probability of component k, at i^{th} time step, $P_F^{i,k}(\omega)$ is compared with a uniformly distributed random number, r generated at each time step. If $P_F^{i,k}(\omega)$ exceeds r then the component k will fail and otherwise

it will continue to operate. This simulation concept is adopted from the research presented in [101]. This process flow of generating the operational status of nodes is illustrated in fig.5.4.

When replicating the hurricane event, the occurrence of 39 mph wind speed which is the threshold speed for a tropical storm is considered as the starting instant of the extreme event. Typically, the damage assessment and network repairing begin when the disastrous winds are over. Therefore, the restoration process begins as soon as the wind profile goes below 39 mph. Implementation of a restoration algorithm is out of focus for this research. Hence, the mean time to restore is assumed as 10 hours and again this value is multiplied by a uniformly distributed random number [39]. The status of each component obtained at each time step through this process is then used to enable faults in the power system dynamically. Power flow analysis is carried out at each time step and the voltage at each critical load location is measured for metric calculations.

5.6 Metric Validation

5.6.1 Network Description

In-order to validate the effectiveness of developed metrics, PDN is modeled using the IEEE 123 bus system in the OpenDSS platform as illustrated in Fig. 5.5. The nominal voltage rating of the feeder is $4.16kV$. The feeder has four voltage regulators and shunt capacitor banks. The substation transformer upstream is connected to node 150 and is the size of $5MVA$, $115/4.16kV, \Delta Y$. The load sizes were modified from the original system and the total sizes after modifying the feeder is around 3.5 MW (active) and 1.8 MVAr (reactive).

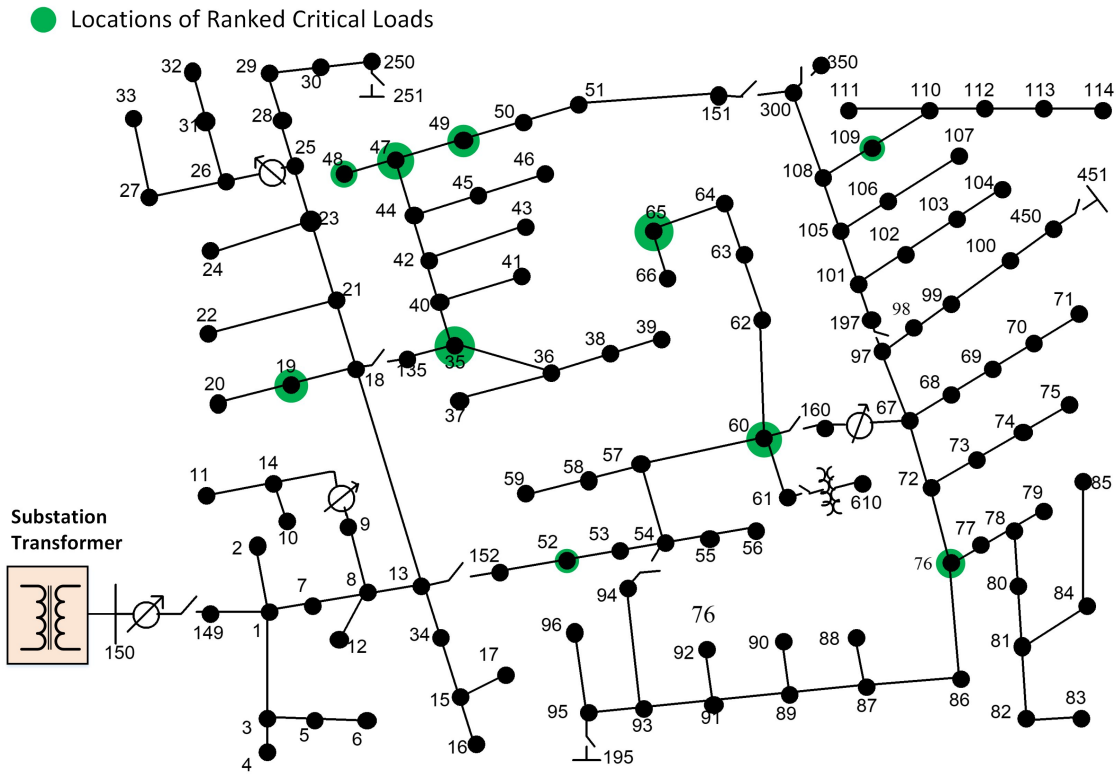

Figure 5.5: IEEE 123 bus network with critical loads marked on it.

This IEEE 123 bus system has 85 total loads and out of them 10 three-phase loads are chosen as critical load nodes for this study. The critical loads are randomly selected across the network and the selected loads are circled in the Figure.4.4. The selected critical loads are ranked according to their criticality using the load prioritization scheme provided in [99] for metric calculations. The load on node 65 is a hospital and node 76 and node 60 are the police and pumping station respectively. Node 47 and 48 are residential loads while node 35 and 49 are supermarkets. There is a shopping mall n node 109 and the fire station is located in the node 19. City hall is located in node 52.

5.6.2 Validation of the Developed Metrics

The developed metrics are scripted and measured in Matlab while it is coupled with OpenDSS through its COM interface to perform power flow analysis at each time step. As mentioned in the Section 5.1, the metrics should be able to justify the actions of resilience enhancements done on the system. In-order to test this, five PV plants are integrated into the PDN and carried out simulations before and after. The PV plants were modeled using GHI profile and temperature data collected from an actual 1.4 MW PV system located on the Engineering campus of Florida International University. Since implementation of restoration algorithm has not been done in this study, it's practically hard to validate the performance of third metric, γ. Hence, the first metric β is validated here.

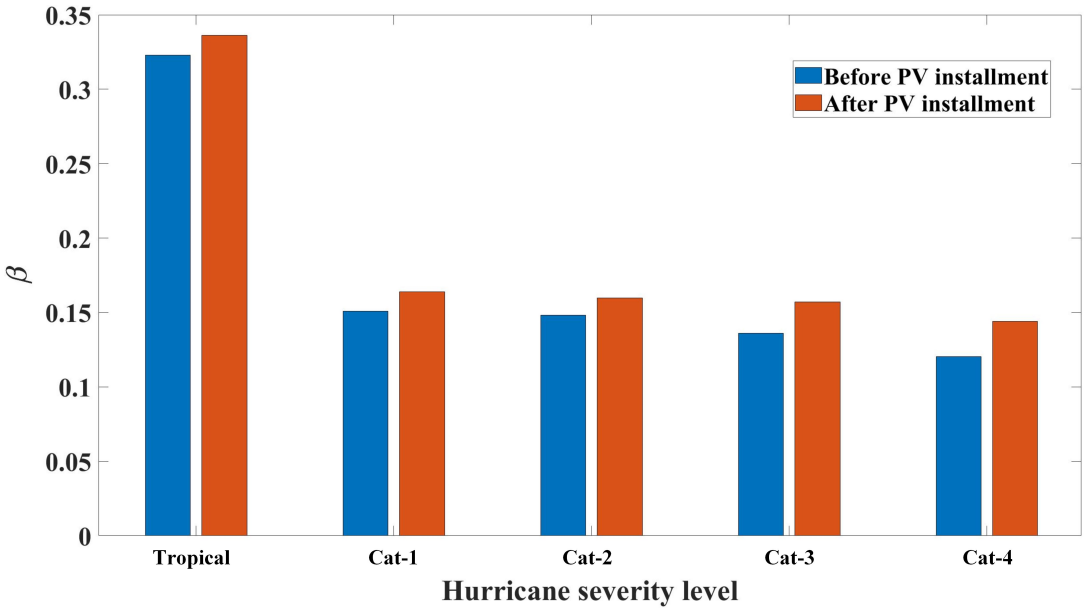

Figure 5.6: The performance of metric, β for wind profiles of different intensities before and after installing PV plants.

In fig. 5.6, the performance of β before and after installing PVs is presented. It can be seen that β has clearly increased after installing PVs in every hurricane

category. But it can also be noted that the increment is higher when the level of intensity is higher. Another information the graph provides is that the metric β reduces when the level of hurricane category go higher. This confirms the conclusion we drawn from fig. 5.1. Similarly, fig. 5.7 depicts the performance of metric breaking wind speed. According to the results, the installations of PV plants increases the breaking wind speed which make sense as installation increases the withstand-ability of the system. Also, it can be observed that the breaking speed stay almost constant for a particular system under different hurricane scenarios.

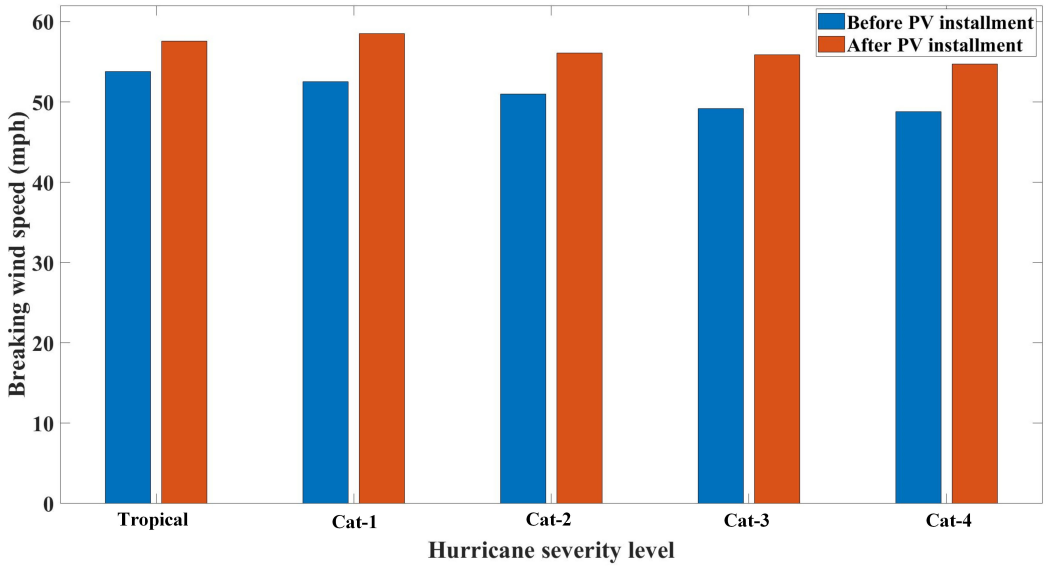

Figure 5.7: The performance of metric, breaking wind speed for wind profiles of different intensities before and after installing PV plants.

5.7 Conclusion & Future Work

In this study, a performance based metrics that represents the three temporal phases of resilience during an extreme event is developed. They are represented as a three dimensional vector. After analyzing the performance of the first two metrics we

can see that the metrics clearly justify the performance enhancement done on the system. Further, the study on level of hurricane intensity shows that these metrics get affected by the event severity.

Based on this work, following research areas are identified for having potential for future investigations.

1. Define and integrate adaptibility measure to the metric vector. Adaptibility will be a long term post-event metric. Probably this metric can be of attribute based, hence the metric scheme would be attribute, performance combined approach.
2. Study the concept of severity of extreme events further, and develop a quantification technique to equalize the performance metrics for extreme events of different severity levels.
3. Come-up with a 3D fragility curve which models the failure probability of components in-terms of both wind speed and the exposure time.

CHAPTER 6

CONCLUSIONS AND FUTURE WORK

The research presented in this dissertation investigates solutions for some of the challenges emerged in the modern PDN. The high penetration of renewable resource based DERs affects the stability of the grid due to their intermittent nature. Again, the proper implementation of DERs has the potential to resolve many aforementioned challenges. In this research, techniques are developed to optimize the benefits of DERs along two main objectives. The first objective is to enhance the performance of DERs by implementing advance control algorithms for the converters.

In chapter 2, a computational complexity reduction technique for FC-MPDPC is presented. This controller is designed for a SI that interlinks BESS to the grid and it facilitates the bidirectional power flow control. The effectiveness of the developed technique is tested for complexity reduction as well as for performance enhancement. For a test case of three-phase two-level converter with 37 candidate voltage vectors, the size of the vector set has reduced to 8. Also, the THD has reduced from 9.7% to 3.89% compared to the conventional FC-MPDPC.

Chapter 3 presents a novel controller development for SIs that interlinks BESS to the grid. It combines the FDM concept to MPC to integrate experience based knowledge to the objective function of the optimization. The objective functions which is designed aggregating the membership functions is capable of dynamically adjusting according to the system state. The designed controller is simulated with Matlab/ Simulink models and is validated.

Chapter 4 develops an optimal DER hosting algorithm to enhance the resilience of PDN where the resilience is defined prioritizing the critical loads. The NSGA-II is applied here to obtain the optimal solution considering the three objectives resilience

enhancement, maximizing PV hosting capacity and minimizing power losses. A hurricane scenario is emulated using probabilistic tools and the developed algorithm is validated. The resilience of the PDN is enhanced by the optimal DER (PV) hosting and placement using the proposed algorithm from a minimum $R_B = 0.51$ to maximum $R_B = 0.94$ and it was able to maximize the DER (PV) hosting capacity from the least value of $0.61MW$ to the highest value of $4.10MW$.

Chapter 5 presents a three dimensional metric vector which follows the performance based approach. The metrics developed here incorporate the critical load prioritization. Further, the impact of the intensity level of hurricane winds over the metrics is analyzed since performance based metrics are event dependent. It is observed that the metrics change with the intensity, therefore do not provide a fair evaluation about the system. This urges the need to quantify the intensity to equalize the magnitudes of metrics for a particular system. The metrics have been validated by evaluating justifications it provide for resilience enhancements.

6.1 Future Work

Based on this research, following topics are identified as potential research directions to explore further.

1. Extend the proposed FDM assisted MPC concept to develop an adaptive, robust controller for autonomous operation of energy storage systems in power smoothing applications considering complex real world constraints and non-linear models.
2. Incorporate appropriate smart inverter functionalities of DERs to enhance the resilience of PDN for an extreme event [102–104].

3. Develop a CL ranking scheme which dynamically change while the extreme event progress.
4. Consider the power transfer from neighboring DERs through system reconfiguration strategies when constructing the optimization algorithm for DER hosting and placement.
5. Incorporate the cost factor of DER installation to the objective function of DER hosting and placement.
6. Combine the impact of two weather events simultaneously when emulating the extreme weather. For an example during a hurricane both the wind and the flooding affects the infrastructure.
7. Develop a resilience metric framework combining attribute and performance based measures and implement a top-down approach where attribute measures gives the general view while performance measures gives the indepth of the specifics that can provide much comprehensive perception on the network resilience.

REFERENCES

[1] S. A. A. Kazmi, M. K. Shahzad, A. Z. Khan, and D. R. Shin, "Smart distribution networks: A review of modern distribution concepts from a planning perspective," *Energies*, vol. 10, no. 4, 2017. [Online]. Available: https://www.mdpi.com/1996-1073/10/4/501

[2] T. O. Olowu, A. Sundararajan, M. Moghaddami, and A. I. Sarwat, "Future challenges and mitigation methods for high photovoltaic penetration: A survey," *Energies*, vol. 11, no. 7, p. 1782, 2018.

[3] A. Khalid and A. I. Sarwat, "Battery module performance analysis under varying interconnection topology for electric vehicles," in *2019 IEEE Transportation Electrification Conference (ITEC-India)*, 2019, pp. 1–5.

[4] M. Moghaddami and A. I. Sarwat, "Single-phase soft-switched ac–ac matrix converter with power controller for bidirectional inductive power transfer systems," *IEEE Transactions on Industry Applications*, vol. 54, no. 4, pp. 3760–3770, 2018.

[5] IEEE Standards Coordinating Committee 21, "IEEE standard for interconnection and interoperability of distributed energy resources with associated electric power systems interfaces," *IEEE Std 1547-2018 (Revision of IEEE Std 1547-2003)*, pp. 1–138, April 2018.

[6] "Fedcenter - eo 13693 (archive) - revoked by eo 13834 on may 17, 2018, sec. 8," 2018. [Online]. Available: https://www.fedcenter.gov/programs/eo13693/

[7] J. D. Taft, "Electric grid resilience and reliability for grid architecture," *Pacific Northwest National Laboratory (PNNL) Technical Report*, March 2018. [Online]. Available: https://gridarchitecture.pnnl.gov/media/advanced/Electric_Grid_Resilience_and_Reliability_v4.pdf

[8] A. Clark-Ginsberg, "What's the difference between reliability and resilience?" *Stanford University Report for ICS-CERT*, March 2016. [Online]. Available: https://ics-cert.us-cert.gov/sites/default/files/ICSJWG-Archive/QNL_MAR_16/reliability\%20and\%20resilience\%20pdf.pdf

[9] M. Panteli and P. Mancarella, "Influence of extreme weather and climate change on the resilience of power systems: Impacts and possible mitigation strategies," *Electric Power Systems Research*, June 2015.

[10] E.P.R.I., "Electric power system resiliency: Challenges and opportunities," *Electric Power Research Institute (EPRI) Technical Report*, February 2016. [Online]. Available: https://www.naseo.org/Data/Sites/1/resiliency-white-paper.pdf

[11] J. McLaren and S. Mullendore, "Valuing the resilience provided by solar and battery energy storage systems," *National Renewable Energy Laboratory (NREL)*, 2018.

[12] A. I. Sarwat, M. Amini, A. Domijan, A. Damnjanovic, and F. Kaleem, "Weather-based interruption prediction in the smart grid utilizing chronological data," *Journal of Modern Power Systems and Clean Energy*, vol. 4, no. 2, pp. 308–315, Apr 2016. [Online]. Available: https://doi.org/10.1007/s40565-015-0120-4

[13] M. Panteli, D. N. Trakas, P. Mancarella, and N. D. Hatziargyriou, "Power systems resilience assessment: Hardening and smart operational enhancement strategies," *Proceedings of the IEEE*, vol. 105, no. 7, pp. 1202–1213, 2017.

[14] M. H. Oboudi, M. Mohammadi, D. N. Trakas, and N. D. Hatziargyriou, "A systematic method for power system hardening to increase resilience against earthquakes," *IEEE Systems Journal*, vol. 15, no. 4, pp. 4970–4979, 2021.

[15] D. B. Wickramasinghe Abeywardana, P. Acuna, B. Hredzak, R. P. Aguilera, and V. G. Agelidis, "Single-phase boost inverter-based electric vehicle charger with integrated vehicle to grid reactive power compensation," *IEEE Transactions on Power Electronics*, vol. 33, no. 4, pp. 3462–3471, April 2018.

[16] Y. Gui, X. Wang, H. Wu, and F. Blaabjerg, "Voltage-modulated direct power control for a weak grid-connected voltage source inverters," *IEEE Transactions on Power Electronics*, vol. 34, no. 11, pp. 11 383–11 395, Nov 2019.

[17] Y. Gui, Q. Xu, F. Blaabjerg, and H. Gong, "Sliding mode control with grid voltage modulated DPC for voltage source inverters under distorted grid voltage," *CPSS Transactions on Power Electronics and Applications*, vol. 4, no. 3, pp. 244–254, Sep. 2019.

[18] S. Vazquez, J. I. Leon, L. G. Franquelo, J. Rodriguez, H. A. Young, A. Marquez, and P. Zanchetta, "Model predictive control: A review of its applications in power electronics," *IEEE Industrial Electronics Magazine*, vol. 8, no. 1, pp. 16–31, 2014.

[19] J. Hu, J. Zhu, and D. G. Dorrell, "Model predictive control of grid-connected inverters for pv systems with flexible power regulation and switching frequency reduction," *IEEE Transactions on Industry Applications*, vol. 51, no. 1, pp. 587–594, 2015.

[20] Y. Zhang and C. Qu, "Model predictive direct power control of pwm rectifiers under unbalanced network conditions," *IEEE Transactions on Industrial Electronics*, vol. 62, no. 7, pp. 4011–4022, 2015.

[21] M. Parvez Akter, S. Mekhilef, N. Mei Lin Tan, and H. Akagi, "Modified model predictive control of a bidirectional AC–DC converter based on lyapunov function for energy storage systems," *IEEE Transactions on Industrial Electronics*, vol. 63, no. 2, pp. 704–715, Feb 2016.

[22] A. Moghadasi, A. Sargolzaei, A. Anzalchi, M. Moghaddami, A. Khalilnejad, and A. Sarwat, "A model predictive power control approach for a three-phase single-stage grid-tied PV module-integrated converter," *IEEE Transactions on Industry Applications*, vol. 54, no. 2, pp. 1823–1831, March 2018.

[23] N. Panten, N. Hoffmann, and F. W. Fuchs, "Finite control set model predictive current control for grid-connected voltage-source converters with LCL filters: A study based on different state feedbacks," *IEEE Transactions on Power Electronics*, vol. 31, no. 7, pp. 5189–5200, 2016.

[24] A. Moghadasi, A. Sargolzaei, A. Anzalchi, M. Moghaddami, A. Khalilnejad, and A. Sarwat, "A model predictive power control approach for a three-phase single-stage grid-tied pv module-integrated converter," *IEEE Transactions on Industry Applications*, vol. 54, no. 2, pp. 1823–1831, 2017.

[25] S. Dharmasena and S. Choi, "Model predictive control of five-phase permanent magnet assisted synchronous reluctance motor," in *2019 IEEE Applied Power Electronics Conference and Exposition (APEC)*, 2019, pp. 1885–1890.

[26] S. . Ho, Li-Sun Shu, and Shinn-Ying Ho, "Optimizing fuzzy neural networks for tuning pid controllers using an orthogonal simulated annealing algorithm osa," *IEEE Transactions on Fuzzy Systems*, vol. 14, no. 3, pp. 421–434, 2006.

[27] T. Chaiyatham and I. Ngamroo, "Improvement of power system transient stability by pv farm with fuzzy gain scheduling of pid controller," *IEEE Systems Journal*, vol. 11, no. 3, pp. 1684–1691, 2017.

[28] R. Arghandeh, M. Brown, A. Del Rosso, G. Ghatikar, E. Stewart, A. Vojdani, and A. von Meier, "The local team: Leveraging distributed resources to improve resilience," *IEEE Power and Energy Magazine*, vol. 12, no. 5, pp. 76–83, 2014.

[29] A. Gholami, F. Aminifar, and M. Shahidehpour, "Front lines against the darkness: Enhancing the resilience of the electricity grid through microgrid facilities," *IEEE Electrification Magazine*, vol. 4, no. 1, pp. 18–24, 2016.

[30] Z. Wang and J. Wang, "Self-healing resilient distribution systems based on sectionalization into microgrids," *IEEE Transactions on Power Systems*, vol. 30, no. 6, pp. 3139–3149, 2015.

[31] A. Khodaei, "Resiliency-oriented microgrid optimal scheduling," *IEEE Transactions on Smart Grid*, vol. 5, no. 4, pp. 1584–1591, 2014.

[32] P. Gautam, P. Piya, and R. Karki, "Resilience assessment of distribution systems integrated with distributed energy resources," *IEEE Transactions on Sustainable Energy*, vol. 12, no. 1, pp. 338–348, 2021.

[33] Z. Li, M. Shahidehpour, F. Aminifar, A. Alabdulwahab, and Y. Al-Turki, "Networked microgrids for enhancing the power system resilience," *Proceedings of the IEEE*, vol. 105, no. 7, pp. 1289–1310, 2017.

[34] V. V. Frederic Petit, "Grid modernization: Metrics analysis (gmlc1.1) – resilience," *Grid Modernization Laboratory Consortium*, April 2020. [Online]. Available: https://gmlc.doe.gov/resources/grid-modernization-metrics-analysis-gmlc1.1-resilience

[35] I. Power and E. S. I. T. S. L. C. T. Force, "Resilience framework, methods, and metrics for the electricity sector," *IEEE Power and Energy Society*, October 2020. [Online]. Available: https://resourcecenter.ieee-pes.org/publications/technical-reports/PES_TP_TR83_ITSLC_102920.html

[36] P. Bajpai, S. Chanda, and A. K. Srivastava, "A novel metric to quantify and enable resilient distribution system using graph theory and choquet integral," *IEEE Transactions on Smart Grid*, vol. 9, no. 4, pp. 2918–2929, July 2018.

[37] S. Chanda and A. K. Srivastava, "Defining and enabling resiliency of electric distribution systems with multiple microgrids," *IEEE Transactions on Smart Grid*, vol. 7, no. 6, pp. 2859–2868, Nov 2016.

[38] X. Liu, M. Shahidehpour, Z. Li, X. Liu, Y. Cao, and Z. Bie, "Microgrids for enhancing the power grid resilience in extreme conditions," *IEEE Transactions on Smart Grid*, vol. 8, no. 2, pp. 589–597, 2017.

[39] M. Panteli, P. Mancarella, D. N. Trakas, E. Kyriakides, and N. D. Hatziargyriou, "Metrics and quantification of operational and infrastructure resilience in power systems," *IEEE Transactions on Power Systems*, vol. 32, no. 6, pp. 4732–4742, 2017.

[40] M. Moghaddami and A. I. Sarwat, "Single-phase soft-switched AC–AC matrix converter with power controller for bidirectional inductive power transfer systems," *IEEE Transactions on Industry Applications*, vol. 54, no. 4, pp. 3760–3770, July 2018.

[41] A. Moghadasi, A. Sargolzaei, M. Moghaddami, A. I. Sarwat, and K. Yen, "Active and reactive power control method for three-phase PV module-integrated converter based on a single-stage inverter," in *2017 IEEE Applied Power Electronics Conference and Exposition (APEC)*, 2017, pp. 1357–1362.

[42] S. Dharmasena and S. Choi, "Model predictive control of five-phase permanent magnet assisted synchronous reluctance motor," in *2019 IEEE Applied Power Electronics Conference and Exposition (APEC)*, March 2019, pp. 1885–1890.

[43] Y. Luo and C. Liu, "Elimination of harmonic currents using a reference voltage vector based-model predictive control for a six-phase pmsm motor," *IEEE Transactions on Power Electronics*, vol. 34, no. 7, pp. 6960–6972, 2019.

[44] T. Wang, C. Liu, G. Lei, Y. Guo, and J. Zhu, "Model predictive direct torque control of permanent magnet synchronous motors with extended set of voltage space vectors," *IET Electric Power Applications*, vol. 11, no. 8, pp. 1376–1382, 2017.

[45] W. Zhu, C. Chen, and S. Duan, "Model predictive control with improved discrete space vector modulation for three-level vienna rectifier," *IET Power Electronics*, vol. 12, no. 8, pp. 1998–2004, 2019.

[46] C. Xiong, H. Xu, T. Guan, and P. Zhou, "A constant switching frequency multiple-vector-based model predictive current control of five-phase PMSM with nonsinusoidal back EMF," *IEEE Transactions on Industrial Electronics*, vol. 67, no. 3, pp. 1695–1707, 2020.

[47] X. Yang, Y. Fang, Y. Fu, Y. Mi, H. Li, and Y. Wang, "Low-complexity model predictive control of AC/DC converter with constant switching frequency," *IEEE Access*, vol. 8, pp. 137 975–137 985, 2020.

[48] M. Parvez Akter, S. Mekhilef, N. Mei Lin Tan, and H. Akagi, "Modified model predictive control of a bidirectional ac–dc converter based on lyapunov function for energy storage systems," *IEEE Transactions on Industrial Electronics*, vol. 63, no. 2, pp. 704–715, 2016.

[49] H. Moon, J. Lee, and K. Lee, "A robust deadbeat finite set model predictive current control based on discrete space vector modulation for a grid-connected voltage source inverter," *IEEE Transactions on Energy Conversion*, vol. 33, no. 4, pp. 1719–1728, 2018.

[50] W. Wang, C. Liu, S. Liu, and H. Zhao, "Model predictive torque control for dual three-phase pmsms with simplified deadbeat solution and discrete space-vector modulation," *IEEE Transactions on Energy Conversion*, pp. 1–1, 2021.

[51] I. M. Hassine, M. W. Naouar, and N. Mrabet-Bellaaj, "Model predictive-sliding mode control for three-phase grid-connected converters," *IEEE Transactions on Industrial Electronics*, vol. 64, no. 2, pp. 1341–1349, Feb 2017.

[52] K. S. Alam, D. Xiao, M. Parvez Akter, D. Zhang, J. Fletcher, and M. F. Rahman, "Modified MPC with extended VVs for grid-connected rectifier," *IET Power Electronics*, vol. 11, no. 12, pp. 1926–1936, 2018.

[53] Y. Zhang, Y. Peng, and C. Qu, "Model predictive control and direct power control for PWM rectifiers with active power ripple minimization," *IEEE Transactions on Industry Applications*, vol. 52, no. 6, pp. 4909–4918, Nov 2016.

[54] X. Liu, D. Wang, and Z. Peng, "A computationally efficient FCS-MPC method without weighting factors for NNPCs with optimal duty cycle control," *IEEE/ASME Transactions on Mechatronics*, vol. 23, no. 5, pp. 2503–2514, 2018.

[55] T. Jin, J. Guo, M. A. Mohamed, and M. Wang, "A novel model predictive control via optimized vector selection method for common-mode voltage reduction of three-phase inverters," *IEEE Access*, vol. 7, pp. 95 351–95 363, 2019.

[56] X. Shi, J. Zhu, L. Li, and D. Dah-Chuan LU, "Low-complexity dual-vector-based predictive control of three-phase pwm rectifiers without duty-cycle optimization," *IEEE Access*, vol. 8, pp. 77 049–77 059, 2020.

[57] Z. Zhou, C. Xia, T. Shi, and Q. Geng, "Model predictive direct duty-cycle control for pmsm drive systems with variable control set," *IEEE Transactions on Industrial Electronics*, vol. 68, no. 4, pp. 2976–2987, 2021.

[58] N. Jin, S. Hu, C. Gan, and Z. Ling, "Finite states model predictive control for fault-tolerant operation of a three-phase bidirectional AC/DC converter under unbalanced grid voltages," *IEEE Transactions on Industrial Electronics*, vol. 65, no. 1, pp. 819–829, 2018.

[59] K. S. Alam, D. Xiao, M. Parvez Akter, D. Zhang, J. Fletcher, and M. F. Rahman, "Modified mpc with extended vvs for grid-connected rectifier," *IET Power Electronics*, vol. 11, no. 12, pp. 1926–1936, 2018.

[60] R. Ortega, N. Barabanov, G. Escobar, and E. Valderrama, "Direct torque control of induction motors: stability analysis and performance improvement," *IEEE Transactions on Automatic Control*, vol. 46, no. 8, pp. 1209–1222, 2001.

[61] B. S. Chen and G. JoÓs, "Direct power control of active filters with averaged switching frequency regulation," *IEEE Transactions on Power Electronics*, vol. 23, no. 6, pp. 2729–2737, 2008.

[62] G. Escobar, A. M. Stankovic, J. M. Carrasco, E. Galvan, and R. Ortega, "Analysis and design of direct power control (DPC) for a three phase synchronous rectifier via output regulation subspaces," *IEEE Transactions on Power Electronics*, vol. 18, no. 3, pp. 823–830, 2003.

[63] S. Vazquez, J. A. Sanchez, J. M. Carrasco, J. I. Leon, and E. Galvan, "A model-based direct power control for three-phase power converters," *IEEE Transactions on Industrial Electronics*, vol. 55, no. 4, pp. 1647–1657, 2008.

[64] A. Vekariya, T. Trivedi, R. Jadeja, and P. Bhatt, "Comparative study of lookup table approach of direct power control for three-phase DC/AC inverter," in *Artificial Intelligence and Evolutionary Computations in Engineering Systems*, S. S. Dash, K. Vijayakumar, B. K. Panigrahi, and S. Das, Eds. Singapore: Springer Singapore, 2017, pp. 419–439.

[65] Y. L. Huang, H. H. Lou, J. P. Gong, and T. F. Edgar, "Fuzzy model predictive control," *IEEE Transactions on Fuzzy Systems*, vol. 8, no. 6, pp. 665–678, 2000.

[66] S. Kayalvizhi and D. M. Vinod Kumar, "Load frequency control of an isolated micro grid using fuzzy adaptive model predictive control," *IEEE Access*, vol. 5, pp. 16 241–16 251, 2017.

[67] B. Wang, L. Yang, F. Wu, and D. Chen, "Fuzzy predictive functional control of a class of non-linear systems," *IET Control Theory Applications*, vol. 13, no. 14, pp. 2281–2288, 2019.

[68] X. Liu, D. Wang, and Z. Peng, "Cascade-free fuzzy finite-control-set model predictive control for nested neutral point-clamped converters with low switching frequency," *IEEE Transactions on Control Systems Technology*, vol. 27, no. 5, pp. 2237–2244, 2019.

[69] A. M. Bozorgi, H. Gholami-Khesht, M. Farasat, S. Mehraeen, and M. Monfared, "Model predictive direct power control of three-phase grid-connected converters with fuzzy-based duty cycle modulation," *IEEE Transactions on Industry Applications*, vol. 54, no. 5, pp. 4875–4885, 2018.

[70] J. M. Sousa, R. Babuska, P. Bruijn, and H. B. Verbruggen, "Comparison of conventional and fuzzy predictive control," in *Proceedings of IEEE 5th International Fuzzy Systems*, vol. 3, Sep. 1996, pp. 1782–1787 vol.3.

[71] J. M. da Costa Sousa and U. Kaymak, "Model predictive control using fuzzy decision functions," *IEEE Transactions on Systems, Man, and Cybernetics, Part B (Cybernetics)*, vol. 31, no. 1, pp. 54–65, Feb 2001.

[72] K. A. Joshi, N. M. Pindoriya, and A. K. Srivastava, "A two-stage fuzzy multiobjective optimization for phase-sensitive day-ahead dispatch of battery energy storage system," *IEEE Systems Journal*, vol. 12, no. 4, pp. 3649–3660, 2018.

[73] C. Bhattacharjee and B. K. Roy, "Fuzzy-supervisory control of a hybrid system to improve contractual grid support with fuzzy proportional–derivative and integral control for power quality improvement," *IET Generation, Transmission Distribution*, vol. 12, no. 7, pp. 1455–1465, 2018.

[74] V. H. Chalishazar, S. Poudel, S. Hanif, and P. Thekkumparambath Mana, "Power system resilience metrics augmentation for critical load prioritization," 1 2021. [Online]. Available: https://www.osti.gov/biblio/1764623

[75] V. B. Venkateswaran, D. K. Saini, and M. Sharma, "Approaches for optimal planning of energy storage units in distribution network and their impacts on

system resiliency," *CSEE Journal of Power and Energy Systems*, vol. 6, no. 4, pp. 816–833, 2020.

[76] R. Eskandarpour, H. Lotfi, and A. Khodaei, "Optimal microgrid placement for enhancing power system resilience in response to weather events," in *2016 North American Power Symposium (NAPS)*, 2016, pp. 1–6.

[77] H. Shirazi, M. Ghiasi, M. Dehghani, T. Niknam, M. G. Garpachi, and A. Ramezani, "Cost-emission control based physical-resilience oriented strategy for optimal allocation of distributed generation in smart microgrid," in *2021 7th International Conference on Control, Instrumentation and Automation (ICCIA)*, 2021, pp. 1–6.

[78] B. Zhang, P. Dehghanian, and M. Kezunovic, "Optimal allocation of pv generation and battery storage for enhanced resilience," *IEEE Transactions on Smart Grid*, vol. 10, no. 1, pp. 535–545, 2019.

[79] V. Widiputra, S. Oh, and J. Jung, "Optimal microgrid formation to improve the resilience of power system withstanding the storm," in *2019 IEEE R10 Humanitarian Technology Conference (R10-HTC)(47129)*, 2019, pp. 228–233.

[80] R. Kizito, X. Li, K. Sun, and S. Li, "Optimal distributed generator placement in utility-based microgrids during a large-scale grid disturbance," *IEEE Access*, vol. 8, pp. 21 333–21 344, 2020.

[81] A. Arshad and M. Lehtonen, "A stochastic assessment of pv hosting capacity enhancement in distribution network utilizing voltage support techniques," *IEEE Access*, vol. 7, pp. 46 461–46 471, 2019.

[82] S. Wang, Y. Dong, L. Wu, and B. Yan, "Interval overvoltage risk based pv hosting capacity evaluation considering pv and load uncertainties," *IEEE Transactions on Smart Grid*, vol. 11, no. 3, pp. 2709–2721, 2020.

[83] R. Torquato, D. Salles, C. Oriente Pereira, P. C. M. Meira, and W. Freitas, "A comprehensive assessment of pv hosting capacity on low-voltage distribution systems," *IEEE Transactions on Power Delivery*, vol. 33, no. 2, pp. 1002–1012, 2018.

[84] F. Ding and B. Mather, "On distributed pv hosting capacity estimation, sensitivity study, and improvement," *IEEE Transactions on Sustainable Energy*, vol. 8, no. 3, pp. 1010–1020, 2017.

[85] N.P.P.D., "Critical infrastructure security and resilience month toolkit," *U.S. Department of Homeland Security (DHS) Technical Report by the National Protection & Programs Directorate*, November 2018. [Online]. Available: https://www.dhs.gov/sites/default/files/publications/CISR-month-toolkit-10292018-508.pdf

[86] A. Almeida, "A multi-criteria methodology for the identification and ranking of critical infrastructures," *Instituto Superior Técnico Report*, pp. 1–10, 2011.

[87] A. Fekete, "Common criteria for the assessment of critical infrastructures," *International Journal of Disaster Risk Science*, vol. 2, no. 1, pp. 15–24, 2011.

[88] K. Barker, J. E. Ramirez-Marquez, and C. M. Rocco, "Resilience-based network component importance measures," *Reliability Engineering & System Safety*, vol. 117, pp. 89–97, 2013.

[89] S. Pinnaka, R. Yarlagadda, and E. K. Çetinkaya, "Modelling robustness of critical infrastructure networks," in *2015 11th International Conference on the Design of Reliable Communication Networks (DRCN)*. IEEE, 2015, pp. 95–98.

[90] S. S. Chopra and V. Khanna, "Interconnectedness and interdependencies of critical infrastructures in the us economy: Implications for resilience," *Physica A: Statistical Mechanics and its Applications*, vol. 436, pp. 865–877, 2015.

[91] L. R. Dauelsberg and A. V. Outkin, "Modeling economic impacts to critical infrastructures in a system dynamics framework," in *Proceedings of the 23rd International Conference of the System Dynamics Society*, 2005, p. 63.

[92] M. Panteli and P. Mancarella, "Influence of extreme weather and climate change on the resilience of power systems: Impacts and possible mitigation strategies," *Electric Power Systems Research*, vol. 127, pp. 259–270, 2015. [Online]. Available: https://www.sciencedirect.com/science/article/pii/S037877961500187X

[93] S. Poudel, A. Dubey, and A. Bose, "Risk-based probabilistic quantification of power distribution system operational resilience," *IEEE Systems Journal*, vol. 14, no. 3, pp. 3506–3517, 2020.

[94] A. Kwasinski, "Quantitative model and metrics of electrical grids' resilience evaluated at a power distribution level," *Energies*, vol. 9, no. 2, 2016. [Online]. Available: https://www.mdpi.com/1996-1073/9/2/93

[95] S. Chanda, A. K. Srivastava, M. U. Mohanpurkar, and R. Hovsapian, "Quantifying power distribution system resiliency using code-based metric," *IEEE Transactions on Industry Applications*, vol. 54, no. 4, pp. 3676–3686, July 2018.

[96] G. Kandaperumal, S. Pandey, and A. Srivastava, "Awr: Anticipate, withstand, and recover resilience metric for operational and planning decision support in electric distribution system," *IEEE Transactions on Smart Grid*, vol. 13, no. 1, pp. 179–190, 2022.

[97] V. Krishnamurthy and A. Kwasinski, "Characterization of power system outages caused by hurricanes through localized intensity indices," in *2013 IEEE Power Energy Society General Meeting*, 2013, pp. 1–5.

[98] C. Hebert, R. Weinzapfel, and M. Chambers, "Hurricane severity index: A more efficient way of predicting a tropical cyclone's destructive potential," May 2010.

[99] S. Dharmasena, T. O. Olowu, and A. I. Sarwat, "Algorithmic formulation for network resilience enhancement by optimal der hosting and placement," *IEEE Access*, vol. 10, pp. 23 477–23 488, 2022.

[100] J. Bennett, C. Trevisan, J. DeCarolis, C. Ortiz-García, M. Pérez-Lugo, B. Etienne, and A. Clarens, "Extending energy system modelling to include extreme weather risks and application to hurricane events in puerto rico," *Nature Energy*, March 2021.

[101] M. Panteli, C. Pickering, S. Wilkinson, R. Dawson, and P. Mancarella, "Power system resilience to extreme weather: Fragility modeling, probabilistic impact assessment, and adaptation measures," *IEEE Transactions on Power Systems*, vol. 32, no. 5, pp. 3747–3757, 2017.

[102] T. O. Olowu, A. Inaolaji, A. Sarwat, and S. Paudyal, "Optimal volt-var and volt-watt droop settings of smart inverters," in *2021 IEEE Green Technologies Conference (GreenTech)*, 2021, pp. 89–96.

[103] T. O. Olowu, S. Dharmasena, A. Debnath, and A. Sarwat, "Smart inverters' functionalities and their impacts on distribution feeders at high photovoltaic penetration," in *2021 IEEE Green Technologies Conference (GreenTech)*, 2021, pp. 97–104.

[104] T. O. Olowu, J. Sarochar, and A. I. Sarwat, "Pareto optimal smart inverter curve selection for high photovoltaic penetration," in *2021 IEEE Green Technologies Conference (GreenTech)*, 2021, pp. 1–6.

VITA

IRESHA SHAMINI D. KONARA MUDIYANSELAGE

October 19, 1988	Born, Gampaha, Sri Lanka
2013	B.Sc., Electrical Engineering University of Moratuwa Moratuwa, Sri Lanka
2016	M.Sc., Electrical Engineering University of Akron Akron, Ohio

PUBLICATIONS AND PRESENTATIONS

[J4] S. Dharmasena, T. O. Olowu and A. I. Sarwat, "Algorithmic Formulation for Network Resilience Enhancement by Optimal DER Hosting and Placement," in IEEE Access, 2022.

[J3] S. Dharmasena, T. O. Olowu and A. I. Sarwat, "A low-complexity FS-MPDPC with extended voltage set for grid-connected converters," IET Energy Systems Integration, 2021.

[J2] T. O. Olowu, S. Dharmasena, A. Hernandez, A. Sarwat, "Impact Analysis of Cyber Attacks on Smart Grid: A Review and Case Study". In: Tyagi H., Chakraborty P.R., Powar S., Agarwal A.K. (eds) New Research Directions in Solar Energy Technologies. Energy, Environment, and Sustainability. Springer, Singapore, 2021

[J1] I. Parvez, A. Ahmed, S. Dharmasena, S. Tufail and A. Sundararajan. "Latency Critical Data Processing in Cloud for Smart Grid Applications". In: Arai K. (eds) Advances in Information and Communication. FICC 2021. Advances in Intelligent Systems and Computing, vol 1364. Springer, Cham.

[C5] S. Dharmasena and A. I. Sarwat, "Fuzzy Decision Making Assisted Model Predictive Direct Power Controller for a Grid-Interlinking Converter of a Battery Energy Storage System," 2020 52nd North American Power Symposium (NAPS), 2021.

[C4] T. O. Olowu, S. Dharmasena, A. Debnath and A. Sarwat, "Smart Inverters' Functionalities and their Impacts on Distribution Feeders at High Photovoltaic Penetration," 2021 IEEE Green Technologies Conference (GreenTech), 2021.

[C3] T. O. Olowu, S. Dharmasena, H. Jafari and A. Sarwat, "Investigation of False Data Injection Attacks on Smart Inverter Settings," 2020 IEEE CyberPELS (CyberPELS), 2020.

[C2] S. Dharmasena, T. O. Olowu and A. I. Sarwat, "Bidirectional AC/DC Converter Topologies: A Review," SoutheastCon, Huntsville, AL, USA, 2019.

[C1] T. O. Olowu, H. Jafari, S. Dharmasena and A. I. Sarwat, "Photovoltaic Fleet Aggregation and High Penetration: A Feeder Test Case," 2019 SoutheastCon, Huntsville, AL, USA, 2019.